OPTICAL-TO-OPTICAL INTERFACE DEVICE

A. JACOBSON

HUGHES RESEARCH LABORATORIES
3011 MALIBU CANYON ROAD
MALIBU, CA 90265

APRIL 1975

CONTRACT NAS 5-23192
FINAL TECHNICAL REPORT
FOR PERIOD 10 FEBRUARY 1973 TO 8 SEPTEMBER 1974

PREPARED FOR

NATIONAL AERONAUTICS AND SPACE ADMINISTRATION
GODDARD SPACE FLIGHT CENTER
GREENBELT ROAD
GREENBELT, MD 20771

UNCLASSIFIED

SECURITY CLASSIFICATION OF THIS PAGE *(When Data Entered)*

REPORT DOCUMENTATION PAGE		READ INSTRUCTIONS BEFORE COMPLETING FORM
1. REPORT NUMBER	2 GOVT ACCESSION NO.	3. RECIPIENT'S CATALOG NUMBER
4. TITLE *(and Subtitle)* Optical-To-Optical Interface Device		5. TYPE OF REPORT & PERIOD COVERED Final Report 7 Feb. 1973-8 Sept. 1974 6. PERFORMING ORG. REPORT NUMBER
7. AUTHOR(s) A. Jacobson, W.P. Bleha, Leroy Miller, J. Grinberg, L. Fraas, and D. Margerum		8. CONTRACT OR GRANT NUMBER(s) NAS 5-23192
9. PERFORMING ORGANIZATION NAME AND ADDRESS Hughes Research Laboratories 3011 Malibu Canyon Road Malibu, CA 90265		10 PROGRAM ELEMENT, PROJECT, TASK AREA & WORK UNIT NUMBERS
11. CONTROLLING OFFICE NAME AND ADDRESS National Aeronautics & Space Administration Goddard Space Flight Center Greenbelt, Maryland 20771		12 REPORT DATE April 1974 13 NUMBER OF PAGES 129
14 MONITORING AGENCY NAME & ADDRESS *(if different from Controlling Office)*		15 SECURITY CLASS *(of this report)* Unclassified 15a DECLASSIFICATION DOWNGRADING SCHEDULE
16 DISTRIBUTION STATEMENT *(of this Report)*		
17 DISTRIBUTION STATEMENT *(of the abstract entered in Block 20, if different from Report)*		
18. SUPPLEMENTARY NOTES		
19. KEY WORDS *(Continue on reverse side if necessary and identify by block number)* Optical Data Processing, Projection Display, Liquid Crystal, Thin Film Photoconductor, Imaging Device		
20 ABSTRACT *(Continue on reverse side if necessary and identify by block number)* This report describes the work done on Contract NAS 5-23192 to extend the performance of a photoactivated liquid crystal light valve. This light valve is designed for incoherent to coherent optical data processing. During this contract period, several innovations were incorporated in an earlier model device. Major innovations are (1) the dc structure used previously was replaced by a novel ac light		

DD FORM 1 JAN 73 1473 EDITION OF 1 NOV 65 IS OBSOLETE

UNCLASSIFIED

SECURITY CLASSIFICATION OF THIS PAGE *(When Data Entered)*

valve structure. This new structure allows long device lifetimes because it eliminates the electrochemical degradation problem present in the earlier dc device. The new structure also allows reflection mode operation with good reading and writing beam isolation. (2) The mode of operation of the liquid crystal was changed from a dynamic scattering mode to a field-effect mode. This change involved the invention of a new hybrid field-effect device. The field-effect mode innovation allows higher image contrast, a cleaner image plane, and lower operating voltages. (3) The liquid crystal layer thickness was reduced from 6 μm to 2.5 μm. This was possible only as a result of the incorporation of the field-effect liquid crystal. Such a thickness reduction allows dramatically increased frame rates. It also allowed an improvement in image resolution.

The developed light valve device consists of a sandwich structure of a thin film photoconductor, light-blocking layer, broad visible spectrum dielectric mirror, and liquid crystal layer. All these layers are sandwiched between two glass electrodes with transparent conductive coatings. There are no matrix elements to limit resolution. Because of the insulating characteristics of the dielectric mirror, it is necessary to use ac voltages to operate the light valve. In operation, the CdS/CdTe photosensor acts as a high resolution imaging light activated voltage gate for the liquid crystal. The CdTe light-blocking layer and dielectric mirror serve to reflect the projection light and prevent this light from reaching the photosensor. Imaging on the light valve can be done with a low intensity P-1 CRT and a lens or by a direct coupling from a fiber optic CRT and a light valve constructed on a mating fiber optic faceplate.

In addition to the performance characteristics of delivered devices, this report presents detailed technical studies on liquid crystal alignment, sputtered CdS photoconductor development, CdS polishing techniques, and device uniformity and cosmetic quality.

TABLE OF CONTENTS

LIST OF ILLUSTRATIONS

I. INTRODUCTION AND PROGRAM SUMMARY

A. Introduction

This report describes the work done on Contract NAS 5-23192, entitled "Optical-to-Optical Interface Device," and covers the entire contract effort, from 10 February 1973 to 7 February 1974, as well as work done during the no-cost extension period through September 1974.

Our program goal during this contract period has been to develop an optical-to-optical interface device, capable of performing real-time incoherent-to-coherent optical image conversion. This function is essential if we are to make practical systems for image information reduction via coherent optical data processing. A practical, high performance device capable of adequately performing this function had not existed previously. The photoactivated liquid crystal light valve developed by Hughes with NASA support (Contract NAS 5-11485) represented a prototype liquid crystal light valve device capable of performing these functions. The present program was implemented to improve that device.

At the outset of this program, the Hughes Photoactivated Light Valve was dc driven and possessed a photoconductor/liquid crystal interface at which electrochemical reactions could occur. These reactions represented the source of a major device lifetime problem. Therefore, we set a specific and overriding goal for this program directed toward improved lifetime of the photoactivated liquid crystal (LC) light valve. Beyond this, we also set goals for improved device uniformity and faster response speeds (both excitation and decay).

B. Program Summary

The program to accomplish these goals was unusually successful. During its course, we succeeded in developing a new device that

realized both high performance and extended lifetime. The particular accomplishments that made this development possible include

- The ac light valve substrate was developed on a parallel IR&D program and was adapted for use as a solution to the lifetime problem for the optical-to-optical device. The ac substrate represents a revolutionary change in the photosensitive substructure of the light valve.

- A chemomechanical polish was developed for the CdS film surface. This polish, combined with improvements in the quality of the glass substrates and of their preparation, represented a solution to the substrate uniformity problem.

- Reactively sputtered CdS films showed dramatically improved response times and sensitivities when compared with thermally evaporated CdS films. The improved response time gave improved device speed of response. However, the improved film sensitivity simply compensated a loss in sensitivity inherent in the change from a dc to an ac device. As a result, no net improvement in sensitivity was realized.

- The liquid crystal mode of operation was changed from a dynamic scattering mode (DSM) to a field effect mode (FEM). This very important change permitted the reduction of the liquid crystal thickness from 6 μm to 2 μm which in turn led to a dramatic improvement in device speed of response. This reduced thickness, combined with a steep threshold in the FEM, also aided in improving the ac device photosensitivity.

- Associated with the liquid crystal FEM were more stringent requirements on liquid crystal alignment. Successful alignment techniques were developed without which high speed field-effect operation could not have been implemented.

This program began with an optical-to-optical dc liquid crystal device and ended with an optical-to-optical hybrid field-effect ac liquid crystal device. This transition represents a major advance in technology. The properties of these two devices are reviewed in the following paragraphs.

1. State of the Art of the Optical-to-Optical Device at the Beginning of This Program

At the beginning of this program the dc activated light valve, though much improved over the original models, still sustained deficiencies in three areas.

a. Lifetime — The average lifetime that could be expected from the optical-to-optical device was 100 hours because of the unavoidable electrochemical degradation between the CdS and the liquid crystal and dopants. This degradation would have destroyed the devices in 8 hours had it continued, even though the discovery of a rejuvenation technique permitted lifetime to extend to 100 hours. Failure of the device was also possible from high current density because of the dc coupled nature of the device, unless extreme care was exercised by the user.

b. Response Time — Response times of the optical-to-optical device remained in the range of several hundred milliseconds. Typically, excitation plus decay required 500 msec. These relatively slow response times were caused by several factors. The use of liquid crystals and dopants that reduced electrochemical degradation was not compatible with optimizing speed of response. Furthermore, CdS film speeds were not precisely controllable and the role of alignment and cell configuration were not thoroughly understood.

c. Cleanliness of the Transform Plane — Residual scattering of light in the transform plane remained a problem largely because of the inherent turbulent character of the dynamic scattering electro-optic effect and also because of nonuniform alignment of the liquid crystal on the CdS surface. The mechanical roughness of thermally evaporated CdS was sufficiently high that the usual alignment techniques (rubbing and use of surfactants) were not adequate to achieve uniform single crystal alignment.

Table 1 shows the level of performance that we had achieved in an optical-to-optical dc device at the conclusion of the previous program. This performance represented the point of departure for the present program.

Table 1. Optical-to-Optical DC Device
Level of Performance of Delivered Item

Resolution	>40 lines/mm
Sensitivity	20 $\mu W/cm^2$
Contrast Ratio	100:1
Excitation Time	100 msec
Decay Time	100 msec
Coherent Light Throughput	95%
Operating Voltage	30 V dc 33 V rms at 20 kHz
Lifetime	<100 hours

T621-R1

1 State of the Art of the Optical-to-Optical Device at the End of This Program

The problem that we faced in order to realize an ac light valve, was the proclivity for the standard dc device to break down and scatter when the CdS electrode swings negative irrespective of the presence or absence of photoactivated light. We solved this problem by developing a new device that replaces the standard CdS/liquid crystal interface blocking contact with a new blocking contact created by adding an insulating layer and a new semiconductor layer between the CdS and the liquid crystal. This new electrical structure permits pure ac activation of the device. But far more important, it leads to two additional features that radically improve the operation of the device and that have the potential to solve the lifetime problem completely. These features are

- The interposed insulating layer can be a dielectric mirror, thereby making the light valve a reflection device.

- A second insulating layer can be deposited to insulate the counter electrode as well as the photoconductor from the liquid crystal, thereby completely isolating the liquid crystal from the electrodes.

As a result of these features, we have a reflection mode device in which the read-light and the write-light are completely independent. But most important, from the standpoint of lifetime, we have the liquid crystal in a glass bottle. Hence, we should be able to realize device lifetimes that approximate the shelf-life of the liquid crystal. This means tens of thousands of hours of operating lifetime should be realizable for the ac light valve.

The ac operated liquid crystal light valve is schematically depicted in Fig. I-1. It comprises four active layers sandwiched between two pieces of glass coated with transparent conductive electrodes. The four layers are the photoconductive layer, a light absorbing layer, the dielectric mirror, and the liquid crystal film. In addition, the counterelectrode is overcoated with SiO_2.

The ac light valve is driven differently from the dc optical-to-optical device. It is driven by an ac power supply at a frequency between 1 and 10 kHz. In operation, the ac voltage capacitively couples current through the insulating layers to excite the liquid crystal. Because of the nature of the blocking layer formed between the CdS and the CdTe, the photoconductor in its dark state has sufficient ac impedance to accept the bulk of the voltage that appears across the cell. When light falls on the photoconductor locally, its ac impedance drops and the ac voltage is switched to the liquid crystal. This describes the operation of the light valve. It should be noted at this point that, although an ac device solves the lifetime problems, it has one disadvantage. The light-induced voltage switching ratio which an ac device can supply to the liquid crystal is limited by film capacitance ratios to values well below switching ratios possible in dc devices. Table 2 shows the level of performance achieved in an optical-to-optical ac device at the end of the present program.

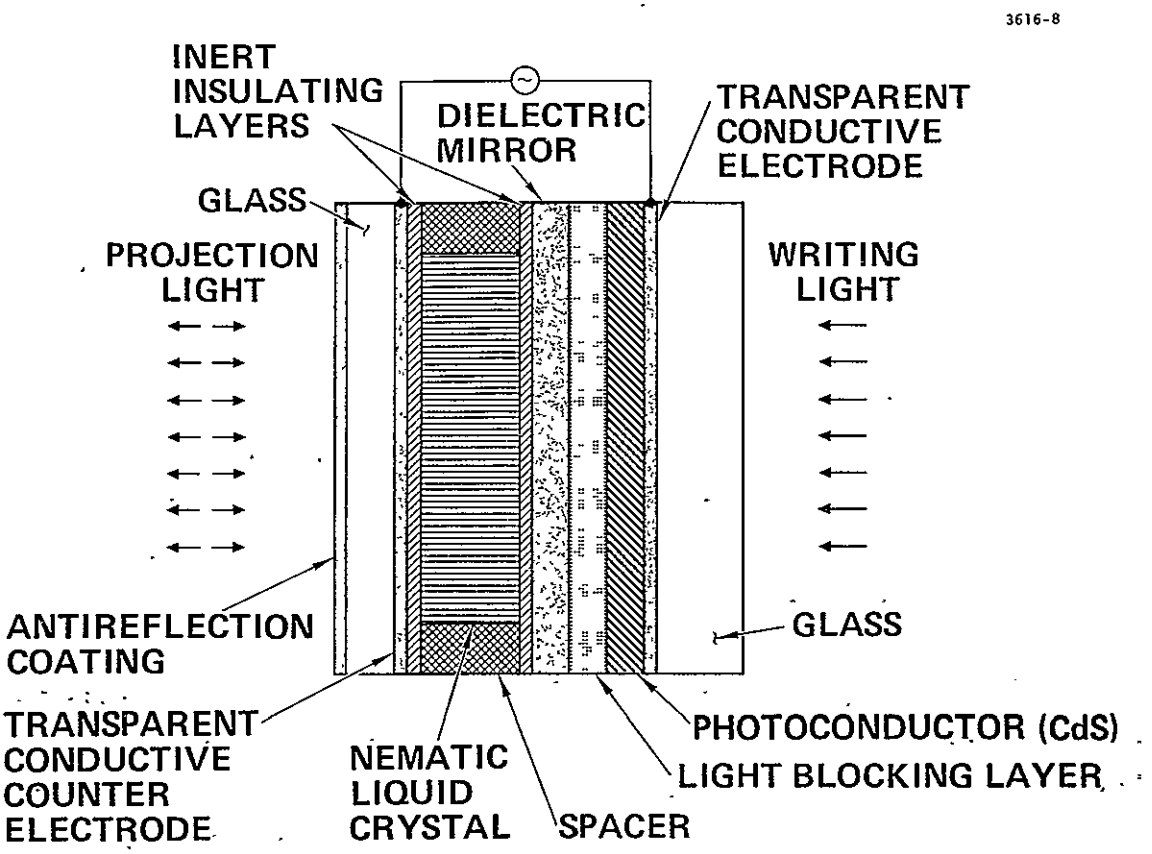

Fig. I-1. Schematic of the ac light valve device.

Table 2. Optical-to-Optical ac Field-Effect Device
Level of Performance of Delivered Item

Resolution	> 60 lines/mm
Sensitivity	60 $\mu W/cm^2$
Contrast Ratio	200:1
Excitation Time	15 msec
Decay Time	20 msec
Operating Voltage at 1 kHz	6 V_{rms}
Lifetime Potential	10,000 hours

The four areas this report focuses on are: (1) liquid crystal studies, (2) substrate thin film studies, (3) device optical quality studies, and (4) completed device evaluation studies. These areas are treated individually in Sections II through V, respectively. As an overview, it can be noted that the liquid crystal studies and the thin film studies were undertaken within the context of the ac light valve format and with the objective of improving the ac device sensitivity, response time, and resolution. The device optical quality studies were initiated because of the need for device uniformity, and because of the critical importance of uniformity for obtaining a thin liquid-crystal layer for improving the liquid crystal response time. The final section on completed device evaluation serves as the section of major concern to the user of a completed device.

II. LIQUID CRYSTAL STUDY

A. Dynamic Scattering Mode

There is a large amount of published material on the dynamic scattering mode (DSM).[1,2] Briefly, DSM may be characterized by electrical current, field-induced hydrodynamic motion. Nematic liquid crystals (LCs) are optically anisotropic (i.e., they have different refractive indices parallel to and perpendicular to the long axes of the molecules). The effect of applying a voltage to and passing a current through a typical LC cell is to disrupt the normally uniform molecular orientation in favor of a large number of small regions (domains) whose molecular orientation is different from those of their neighbor domains. This appears to the light passing through the cell as closely-spaced refractive index boundaries. These index boundaries cause the light to be refracted at various angles (i.e., scattered). Thus we have a system that, when no voltage is applied, appears optically homogeneous and transparent, and when voltage is applied, appears highly diffusing or scattering.

In our review of the liquid crystal (LC) requirements for the optical star field tracker, we decided that for our initial investigation the dynamic scattering mode LC is best fitted for this device. All dynamic scattering mode liquid crystal mixtures that were investigated during this contract were chosen for their relatively fast response time and good contrast.

The two types of liquid crystal compositions investigated in detail were the ester type mixtures and Schiff base mixtures. The ester types are mixtures of four to nine esters with general formulas of

$$R_1 - 0 - \phi - COO - \phi - R_2 \quad ,$$

where R_1 and R_2 are alkyl groups with one to eight carbon chain. While the Schiff base mixtures consist of

$$R_1 - 0 - \phi - CH = N - \phi - R_2$$

and

$$R_3 - 0 - \phi - CH = N - \phi - OOC - R_4$$

components where R_1 R_2 R_3 R_4 are one to four carbon alkyl groups. To assure the homogeneous or homeotropic alignment of liquid crystal between the electrodes, appropriate dopants were added to the mixtures. Tetrabutyl ammonium perchlorate (TBAP) in esters yielded parallel alignment while hexadecyltrimethyl ammonium stearate in esters or in Schiff bases provided perpendicular alignment.

For initial testing and evaluation of these liquid crystal compositions, low frequency ac was applied in pulses together with a continuous superimposed 10 kHz high frequency signal. Transmission mode devices for this testing were fabricated of liquid crystal sandwiched between two conductive In_2O_3 electrodes separated by a 1/4 mil mylar spacer. Voltage versus scattering curves in Fig. II-1 show threshold voltages between 7 to 12 V rms with no background scattering below the threshold voltage, which is advantageous for high contrast ratio.

Further testing of the liquid crystals was done by using a 20 msec, 100 Hz pulse together with a superimposed 10 kHz high frequency voltage, measuring delay time, rise time, decay time, and scattering. Experimental results are summarized in Table 3.

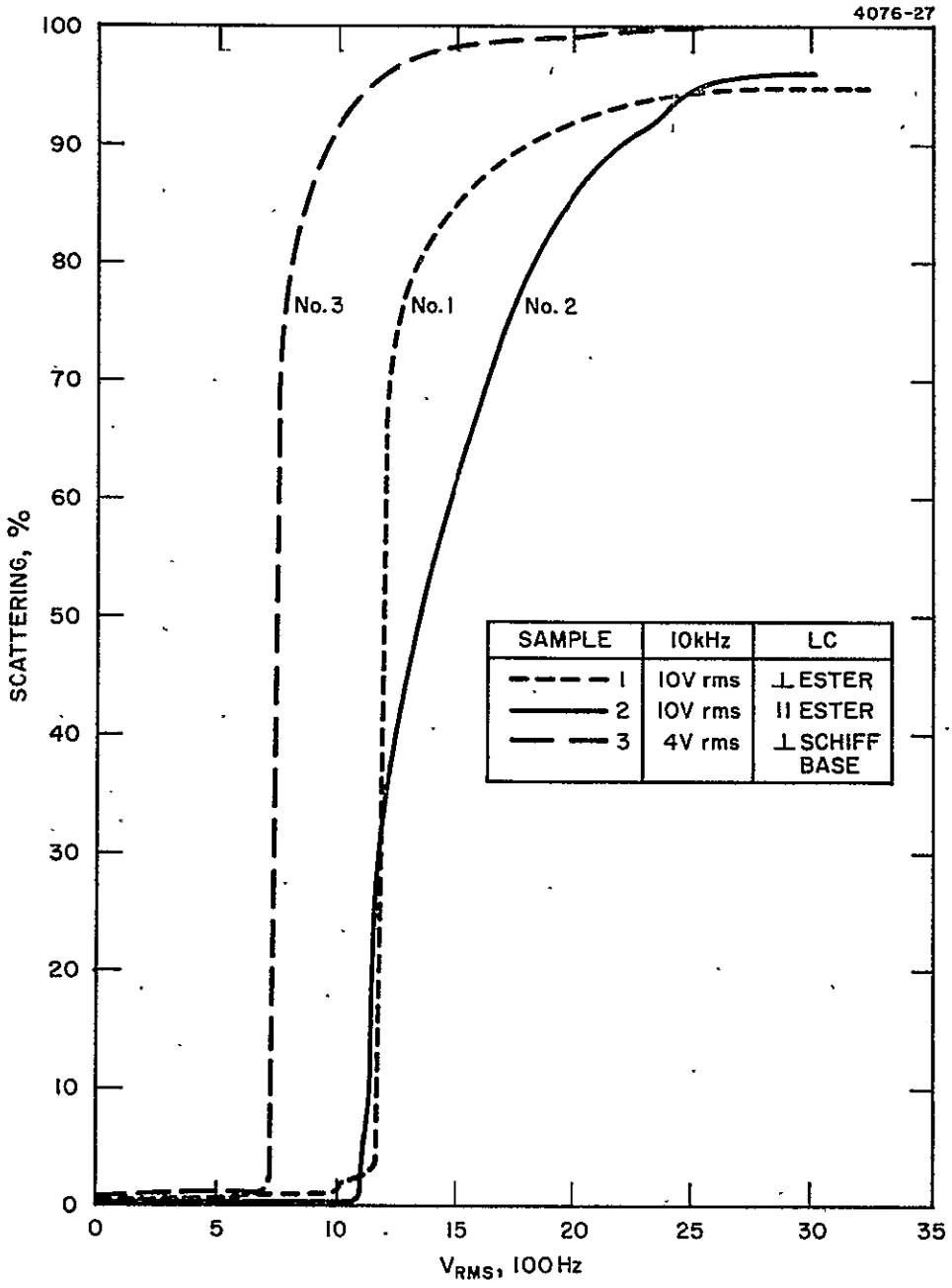

Fig. II-1. Liquid crystal light scattering curves versus applied root mean square ac voltage.

Table 3. Time Response and Scattering Data for DSM Liquid Crystals

LC	10 kHz, V rms	100 Hz, V rms	T delay, msec	T rise, msec[a]	T decay, msec[a]	Scattering, %
1	15	20	15	3	10	5
	15	30	5	6	350	75
	15	40	2	8	600	88
2	15	23	14	5	5	15
	15	30	8	12	20	60
	15	40	2	11	60	85
3	4	14	10	8	30	13
	4	20	5	8	370	95
	4	25	5	8	500	99

[a] Rise time and decay time measured between 10% and 90% of scattering.

T1649

In conclusion, the best LC mixture is No. 3 with low operating voltages and very high scattering. However, a major disadvantage of this composition, which is Shiff's base-type LC, is its chemical and photochemical instability. The chemical decomposition caused by moisture could be controlled by preparing and sealing the cells in an inert dry atmosphere. The parallel aligned LC No. 2 has much faster decay time than any of the other mixtures.

Our initial work with the dynamic scattering mode liquid crystals have been successful, since we have developed materials that switch on to full scattering in 10 to 13 msec. However, to produce maximum scattering in a device an off-to-on switching ratio of three was necessary. This high switching ratio was found to be incompatible

with the thin film ac light valve substrate requirements. Hence, we decided to investigate other liquid crystal electro-optic effects with lower switching ratio requirements.

B. Voltage Tunable Birefringence

1. Field Effect for Optical Data Processing Light Valve

On the basis of the results described previously we decided that the DSM mode is not suitable for the optical data processing (ODP) application. It suffers from several drawbacks. It exhibits extensive noise in the Fourier plane because of the turbulent character of the DSM effect. The response time with switching ratios of 2:1 or smaller is slow. For these switching ratios the contrast is limited to about 10:1. The field-effect mode is a natural candidate to overcome these problems. In this mode, all molecules are tilted together. This is equivalent to a rotation of a solid-state crystal and one does not expect to generate any Fourier plane noise by this action. Furthermore, in this mode, very thin layers can produce very high contrast, which is impossible in the DSM, and in general, the time response in liquid crystals is proportional to the square of the thickness.

2. Birefringence Effect in Liquid Crystals

We investigated the birefringent FEM first. The liquid crystal molecules are highly asymmetric. When aligned, the created crystal exhibits macroscopic optical anisotropy. The refractive index along the molecules (n_e) is higher than the indices perpendicular to the long molecular axis (n_o). The last two are equal, so the crystal is uniaxial with the optical axis along the molecules.

To understand how the birefringent effect works in a liquid crystal light valve, a gedanken experiment is described. Assume that a liquid crystal layer is located in the XY plane with the optical axis parallel to X, and assume that a linearly polarized light beam propagates along the Z axis with the polarization in the XY plane, 45^o to the X axis. In the liquid crystal medium, the beam is divided into

an extraordinary beam with the polarization parallel to the liquid crystal optical axis (X) and an ordinary beam with the polarization parallel to the Y axis. The X axis beam propagates with phase velocity C_o/n_e and the Y axis beam with C_o/n_o. As the two beams propagate through the medium, a different phase is created that is proportional to the thickness, to the index difference $n_e - n_o = \Delta n$ (which is called the birefringence coefficient), and to the inverse of the light wavelength. This phase difference changes the character of the polarization from linear to elliptical, then circular, elliptical, and again linear, 90^o shifted with respect to the input. This cycle can be repeated many times.

Generally, the transmission of a birefringent layer between cross polarizers is expressed as

$$T = \sin^2 2\phi \sin^2 \frac{\pi d \Delta n \sin^2 \theta}{\lambda} .$$

where θ is the angle between the liquid crystal optical axis and the incident light, ϕ is the angle between the input polarization and the direction of the liquid crystal optical axes tilt, and d is the cell thickness. See Fig. II-2.

The optical effect, which the liquid crystal has on the projection light beam, has been treated as a function of the orientation of the liquid crystal molecules. Now, we turn to the effect of an applied voltage on the liquid crystal orientation.

If the liquid crystal has a positive dielectric anisotropy (the dielectric dipole moment is parallel to the optical axis) a voltage above a certain value will tilt the liquid crystal molecules. This corresponds to a change in the angle θ (in the above case, from 90^o to lower values) which means a change in the optical retardation and thus a change in the transmission. In general, the optical transmission is a multiple peaked function of the applied voltage (Fig. II-3).

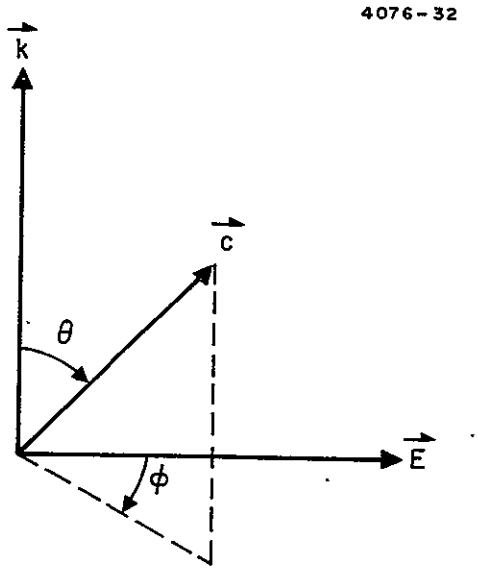

$\vec{k}$ = light propagation wave vector

$\vec{E}$ = light polarization vector

$\vec{C}$ = liquid crystal optical axis

Fig. II-2.
Diagram defining the polar and azimuthal angles relating the liquid crystal optical axis to the light polarization and propagation directions.

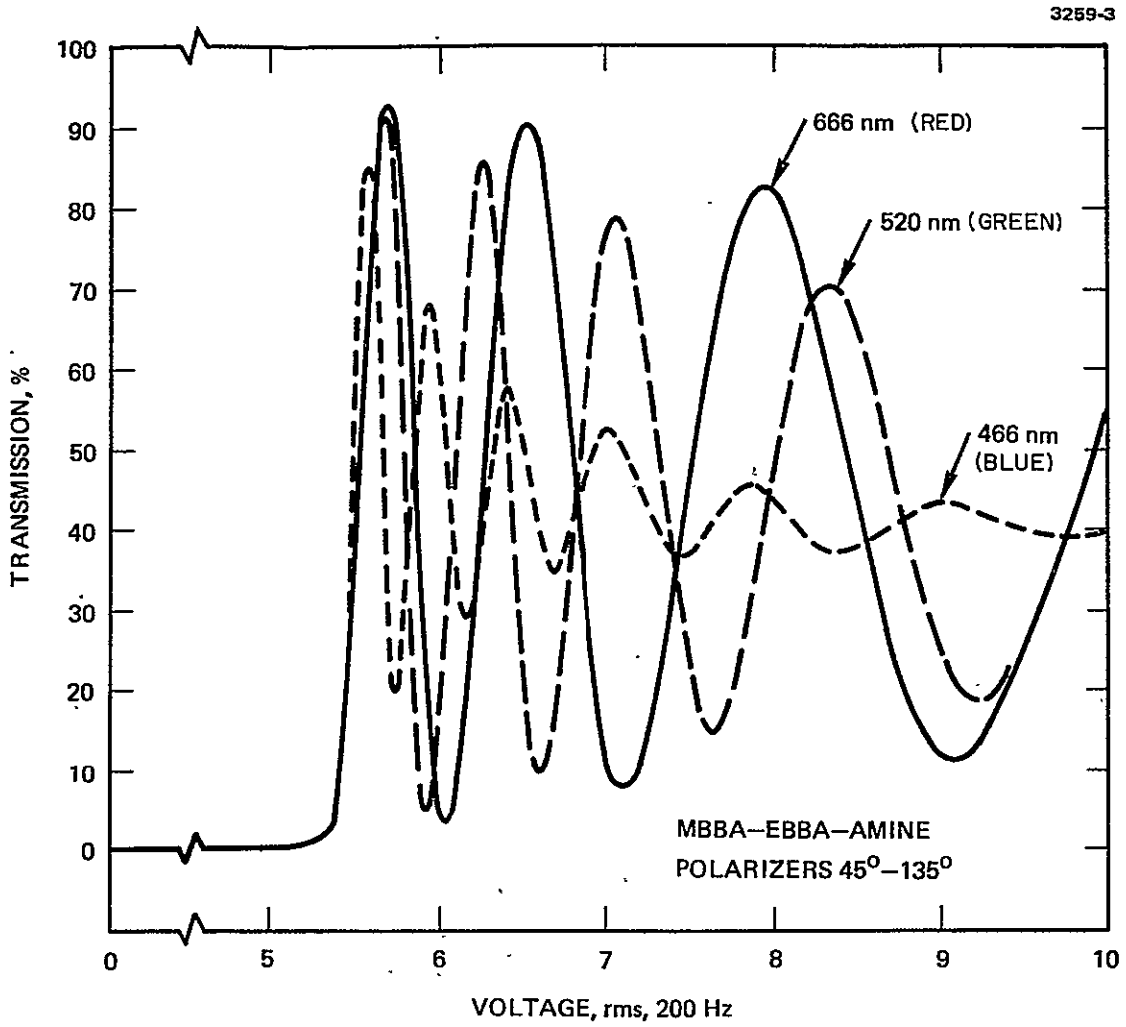

Fig. II-3. Birefringent liquid crystal response characteristic.

From the above discussion, it is clear that a voltage applied to the liquid crystal in the indicated alignment configuration can modulate optical transmission. This is important for our device. To examine this effect in more detail, first note that for an ODP application, multiple transmission peaks are undesirable. We would like to have a monotonically increasing transmission function above the threshold, and this transmission function should reach saturation at a value close to 100%. Recalling that the optical phase retardation is proportional to the cell thickness, it becomes clear that an optimal cell thickness exists for a monotonically increasing transmission function which peaks at near 100% at the peak light activated voltage for a light valve. The optimal thickness must be determined experimentally. We will treat this question in the next section.

Fortunately, decreasing cell thickness not only decreases the number of transmission peaks, but it also decreases the liquid crystal response time. The time response is proportional to the square of the thickness

$$T_r = \frac{\gamma_1 d^2}{|\epsilon_a| \epsilon_o \left[V^2 - V_{th}^2\right]}$$

$$T_f = \frac{\gamma_1 d^2}{|\epsilon_a| \epsilon_o V^2}$$

where T_r and T_f are the rise and fall times, γ_1 is the viscosity coefficient, ϵ_a is the dielectric anisotropy, and V and V_{th} are the applied and the threshold voltages.

3. Experimental Results Relating to Birefringence

The measured transmission versus voltage curves for an ester, negative-anisotropy liquid crystal are in agreement with the above equations. Our measurements show two transmission minimum-maximum cycles for cells that are 1/2 mil thick, and only one cycle for cells 1/4 mil thick. For application in the optical correlator we would like to reduce the number of cycles to one-half, so that the transmission will vary from a minimum of 1 to 2% to a maximum of 90 to 100%. In this way we can control the stability of the signal on the device with better effect. The 2 to 3 μm thickness spacer needed for one-half cycle transmission response from our present liquid crystal is not commercially available. Therefore, to determine if we could obtain very fast response, we fabricated a very thin cell by simply not using a spacer. The cell proved to be too thin so that the maximum transmission was only 50%, however, it had a very fast response time of 5 msec as shown in Table 4. Experimental data collected at 200 Hz frequency using crossed polarizers at 45° and 135° provided the data for this table.

Table 4. Time Response Versus Thickness Data for Birefringent Liquid Crystal

d	T_{min}	T_{max}	V_{ratio}	T_{rise}, msec	T_{decay}, msec
1/2 mil	10% at 4.4 V	80% at 5.6 V	1.3	1400	1200
1/4 mil	4% at 5.0 V	94% at 7.5 V	1.5	380	550
no spacer	4% at 4.5 V	50% at 11.2 V	2.5	5	30

T1656

4. Limitations of the Birefringence Effect for the ODP Application

Two off-state liquid crystal alignments should be considered for the birefringent cell — the parallel and the perpendicular. In the parallel case, the long molecular axis is parallel with the electrodes and in the perpendicular case, it is perpendicular. To be able to activate the liquid crystal (to tilt the molecules by means of electrical field) in the parallel case, the dielectric anisotropy must be positive, and in the perpendicular case it must be negative (the electric dipole moment must be parallel with the optical axis in the parallel case and perpendicular in the perpendicular case. For an incident beam along the Z axis, the perpendicular alignment exhibits no birefringence because the perpendicular refractive indices are equal. So independent of the thickness, the input polarization is not affected by the liquid crystal (and the transmission with cross polarizers is close to zero). In the parallel alignment case, the birefringence is at maximum so the retardation is $d\Delta n$ and the transmission depends on the thickness.

In the perpendiulcar case, high contrast can be achieved but the response time is slow because high negative dielectric anisotropy materials are not available (the useful materials have $|\epsilon_a| < 1$). However, there are good liquid crystals with high positive dielectric anisotropy ($\epsilon_a > 10$). Thus fast response times in the range of a few milliseconds with a switching ratio of 1.5:1 are possible for the parallel alignment case. Unfortunately, the thickness dependence of the off-state transmission seriously limits the contrast and the uniformity in cases where this state is made into the low transmission state. It would be a mistake to try to produce the "black screen" state by the on state because of the nonuniformity of the latter. Generally, in well-designed light valves, the off-state should correspond to a "black screen," and this condition should be independent of the liquid crystal thickness. From our experience, this is the only way to achieve high contrast and uniformity. To produce a contrast of 100:1 for instance, the light valve must block at least 99% of the light in the black-screen state. If the nonuniformity of the blocking effect is

only 1% (98% blocked) the contrast drops to 50:1. So the black screen state must be extremely uniform. The on state is the activated state and naturally, it tends to be more nonuniform than the passive state, which is the off state. It is almost impossible to achieve an on state which has the required light blocking efficiency and uniformity. On the other hand, if the on state is made into the high transmission state, much higher nonuniformity can be tolerated. For instance, if the transmission changes from 99 to 98% e.g., for a cell with a nonuniformity 1% and an off state of 1% transmission, the change in contrast is only 1%. Therefore, we conclude that the perpendicular alignment case suffers from slow response times and the parallel alignment case suffers from limited contrast and high nonuniformity. At this stage, we began to look for an effect that will utilize the fast, high dielectric anisotropy liquid crystals and will produce a dark off state, independent of the thickness nonuniformity. In other words, we looked for an effect that would combine the good features of both alignments and would exclude the drawbacks.

C. Twisted Aligned Nematics in the Reflection Mode

1. The Off State

As described in Section II-B, the nematics used for parallel alignment exhibit much faster response times than those used in perpendicular alignment. On the other hand, when using parallel alignment, it is very difficult to achieve high contrast and good uniformity. We now introduce the twisted-nematic alignment. This provides a dark off state screen, independent of the thickness, and permits the use of high dielectric anisotropy materials; thus one expects to achieve fast response. Unfortunately, the twisted-nematic effect is canceled in reflection, so it is impossible to implement this alignment in a normal fashion and we had to invent a new twisted-nematic/birefringent mode. We continued to use the reflection mode because this enables us to use the high efficient fiber optics coupling between the light valve and the image intensifier (or CRT). This also simplifies the system and improves the overall sensitivity.

Before we describe the mode actually used in the device, we first describe the operation of the normal twisted-nematic alignment in transmission. In the off state the optical axes of the molecules are parallel with the electrodes but the directions of the molecules on the two electrodes form an angle, normally 90°. The direction of the optical axis varies linearly with the Z coordinate from one electrode to another and creates a helix. This is depicted in Fig. II-4. This alignment exhibits the following optical activity features. When linearly polarized light enters the liquid crystal layer with the polarization along the liquid crystal optical axis (or perpendicular to it) the polarization is rotated as the light propagates through the layer. The rotation follows the rotation of the liquid crystal optical axis. So the output polarization is rotated with respect to the input, by the liquid crystal twist angle. In a later calculation we will show that if the cell is thick enough the angle of rotation is independent of the wavelength (through the visible spectrum), independent of the cell thickness, and the ellipticity is very low. On the basis of these characteristics, a simple transmission mode display device can be made. If we place, for instance, a 90° twisted nematic cell between parallel polarizers and pass light through it, we observe a dark off state on a viewing screen (the polarization is rotated 90° by the liquid crystal and it is blocked by the analyzer). If the liquid crystal has positive dielectric anisotropy and a sufficient electric field is applied, the alignment switches from parallel to homeotropic (perpendicular). Since the homeotropic alignment has neither rotatory power nor birefringence, the light will propagate unchanged through the liquid crystal and the system will have a high transmission coefficient in this state. The contrast ratio (which is the transmission ratio of the on to off states) will be limited by the transmission in the off state. The time response is proportional to the square of the thickness, so obviously we are interested in minimizing the thickness, but the twisted-nematic effect (the rotation of polarization) as we described before works well only above some thickness value. So it is important to find the limiting thickness value,

the price that one pays for approaching this limit, and how the parameters can be manipulated to obtain best performance. In the literature we found two methods to calculate the twisted-nematic liquid crystal behavior. One method, presented by Berreman,[3] consists of a computer numerical calculation. We found this method awkward because of the lack of an analytical expression. This made it difficult to judge the relationships and the influences of the different parameters. The other method[4] is based on the Poincaré sphere. It is more qualitative, but not accurate enough.

The model that we postulated for this calculation consists of a large number of very thin parallel-aligned nematic liquid crystal layers, stacked one on the other, and rotated by a small angle ϵ around the Z axis, one with respect to the other (Fig. II-5). Assigning N for the number of layers and α for the twist angle, we have $\epsilon = \alpha/N$. The thickness of the infinitesimal layer will be $\Delta Z = d/N$. Now, we look at some layer n so that $1 < n < N$ and we assume that the input polarization to that layer is represented by $P_{x(n-1)}$ and $P_{y(n-1)}$. Note that x(n-1) and y(n-1) are the directions of the optical and ordinary axes, respectively, of the (n-1) layer. Both $P_{x(n-1)}$ and $P_{y(n-1)}$ are complex numbers because they include the phase relationship. Referring to Fig. II-5, we can express P_{xn} and P_{yn} in the following way:

$$\left.\begin{aligned} P_{xn} &= P_{x(n-1)} \cos\epsilon - P_{y(n-1)} \sin\epsilon \\ P_{yn} &= P_{y(n-1)} \cos\epsilon + P_{x(n-1)} \sin\epsilon \end{aligned}\right\} \qquad (1)$$

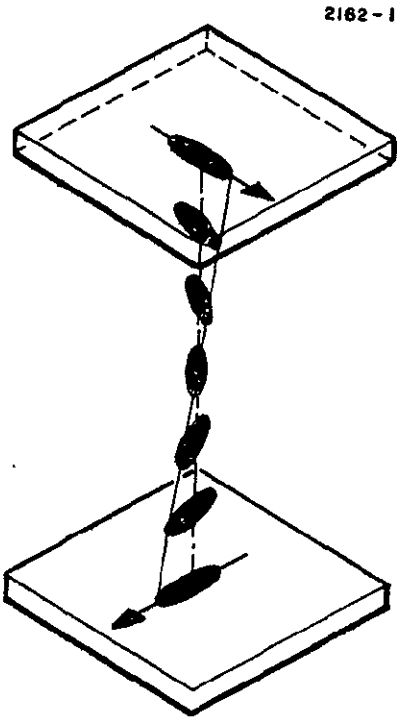

Fig. II-4.
Twisted-nematic configuration.

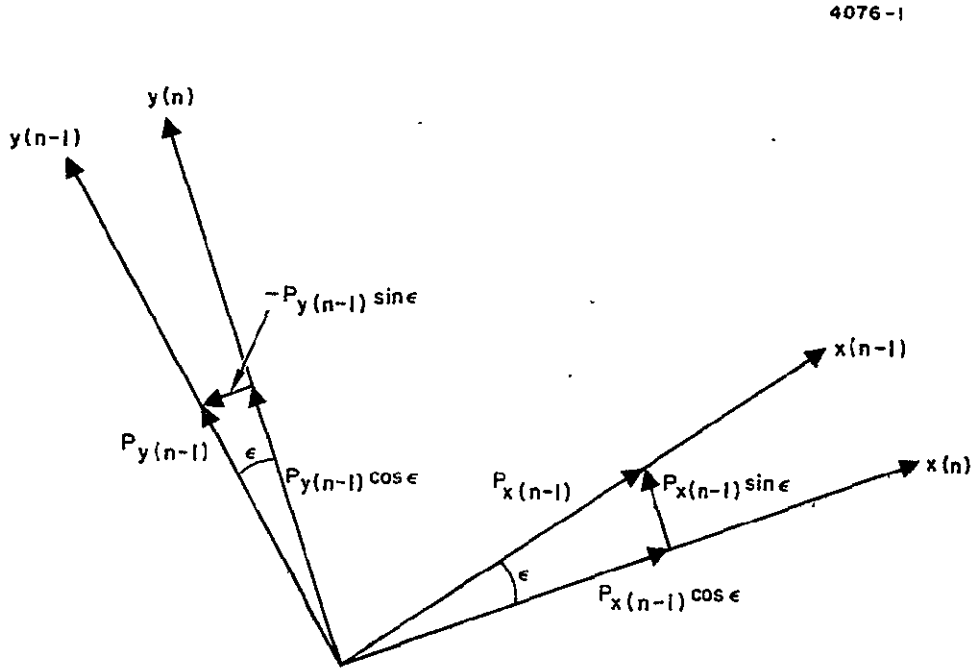

Fig. II-5. Change in polarization splitting between the (n - 1) and n axes.

For each layer, we take as a phase reference the ray that propagates through the extraordinary axis only. The polarization at the output of the infinitesimal n layer will be described by

$$P_{xn} = P_{x(n-1)} \cos \epsilon - P_{y(n-1)} \sin \epsilon$$

$$P_{yn} = \left(P_{y(n-1)} \cos \epsilon + P_{x(n-1)} \sin \epsilon \right) e^{i2\pi\Delta n_o \Delta z} \tag{2}$$

We will show here the calculation for a simple case where the polarization of the input light is parallel to the liquid crystal optical axis at the first electrode and the analyzer is perpendicular to the liquid crystal optical axis at the second electrode. (Calculations for the more general case of the relative directions of the polarizer, the cell axes, and the analyzer are in progress, as are the calculations for the on state.)

For this simple case we are interested only in the ratio

$$R_n = \frac{P_{yn}}{P_{xn}} \tag{3}$$

The transmission will be given by

$$T = R_N R_N^* \tag{4}$$

When we substitute eq. (2) into eq. (3) and define

$$\left.\begin{aligned} \tan(\epsilon) &\equiv a \\ e^{\frac{i2\pi\Delta n_o \Delta z}{\lambda}} &\equiv e^{i\phi} \equiv b \end{aligned}\right\} , \tag{5}$$

we obtain

$$R_n = \frac{\left(P_{y(n-1)} + a\,P_{x(n-1)}\right)b}{P_{x(n-1)} - aP_{y(n-1)}} \tag{6}$$

Or by dividing eq. (6) by $P_{x(n-1)}$ we obtain

$$R_n = \frac{\left(R_{n-1} + a\right)b}{1 - a\,R_{n-1}} \tag{7}$$

To express the R_n as a function of a, b, n and the input light polarization we will try to find the general term by induction, starting with R_0, R_1, R_2 and so on.

For the simple case mentioned above, the initial conditions are

$$P_{yo} = 0, \quad P_{xo} = \tag{8}$$

$$R_0 = 0$$

$$R_1 = ab$$

then

$$R_2 = \frac{ab^2 + ab}{1 - a^2b}$$

$$R_3 = \frac{ab^3 + ab^2 + ab - a^3b^2}{1 - 2\,a^2b - a^2b^2}$$

$$R_4 = \frac{a\sum_{k=1}^{4} b^k - 2a^3b^2 - 2a^3b^3}{1 - 3a^2b - 2a^2b^2 - a^2b^3 + a^4b^2}$$

$$R_5 = \frac{a \sum_{k=1}^{5} b^k - 3a^3b^4 - 4a^3b^3 - 3a^3b^2 + a^5b^3}{1 - a^2 \sum_{k=1}^{4} (5-k)\, b^k + 3a^4b^2 + 2a^4b^3}$$

Recall that $a = \tan \epsilon$ is a small number. Thus, if we neglect the terms that include powers of a larger than 2, we have a simple expression for R_n

$$R_n = \frac{a \sum_{k=1}^{n} b^n}{1 - a^2 \sum_{k=1}^{n-1} (n-k)\, b^k} \tag{9}$$

Below we give some physical interpretation to the terms in this equation.

For the zero approximation the only term in eq. (9) is the one in the denominator. The rest are zero

$$R_n^{(0)} = 0 \tag{10}$$

The term in the numerator expresses the first approximation. Thus

$$R_n^{(1)} = a \sum_{k=1}^{n} b^k \tag{11}$$

and the second approximation is expressed by eq. (9) carried out to include a^2 terms. A second term appears in the denominator. Using the same method one can obtain higher orders of approximation. For

instance in the case of the third approximation another term appears in the numerator, which is

$$-a^3 \sum_{\ell=1}^{n-2} b^{n-\ell-1} \sum_{k=1}^{\ell} (\ell-k+1)\, b^k \qquad (12)$$

and in the case of the fourth approximation, a positive term which includes a triple sum and a^4 is added in the denominator and so on. Next we discuss the physical meaning of the different approximations. For this calculation we assumed that the input polarization is linear and directed along the optical axis at the first electrode. Generally, as this polarization propagates through the rotated liquid crystal layers it is divided into components along the main axes of the layers. In this case a perpendicular component builds up (Fig. II-6). The zero approximation neglects this component so the polarization remains linear as it is rotated and $R_n^{(0)} = 0$. The first approximation summarizes the contributions to the perpendicular polarization created at each step, but assumes that the main component (that parallel to the optical axis) is unchanged. In other words, the first approximation neglects the contributions back from the perpendicular to the parallel polarization. The contribution that was generated at the first layer, propagates along the ordinary axis through all the thickness, so its phase with respect to the parallel polarization is b^n. The contribution that was generated at the second layer, propagated through the first layer as parallel and only n-1 layers as ordinary, so its phase will be b^{n-1}. Generally, the phase of the one that was created in layer ℓ will be $b^{n-\ell}$. In Fig. II-7 it is shown that the locus of the b^k vectors in the complex plane is a circle that crosses the center of the coordinates. The phase relationship of the b^k vectors allows the possibility of making the $P_{yN} = 0$ by adjusting the overall retardation to $2K\pi$. The term in the denominator which gives the second approximation expresses the back contributions of the built-up perpendicular polarization. In this case, the number of the

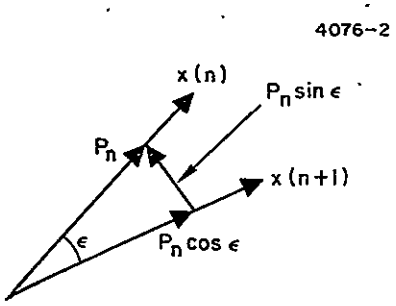

Fig. II-6.
Buildup of perpendicular polarization by the rotation of liquid crystal optical axis.

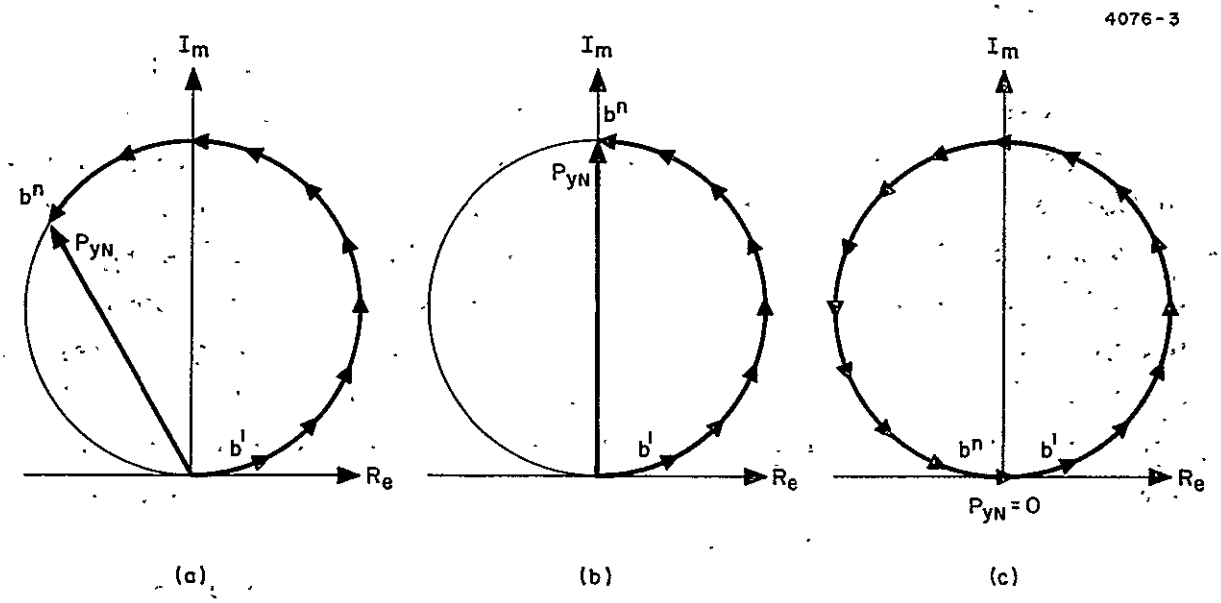

Fig. II-7. Locus of b^k vectors. (a) General case of the overall retardation. (b) The special case when retardation is π (or $2(k - 1)\pi$) with the result that the P_{yN} is maximum. (c) When the retardation is 2π (or $2k\pi$) the $P_{yN} = 0$.

b^k vectors depends on k, and this number is larger as k is smaller. Each time a contribution to the perpendicular polarization is generated, it immediately generates back a contribution to the parallel polarizations which are shifted in phase only by b. The number of contributions to the perpendicular polarization is (n-1) so the number of $-a^2b$ vectors is (n-1) too. Similarly, one can explain the (n-2) $-a^2b^2$ vectors and so on. The third approximation is the contributions of these vectors to the perpendicular polarization.

The effect that rotates the polarization in the twisted nematic cell is simple to explain. The fact that the layers are rotated and the polarization each time is split into axes that are rotated by a small angle with respect to each other, is enough to cause the rotation. If we would have such a medium, even without birefringence, and that layer split the polarization in this way, we would obtain the polarization rotation effect. To illustrate this, imagine a stack of an infinite number of linear, absorption-type, ideal polarizers. The polarizers are rotated by an angle ϵ one with respect to the other. The angle difference between the first and the last one is α. The polarization vector emerging from the first one has a magnitude of one and is divided into two components by the second one, cos ϵ, parallel with the direction of polarization and sin ϵ, perpendicular. The two components are totally transmitted and totally absorbed by the second polarizer because we assumed ideal polarizers. Then the magnitude of the polarization vector emerging from the third one will be $\cos^2\epsilon$ and so on. The magnitude emerging from the last one will be $\cos^n\epsilon$ (assuming n+1 polarizers).

$$A = \lim_{n\to\infty} \cos^n \epsilon \tag{13}$$

or using the approximate expression for $\cos \epsilon \simeq 1 - (\epsilon^2/2)$

$$A = \lim_{n\to\infty} \left(1 - \frac{\alpha^2}{2n^2}\right)^n \tag{14}$$

Next, find the limit of ln A.

$$\ln A = \lim_{n \to \infty} \frac{\ln\left(1 - \frac{\alpha^2}{2n^2}\right)}{1/n} \tag{15}$$

and using the L'Hopital law we find ln A = 0 or A = 1. Therefore, we expect full rotation of the input polarization independent of the light wavelength. For the same reason the cos ϵ (see Fig. II-5) does not have an influence on eq. (9). The possibility of splitting the polarization by continuously, slightly rotated coordinates is the main twisted-nematic effect. The minor effects are the correction terms that are caused by the build up effects of the perpendicular polarization.

Now, evaluate the sums in eq. (9).

$$\sum_{k=1}^{n} b^k = b \frac{b^n - 1}{b - 1} \tag{16}$$

and

$$\sum_{k=1}^{n-1} (n-k)\, b^k = \sum_{m=1}^{n-1} \sum_{k=1}^{m} b^k = \sum_{m=1}^{n-1} b \frac{b^m - 1}{b-1}$$

$$= \frac{b}{(b-1)^2}\left[b^n - 1 - n\,(b-1)\right] \tag{17}$$

Substituting (16) and (17) into (9) one obtains

$$R_n = \frac{\frac{ab}{b-1}\,(b^n - 1)}{1 - \frac{a^2 b}{(b-1)^2}\left[b^n - 1 - n(b-1)\right]} \tag{18}$$

To demonstrate the polarization ratio at the output of the liquid crystal layer, substitute n = N, and then

$$b \simeq 1 \quad , \quad b - 1 \simeq i\phi \quad , \quad (b-1)^2 = -\phi^2$$

$$a \simeq \frac{\alpha}{N} \quad , \quad N\phi = \frac{2\pi\Delta n_o d}{\lambda} \equiv \beta \quad , \tag{19}$$

and we obtain a simple expression for R_N

$$R_N = \frac{\left(\frac{\alpha}{i\beta}\right)(\cos\beta - 1 + i\sin\beta)}{1 + \left(\frac{\alpha}{\beta}\right)^2\left[\cos\beta - 1 + i(\sin\beta - \beta)\right]} \tag{20}$$

The transmission through the analyzer according to eq. (4) will be

$$T = \frac{2\left(\frac{\alpha}{\beta}\right)^2(1 - \cos\beta)}{1 - 2\left(\frac{\alpha}{\beta}\right)^2(1 - \cos\beta) + \left(\frac{\alpha}{\beta}\right)^4\left[(2 - 2\cos\beta - 2\beta\sin\beta + \beta^2)\right]} \tag{21}$$

The dependence of T on the thickness, on the light wavelength and on the liquid crystal birefringence is through β. For thick cells, β is large and the transmission is low, independent of the three parameters mentioned above because the term $(1-\cos\beta)$ has an upper limit $0 \leq (1 - \cos\beta) \leq 2$. As we already pointed out, to get fast response we have to make the cell as thin as possible and then the factor α/β becomes large. In this case, for a given wavelength, the term

$(1-\cos\beta)$ allows us to obtain a low off-state transmission light value. We must tune the thickness to such a value that

$$\beta_o = \frac{2\pi\Delta n_o d_o}{\lambda} = 2K\pi \quad , \tag{22}$$

where K is an integer. In terms of the diagram in Fig. II-7 this corresponds to a case, where the phase difference between all the contributions to the perpendicular polarization is such that they cancel themselves out. However, this compensation causes a dependence of T on d, λ, and Δn. We disqualified the birefringence effect in the parallel (homogeneous) alignment because the off state transmission was dependent on the same parameters. The following calculation explains why we use the twisted nematic alignment even though it has the same qualitative bad features (in a thin cell) as the homogeneous alignment. As we recall, Section II-B, the transmission of a birefringent cell is given by $T = \sin^2 2 \quad \sin^2\beta$. Assuming that $\sin^2 2 = 1$ and the cell is tuned to β_o (eq. (22)), the transmission is a function of the tuning inaccuracy

$$T \simeq \frac{\Delta\beta^2}{2} \tag{23}$$

Making the same calculation for the twisted nematic, using for simplicity only the first approximation, we find

$$T \simeq 2\left(\frac{\alpha}{\beta}\right)^2 (1-\cos\beta) \simeq 2\left(\frac{\alpha}{\beta}\right)^2 \frac{\Delta\beta^2}{2} \tag{24}$$

The sensitivity of the twisted nematic cell compared with the birefringent cell, to inaccuracy in β is lower by a factor of $(2(\alpha/\beta)^2)^{-1} = 25$. This is calculated for a 2.5 μm thick cell with $\Delta n_o = 0.23$, $\lambda = 0.63$ μm, and a twist angle of 45^o operating in reflection mode. This is a very significant factor! One can use eq. (21), with good approximation for the reflection mode, if one doubles the twist angle α and the thickness

d when substituting the values in eq. (21). In addition, one must remember that the rotation is canceled on reflection. The tuned thicknesses for Δn_o and λ as a function of the K value (eq. (22)) are presented in Table 5.

Table 5. Optimal Thickness for $\lambda = 0.63$ as a Function of Mode Number K

K	1	2	3	4
$d_o(\mu)$	1.37	2.74	4.11	5.48

It is necessary to make the following consideration when choosing the desired K number. As the cell gets thinner the off state transmission depends more critically on the thickness.

$$T \simeq \left(\frac{\pi \Delta d}{d}\right)^2 \tag{25}$$

where Δd is the inaccuracy of the thickness. The difference is between the actual thickness d and the tuned d (eq. (22)). On the other hand, the response time decreases with the square of the thickness. Therefore, some tradeoff is necessary. Another consideration is the on state transmission function (see next section). When the cell is too thick the on state transmission is a multipeaked function.

We have measured the response time of the following liquid crystal cells. For a 3 μm cell and a switching ratio of 2:1, we measured a rise time of 15 msec, for a 1/4 mil and a 1/2 mil cell and a switching ratio of 3:1, we measured 30 msec and 100 msec, respectively. Using the equation (from the section on birefringence) to translate all the rise times, to the same, more realistic switching ratio 2:1, one gets the following result:

$d(\mu)$	12	6	3
t_r(msec)	270	80	15

There is no reason to try to use K = 1 (Table 5) because the response time will be limited by the substrate (see Section III-b). On the other hand, the K = 3 choice will slow down the device, so we have chosen to operate at K = 2. This requires reasonable thickness control and gives also good on state transmission (see next section).

2. On State

The off state of the "normal," twisted-nematic transmission mode rotates the polarization by the twist angle α (usually 90^{o}) (Fig. II-8(a)). In the on state the liquid crystal exhibits neither optical activity nor birefringence, so the light polarization is unchanged by passing through the liquid crystal layer (Fig. II-8(b)). Thus, in the transmission mode, the off and the on states are easily distinguishable states.

On the other hand, in the off state of the reflection mode the optical activity is canceled, or the output polarization is like the input and there is nothing to distinguish between this state and the on state. The on state in the reflection mode is similar to the on state in the transmission mode.

To circumvent this difficulty, we have invented a new electro-optic mode — the hybrid field effect mode — which utilizes the twisted alignment effect (described above) in the off state (no voltage on the liquid crystal) in combination with the birefringence liquid crystal effect in the on state (voltage on the liquid crystal). As shown in Fig. II-9(a), we use crossed polarizers in the incident and the reflected beams to obtain a dark off state; the dark off state results because after reflection from the dielectric mirror, the light is polarized in the same direction as was the incident light (the twist is untwisted upon reflection), and is then blocked by the crossed analyzer. Using a positive dielectric anisotropy liquid crystal and applying voltage, we can change the alignment to perpendicular as in the conventional twisted nematic device. If the alignment in the on state (Fig. II-8(b)) is perpendicular and the incident projection beam is incident perpendicular

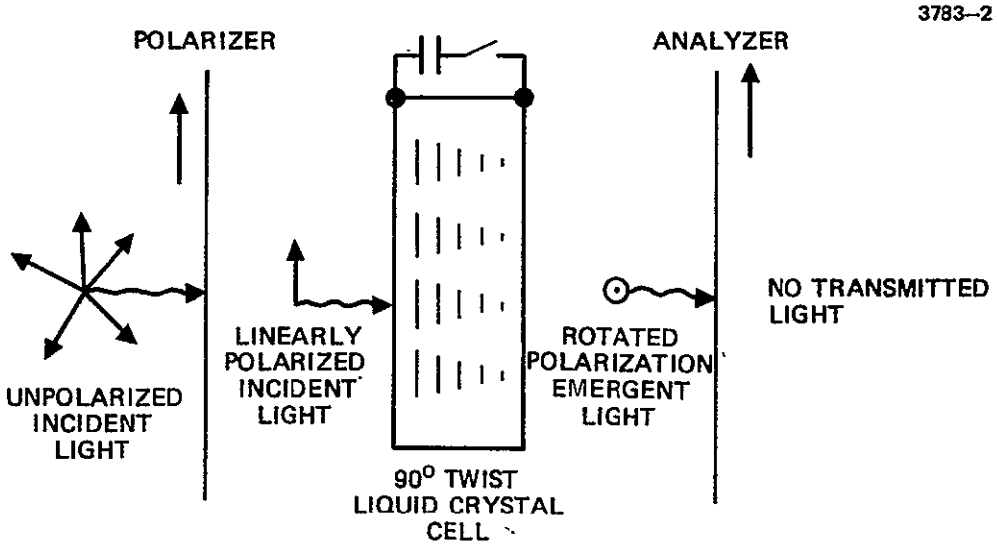

a) OFF-STATE

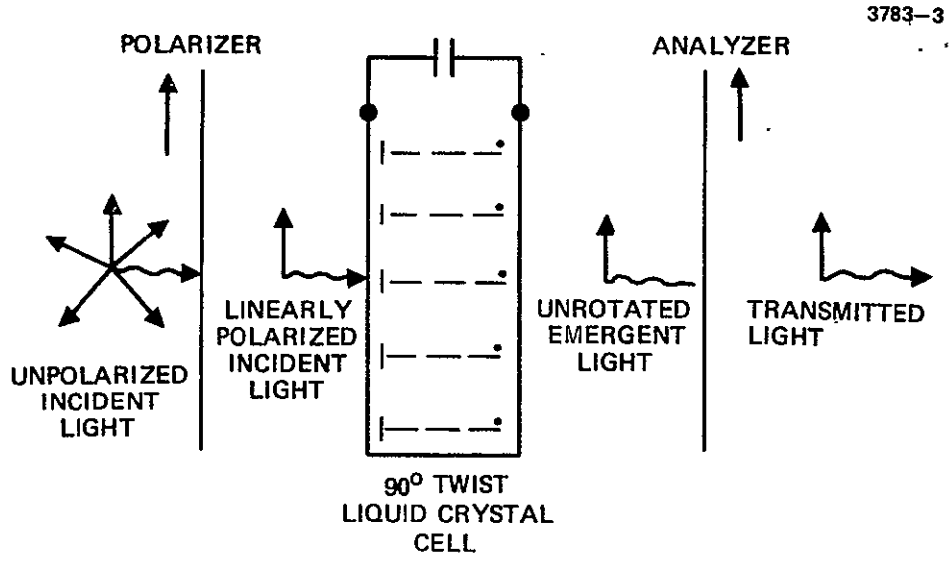

b) ON-STATE

Fig. II-8. Principle of operation of conventional transmission mode twisted nematic liquid crystal device.

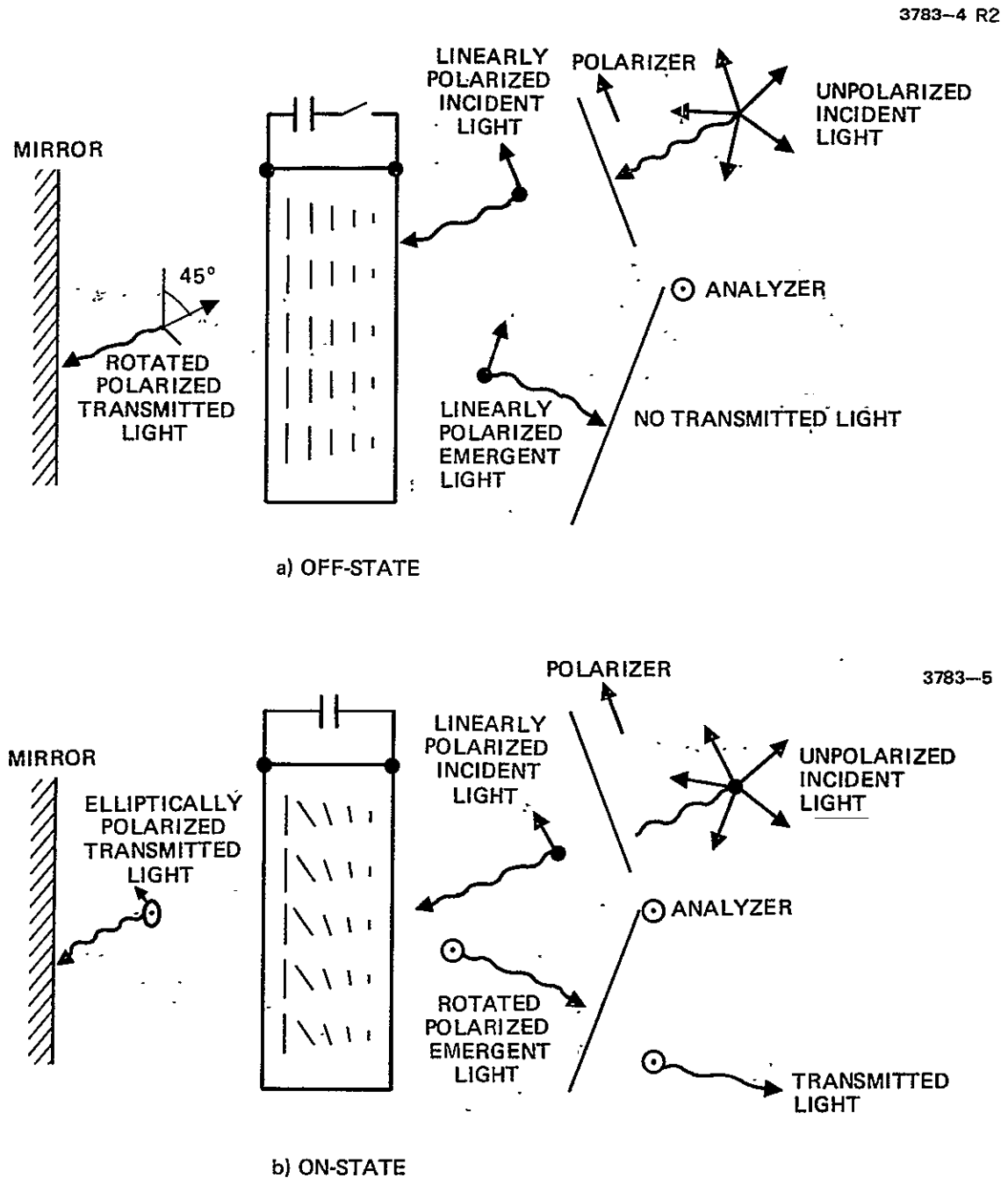

Fig. II-9. Principle of operation reflection mode hybrid field-effect liquid crystal device.

to the cell aperture, the effective birefringence of the liquid crystal is reduced to zero, because in the perpendicular state the polarization of the light is perpendicular to the optical axis of the liquid crystal. To introduce birefringence in the on state we use a 45^{o} twist instead of the conventional 90^{o} twist that is characteristic of the usual twisted nematic liquid crystal devices (Fig. II-8(b)). This has the desirable effect of orienting the polarization of the transiting light at an angle 45^{o} with respect to the extraordinary axis of the liquid crystal molecules. This orientation is optimum for inducing the birefringent effect. To understand qualitatively how this occurs, refer to Fig. II-10. In this figure, we show calculated values for the twist angle as a function of distance into the layer when the voltage across the liquid crystal layer is fully on. As shown in the figure, the effect of the voltage on the twisted structure of the liquid crystal is to destroy the twist spiral. Half the molecules in the layer adopt the preferred alignment direction associated with one electrode and the other half adopt the alignment direction associated with the other electrode. The physical explanation for this behavior is as follows. The calculated tilt angle, as a function of Z along the cell thickness is shown in Fig. II-10. Close to the electrodes, the tilt angle is small, and at the center, where the influence of the electrodes is the smallest, it is large. Generally, as the tilt angle is larger, the transmittance of the twist, from layer to layer, is less effective. For a perfect perpendicularly aligned layer the transmittance is zero. We can describe the twisted nematic alignment as a chain of molecules that would like to be parallel to each other, but the electrode forces twist the chain (Fig. II-4). The switching of the molecules to perpendicular alignment at the center of the cell corresponds to cutting the chain at the point $Z = d/2$. In this case the two halves of the cut chain will spring back to the unperturbed position. This corresponds to disappearance of the twist and alignment of the molecules in the two halves of the cell parallel with the electrodes. (Fig. II-10 illustrates the ideal case.) Because the tilt angle never reaches 90^{o} for finite switching ratios, the calculated curve differs

from the ideal. Since the polarization of the incident light is along the preferred direction of the electrode through which the light enters the cell, and since the molecules in this half of the liquid crystal layer are lined up parallel with this direction, then the polarization of the light beam is unaffected by transit through the first half of the layer. As a result, the polarization of the light makes an angle of 45° with respect to the molecules in the second half of the cell. This orientation is ideal for maximizing the birefringent effect. Any angle different from 45° between the polarization of the light and the optical axis of the liquid crystal in the second half of the layer would lead to a smaller birefringent effect. Hence, 45° is the optimum angle (at least for the ideal case shown in Fig. II-10). However, if we consider the actual case illustrated by the calculated curve in Fig. II-10, we find that some molecules in both halves of the layer deviate from the preferred directions of their respective electrodes. Hence, the twist angle may have to deviate slightly from the 45° ideal angle to maximize the birefringent effect. The twist angle should be set so that light entering the second half of the device is polarized at an angle of 45° with respect to the molecular direction there. This optimization process is described in more detail in proposal 74M-5470/04392. In this contract period, we made some coarse changes of the twist angle. We have found that the residual tilt and the relevant birefringence are functions of the angle and the cell thickness. We would like to have the transmission curve, as a function of the input voltage, in the form of a step function. The hybrid field-effect device satisfies the condition of very low transmission below the threshold voltage, which provides high contrast. Above the threshold the transmission depends on the tilt angle, the direction of the tilt, the birefringence of the liquid crystal, the angle of the twist and the cell thickness. In general, the transmission through the birefringence cell between crossed polarizers is given by (refer to the voltage tunable birefringence discussion in Section II-B)

$$T = \sin^2 (2\phi) \sin^2 \frac{(\pi d \Delta n)}{\lambda}$$

Therefore, for a thick cell it is not to be expected that we will have a monotonic transmission function above the threshold voltage.

To identify the influence of the different parameters, we have built first some thick cells with twist angles of 90°, 45°, and 30°. The thicknesses were 1/2 mil and 1/4 mil (see examples in Figs. II-11 and II-10). We tested the transmission of these devices as a function of voltage and as a function of the direction of the input polarization. In all cells the best results were obtained when the input polarization was parallel with or perpendicular to the direction of the liquid crystal alignment on the front electrode. The 90° cells (not shown) had low thresholds (1.5 V to 2 V) and narrow maximum transmission peaks as we expected. The 45° cells had one narrow and low transmission peak followed by a high (80%) and very broad transmission peak. The threshold was 3 to 4 V and the peak extended up to 15 V. In the case of the 30° devices, the peak was lower (70%) and somewhat narrower. Decreasing the thickness sharpens the threshold and slightly lowers and narrows the major peak, but the effects are much less than proportional to the decreased thickness. Thus for a given voltage, the off-state perpendicular tilt increases as the cell thickness is reduced. This is explained by an increasing influence of the wall forces. This latter effect compensates for the smaller thickness, leaving $d\Delta n$, in the full on state, almost unchanged with decreasing thickness (compare 1/2 and 1/4 mil cells, Fig. II-11). This fact gave us reason to believe that it would be possible to construct a very thin cell for fast response while still maintaining a very high on-state transmission.

The other effect of thickness decrease is the decrease of the number of peaks. We would like to have one broad step peak. We have also observed that the off-perpendicular tilt is larger as the twist angle becomes smaller, being the largest for a parallel aligned cell. This can be explained by the algebraic addition of the wall forces on the liquid crystal molecules when the alignment directions on the two electrodes are parallel as opposed to the vector addition when the alignment directions are at 90°. This is also the reason that the

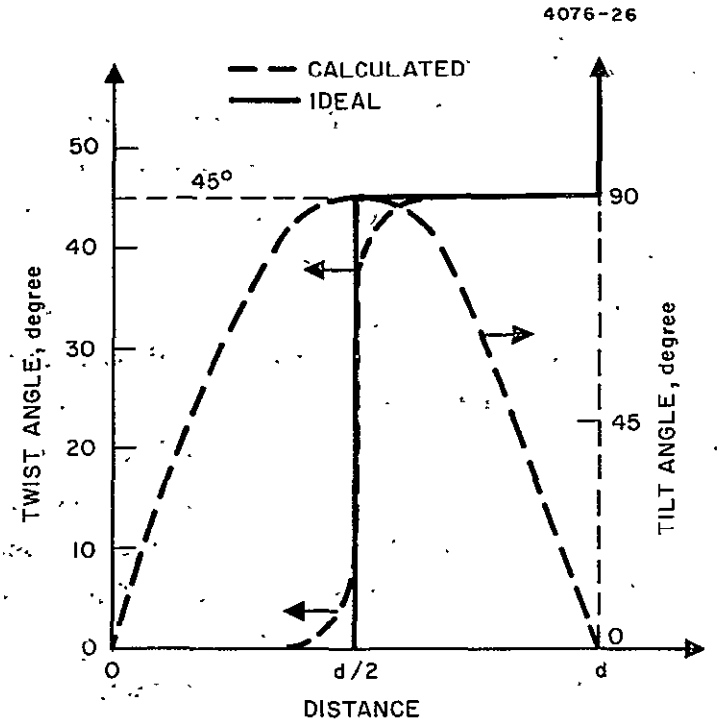

Fig. II-10.
Twist angle versus distance with the voltage on. The axis on the left refers to twist angle. The axis on the right refers to tilt angle.

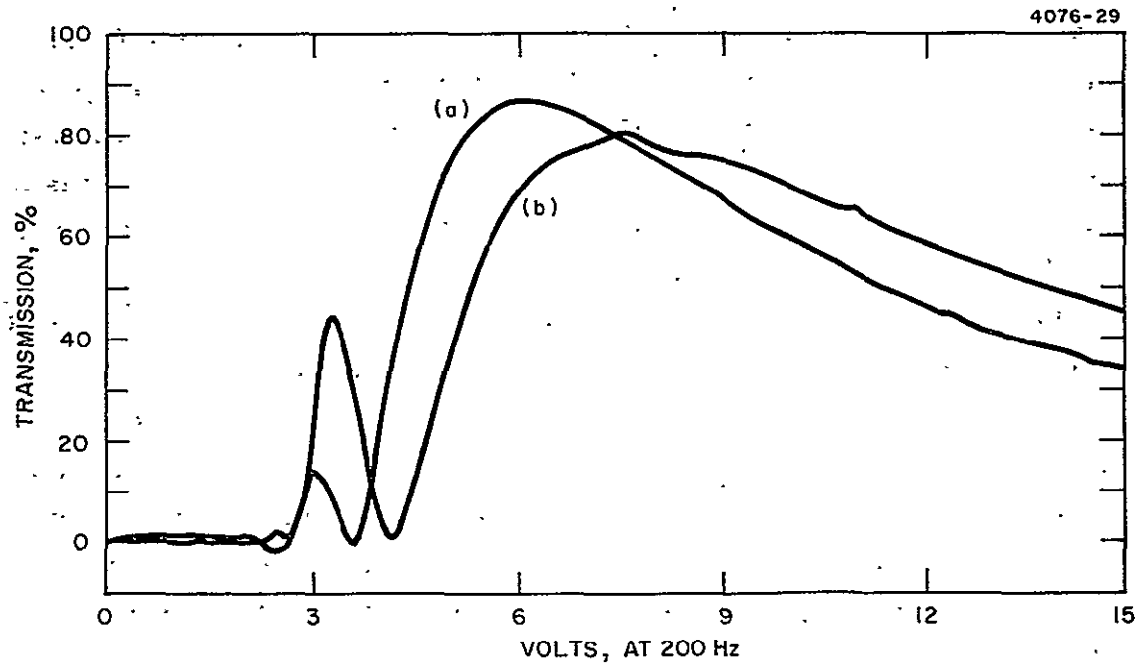

Fig. II-11. Transmission of the 45° twist cell as a function of the applied voltage (reflection mode). (a) Thickness 6 μm. (b) Thickness 12 μm.

threshold for a 45° cell is higher than for a 90° cell. The last peak of the 30° cell is narrower than in the case of the 45° cell because the birefringence effect is not optimized as was explained before (Fig. II-12).

On the basis of these measurements and on some approximate calculations, we built a 2 μm thick, 45° twist cell. As we expected, we observed one peak (Fig. II-13). The peak appeared at a voltage 1.4 times the threshold voltage. Although this peak had a sharp rise, the peak was rather narrow. Peak transmission was 86% for this cell, and at two times the threshold voltage it decreased to 70%. The narrower peak shows that the wall forces are not strong enough to compensate fully for the large decrease in cell thickness. We also tested other twist angles in the 2 μm cell case.

To increase the birefringence of the on state even further, we can illuminate the cell with an off-axis projection beam. When the incident light angle deviates from perpendicular, the effective birefringence is not zero, even when the alignment is ideally parallel. On the other hand, no significant change is observed in the twisted nematic behavior so long as the incidence angle is smaller than 20 to 30°. Combining these two improvements (45° twist and off-axis projection), (Fig. II-14), we have obtained very good contrast and high speed. With the incident light falling on the cell at an angle of 25°, we obtained the following results:

Off-state transmission	2%
Peak transmission	95% at switching ratio of 1.5:1
Flatness of the peak	5% change in transmission for a variation of switching ratio from 1.5:1 to 2.0:1
Rise time	15 msec for a switching ratio of 2.0

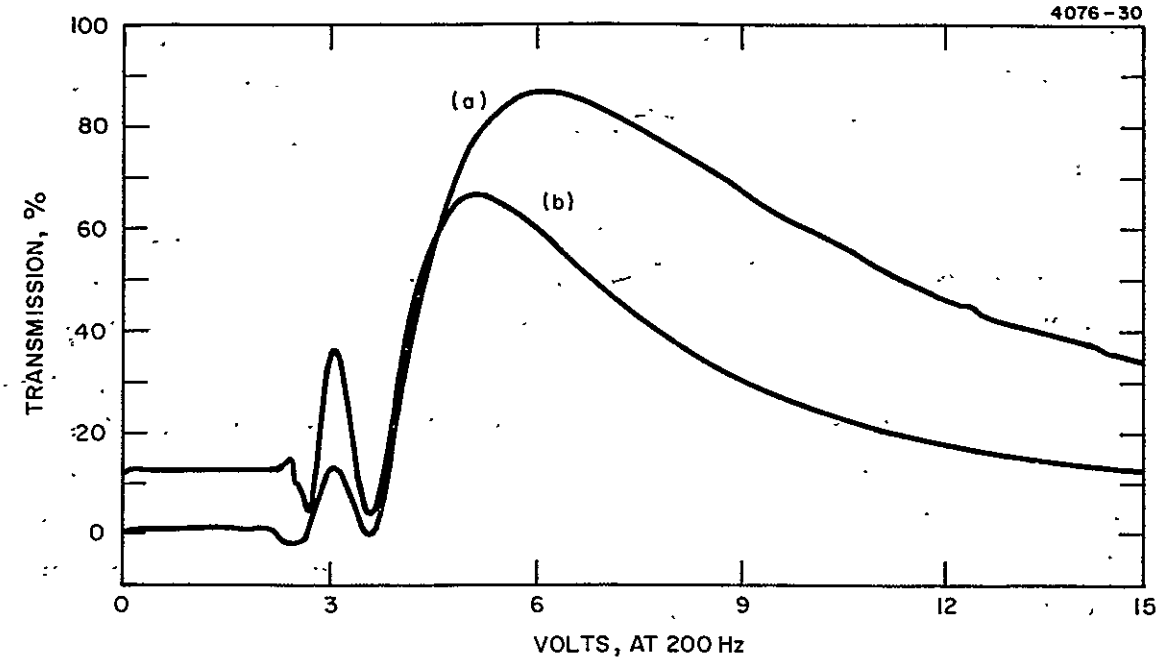

Fig. II-12. Transmission of 6 μ twisted nematic cells as a function of the applied voltage (reflection mode). (a) 45° twist angle; (b) 30° twist angle.

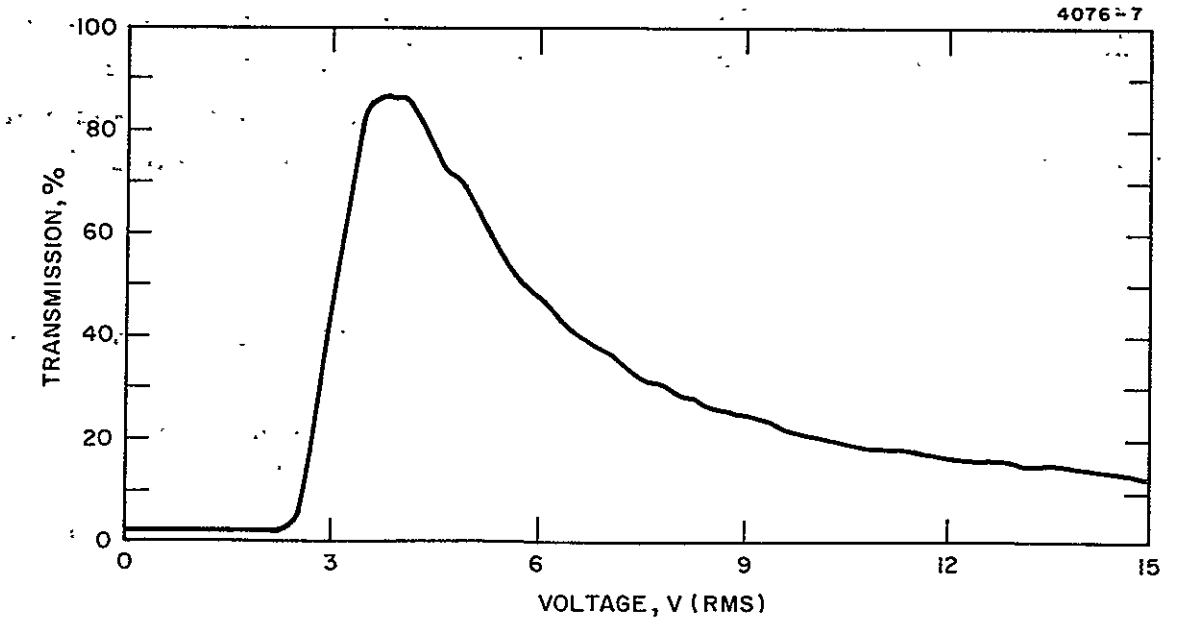

Fig. II-13. Transmission of a 2 μm thick 45° twisted nematic cell as a function of the applied voltage (reflection mode).

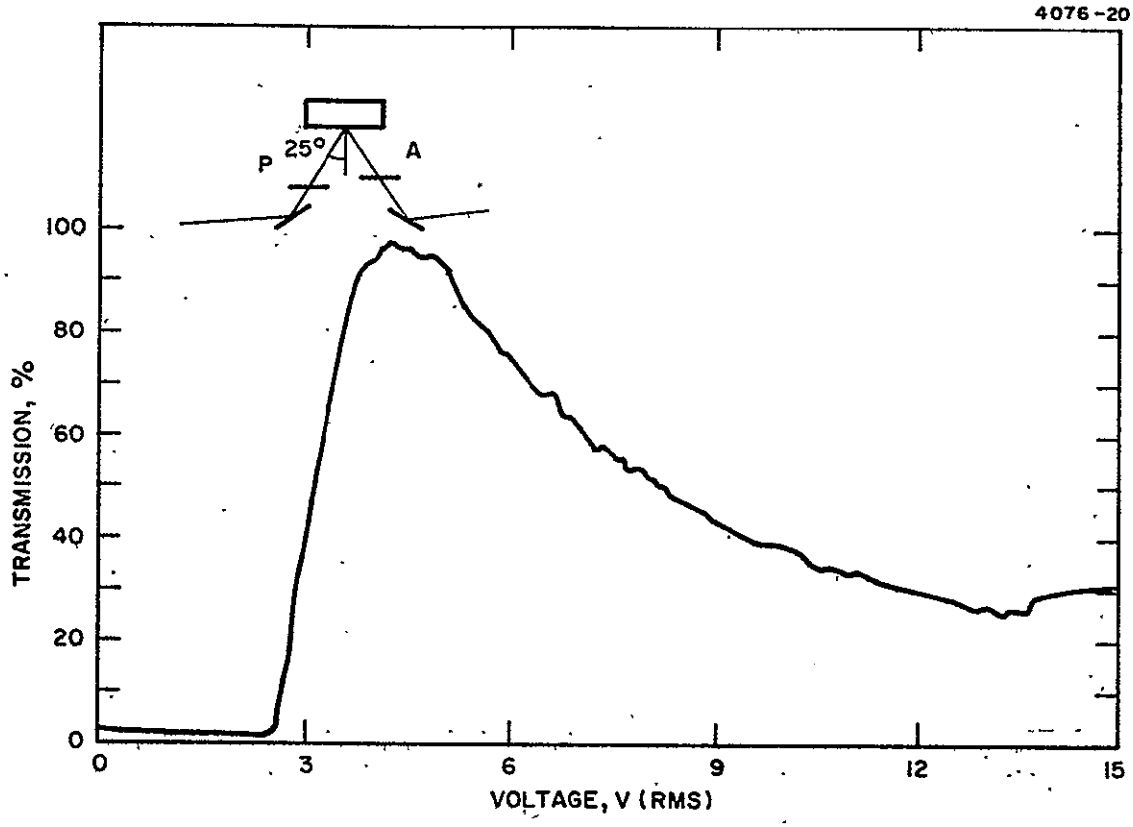

Fig. II-14. Transmission of a 2 μm thick 45° twisted nematic cell as a function of the applied voltage. The reading beam was 25° off the cell perpendicular.

Another advantage of this mode of operation is the sharpness of the threshold, as compared with DSM. In most cases, we find that off-axis operation is not necessary to obtain very high contrast (>100:1).

We have also measured the effect of the switching ratio on the response time. We carried out these measurements on 1/2 mil cells with 90° twist using 200 Hz ac. The voltage was switched between a threshold voltage of 0.9 V rms and the operating voltage, V, listed in the table below.

Table 6. Cell Transmission and Rise Time Data Versus Voltage Switching Ratio for Twisted Nematic Liquid Crystal

V/Vth	Transmission Range, %	T_{rise}, msec [a]	$T_{rise\ (2\mu)}$, msec [b]
2.0	8 to 90	500	14
5.0	5 to 98	40	1.1
10.0	7 to 97	20	0.55

[a] The measurement of time response was made from 10 to 90% of the total transmission to determine the time response at high contrast (1/2 mil thick cell).

[b] The T_{rise} (2 μm) are projected values for a 2 μm thick cell.

T1657

Unfortunately, switching ratios higher than 2 are unobtainable in the present ac mode substrate. Still this 15 msec time response projected for the 2 μm cell with the obtainable switching ratio of 2:1 offers promise for many applications.

The temperature effect on response time was investigated using a 200 Hz signal switched between 0.9 V rms and 1.95 V rms with parallel polarizers. For a 1/2 mil, 90° twist cell the results are summarized below:

Temperature	T_{delay}, msec	T_{rise}, msec	T_{decay}, msec
23°C	180	370	460
40°C	100	240	340
60°C	50	175	240

In summary, we have a liquid crystal light valve that is particularly well suited for optical data processing — one that utilizes the twisted nematic alignment in the off state and the birefringence effect of the liquid crystal in the on state. To increase the birefringence in the on state (which for homeotropic alignment normally is zero), we implement a 45° twist angle by means of alignment forces on the electrodes and we can use off-axis incidence of the readout light.

D. Alignment Studies

A controlled, uniform liquid crystal alignment is essential for the satisfactory performance of any liquid crystal display, and it is particularly important for achieving the high resolution required of the optical-to-optical interface device. Hughes is supporting a continuing study of alignment techniques which are applicable to all of the liquid crystal devices under development at Hughes. The techniques described here were developed with IR&D funds, but a description is nevertheless provided for informational purposes so that the construction and functioning of the devices prepared for study on this program may be clearly understood.

There are two basic boundary conditions where a liquid crystal comes in contact with a solid surface. The liquid crystal molecules can be oriented with their long molecular axes essentially parallel with the surface, or they can be oriented essentially perpendicular to the surface. When the orientation is perpendicular at both surfaces of a liquid crystal cell, the alignment is termed homeotropic or perpendicular. When the orientation is parallel at both surfaces and the molecular axes are uniformly aligned in a single direction, the alignment is said to be homogeneous or parallel. If the parallel orientation at one surface differs in direction from the parallel orientation at the opposing surface, the liquid crystal in the bulk accommodates for the difference by assuming a helical twist from one surface to the other, and the alignment is twisted parallel or twisted nematic. Additional distinctions can be made if the alignment is not truly parallel or perpendicular at the boundaries but is tilted at some angle from these positions. In these cases we may speak of such alignments as being tilted parallel or tilted perpendicular, or even tilted twisted parallel and twisted tilted perpendicular.

1. Dynamic Scattering Mode Devices

Any of these alignment modes can be used in a dynamic scattering device, although each will have its own unique dynamic scattering patterns, light scattering characteristics, and response-curves. In field-effect devices an alignment that is essentially perpendicular will be used with a liquid crystal having a negative dielectric anisotropy so that the field will tilt the molecules toward a parallel orientation, as in the birefringent cell. An alignment that is essentially parallel or twisted parallel will be employed with a liquid crystal having a positive dielectric anisotropy, so that the field will tilt the molecules toward a perpendicular orientation. If a twist is present, it will be gradually lost at some stage during the process of re-orientation by the field. In each device the positioning of polarizers, if they are used, will depend on the alignment of the liquid crystal in the off state, the orientation by the field in the on state, and the type of effect being exploited.

Conventional electrode surface materials, such as indium-tin-oxide or silica, are strongly polar. Since the centers of nematic molecules are considerably more polar than the ends, interaction of the molecules with the polar surface can be maximized only by aligning parallel to the surface and adsorption onto it. Although the directors will be aligned in a uniform direction locally, the orientation on an untreated surface varies in a more or less random fashion from one small region to the next, with twists or disclinations accommodating for the conflicts between them. In the absence of any other influence, the liquid crystal assumes the alignment direction in which it first meets the surface, and the pattern formed when the liquid crystal first flowed over an untreated surface can readily be discerned with a polarizing microscope. This pattern is extremely resistant to change, even by prolonged heating above the nematic-isotropic transition temperature. Therefore, for parallel alignment it is necessary to provide direction for this tendency to adsorb on the polar surface. For perpendicular alignment it is necessary to make the surface nonpolar so that the nonpolar ends of the molecules will be attracted to it more than their polar centers.

One method of making the surface nonpolar is to dissolve a perpendicular aligning agent in the liquid crystal. Such an aligning agent will have a polar group at one end of a long, nonpolar, aliphatic hydrocarbon chain. The polar end will be attracted to the polar surface preferentially, thereby coating the surface and presenting the nonpolar aliphatic chains as a new surface in contact with the liquid crystal. On this program we generally used hexadecyltrimethylammoniumstearate as such an aligning agent, since both the anion and the cation of this salt have the required structure. Hexyloxybenzoic acid served a similar purpose in at least one liquid crystal mixture.

An alternative method of inducing a perpendicular alignment is to coat the surface permanently with a nonpolar material, such as silicone with long, nonpolar substituents.[5] Hughes has developed an alternative method that is specific for such materials as SiO_2, which have reactive hydroxyl groups on the surface. This method consists of heating the substrate in a melt of a long chain aliphatic alcohol

(typically hexadecanol or tetradecanol) and an amine (typically hexadecylamine) as a catalyst. The treatment usually is carried out at ~120°C for periods of four to 24 hours, after which the surfaces are washed thoroughly with clean organic solvents (e.g., hexane and methanol). During this treatment the alcohol reacts chemically with the surface hydroxyls to form long chain alkoxy groups that make the surface nonpolar. We have found it necessary to resort to the alcohol-amine treatment to obtain perpendicular alignment in 2 μm cells, in which the stearate aligning agent fails to function satisfactorily. The alcohol-amine treatment does not alter the conductivity of the liquid crystal, whereas the stearate is both a conductive dopant and an aligning agent.

2. Hybrid Field-Effect Device

The oldest and most convenient method of producing parallel alignment is to rub the surface. Although a wide variety of materials have been suggested for use in rubbing, we prefer to use a lens tissue with a few drops of India ink. Rubbing leaves striations which differ slightly in alignment direction and which are readily visible under a polarizing microscope. Nevertheless, the technique is adequate for routine testing and noncritical applications, and we used it only for such purposes.

A much more uniform parallel alignment can be achieved by shallow angle ion beam etching. This method works extremely well on silica and certain other surfaces but fails on indium-tin oxide. Generally we deposit 1500 to 3000 Å of SiO_2 by sputtering with a radio frequency argon plasma while the substrate is at ground potential. This coating is then ion beam etched in the Veeco Microetch with an argon ion beam to a depth of 200 to 900 Å with an etching angle of ~60 to 80° from normal. Best results are obtained with these surfaces when the liquid crystal is allowed to flow parallel with the etch direction during cell assembly, whenever this is possible. The resulting parallel (or twisted parallel) alignment is extremely smooth and free of striations; however, we have found that the direction of alignment is not entirely constant across a one-inch cell because of divergence of

the ion beam. This divergence has been found to be approximately 5 to 6° per inch. Efforts are currently being made to reduce the divergence through better collimation of the ion beam. The amount of divergence is important for a twisted nematic cell which is viewed or projected with crossed polarizers. Deviations of a few degrees can substantially increase the light transmitted in the off state.

There is some evidence that parallel alignment obtained by ion beam etching is not truly parallel but is slightly tilted. The tilt angle has not yet been measured, but the molecules appear to be tilted out of the surface toward the ion beam source. Tilting uniformly in a given direction in the off state can be very useful, because it determines the direction of tilt when a field is applied. However, if this tilt angle is too large, the effect is equivalent to the application of a low strength field, and the result is reduced contrast. Measurement, control, and selection of the optimum tilt angle is the subject of a continuing study.

A small, uniformly directed tilt is also desirable in a perpendicular alignment, since it will control the direction of tilt in an applied field. Tilted perpendicular alignment is obtained in birefringent cells by combining the techniques for perpendicular alignment with those for parallel alignment, e.g., the shallow angle ion beam etched surfaces are either given the alcohol-amine treatment or are used with a stearate aligning agent. The tilt angle can be controlled by varying the chain length of the alcohol or by adjusting the stearate concentration.

This summary has briefly described the alignment methods used on the NASA program. Hughes is continuing to make progress in understanding and taking advantage of the subtleties of these techniques.

SUBSTRATE STUDIES

A. DEVICE CONFIGURATION STUDIES

1. Transmission Mode Light Valve With External Dichroic Mirror

As discussed in Section I, the lifetime limiations of the dc optical-to-optical device light valves made it necessary to provide an inert interface between the photoconductor and the liquid crystal in the next generation of devices. Efforts to solve this problem resulted in the reflection mode ac light valve with a light-blocking layer and internal dielectric mirror/inert interface layer separating the photoconductor and liquid crystal. While this design was very successful for large screen projection display, it had several initial limitations for use as a high speed dynamic scattering mode optical data processing device:

a. The photoactivated current-switching ratio was severely limited in the ac device by the high capacitive dark current. In order to achieve fast response in the dynamic scattering mode, high current switching ratios are necessary. See Section II-A.

b. The current switching ratio was further limited by the thickness associated with the dielectric mirror and light-blocking layer.

c. The imaging light sensitivity and resolution were degraded because it was not possible to image directly into the interface junction region. Instead, the imaging light was incident through the back interface of the photoconductor, which resulted in image spreading and an exponential decrease of imaging light intensity through the insensitive region of the photoconductor.

d. The photoconductor surface on which the internal mirror was deposited had a polycrystalline texture and thus was nonspecular. This resulted in noise in the coherent readout image.

These problems were formidable in terms of achieving a practical ODP device. The initial approach taken to solve them was to convert the basic reflection mode device to a transmission mode of operation. The advantages of this mode will be outlined below. A transmission mode device could be constructed by replacing the light blocking layer/internal dielectric mirror combination with a transparent insulator that provided high dc resistance, an inert interface with the liquid crystal, and formed a highly light-sensitive junction (similar to CdTe) with the CdS photoconductor. While there still was a basic limit to current switching ratio imposed by the ac operation, the thinness of this transparent blocking layer would not further limit the switching ratio. Calculated values under these conditions showed that switching ratios sufficient for high speed dynamic scattering mode operation could be obtained. And because the imaging light would again be directly incident into the junction through the transparent blocking layer, higher sensitivity and resolution would result.

However, because of the requirement for the use of an image intensifier tube, the light valve must still be used in the reflective mode. This could be accomplished with the transmission mode device by the use of an external dichroic mirror as shown in Fig. III-1, which is a schematic of the proposed use of the transmission device in a reflection mode system. On the mating fiber optic faceplate to the fiber optic image intensifier, a dichroic mirror which transmits 525 nm but reflects 633 nm is deposited. Over the dichroic mirror the indium tin oxide (ITO) conductive counter electrode and SiO_2 inert barrier are added. This forms one electrode for the liquid crystal layer. The other electrode is the light valve substrate, consisting of the transparent blocking layer, CdS photoconductor, and ITO transparent electrode deposited on glass. In operation the green imaging light from the P-1 phosphor of the intensifier tube passes through the dichroic mirror, liquid crystal, and transparent blocking layer to the CdS junction region to activate the light valve. The red readout laser light passes through the CdS, but does not photoactivate it. The laser light is then modulated by the liquid crystal and returns through the light

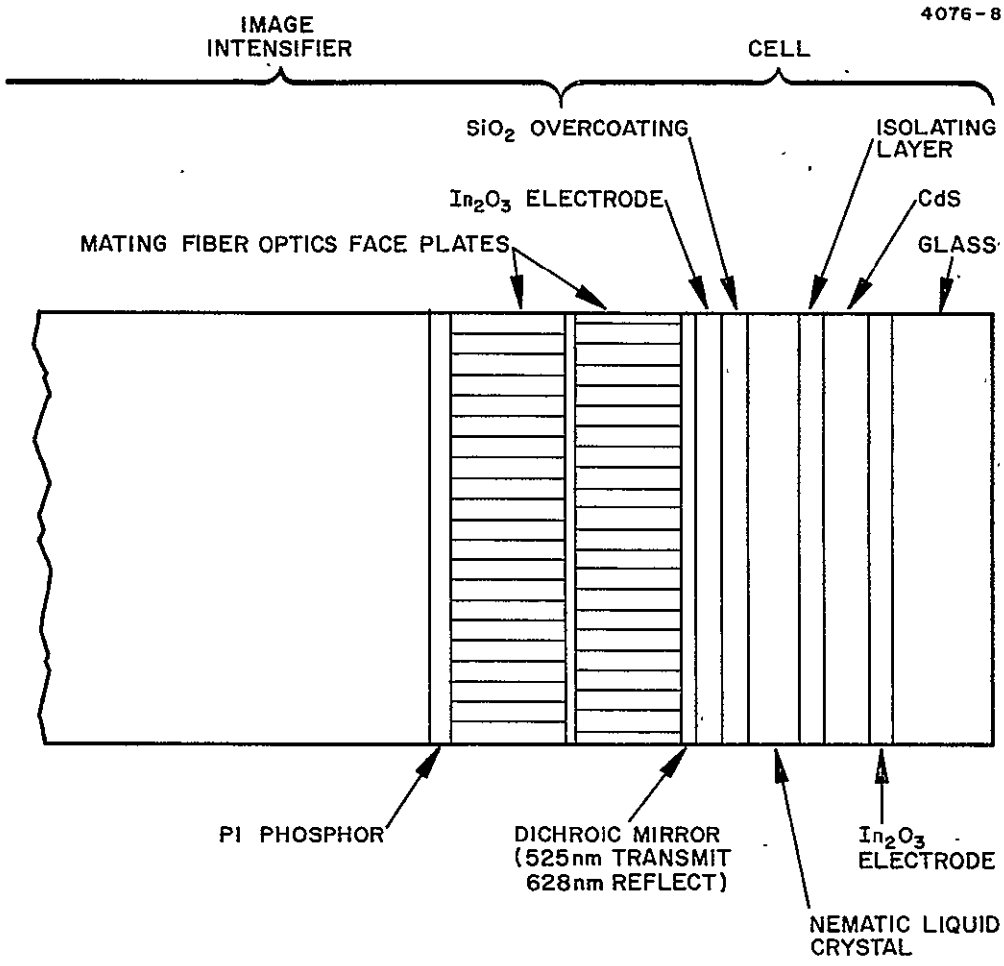

Fig. III-1. Transparent ac light valve for use with image intensifier.

valve substrate after being reflected by the dichroic mirror. Also, because the laser reflecting dichroic mirror is placed on a highly polished, flat faceplate, the noise associated with a mirror on a rough surface is eliminated.

The principal problems with the experimental realization of this device are incorporating a transparent blocking layer that meets the requirements imposed on it, while concurrently optimizing the CdS film properties.

The next section will consider the optimization of the thermally evaporated CdS heat treat process in H_2S. This will be followed by the considerations of materials for the transparent blocking layer. Then results will be presented for the substrates tested both with metal contacts and in a light valve configuration. Finally, the problems inherent in this configuration will be discussed.

2. Optimization of CdS Heat Treatment

The thermal evaporation of CdS results in films that are highly nonstoichiometric. There is an excess of cadmium and thus the films have relatively high n-type conductivity. For use in high impedance photoconductor applications, such as the liquid crystal light valves, it is necessary to compensate the films with sulfur. This has been accomplished by thermal processing in flowing H_2S. The standard process has been at a flow rate of 115 scc/min (scc = standard cm^3) at 475°C for 30 min. A second, similar flash process was done with a flow rate of 10^3 scc/min at 490°C for 10 min. Both of these processes are non-equilibrium in that the sulfur compensation is not carried to completion through the entire thickness of the CdS film. These processes do result in the necessary high resistivity region near the junction, but they are not highly reproducible. The nonreproducibility is caused by very small changes in the thermal processing parameters and in the initial stoichiometry of the films that change the compensation level reached. The precision of control necessary can be seen from the fact that one part in 10^6 excess cadmium results in conductivity too high for light valve operation.

To circumvent this problem, a new process which proceeds to complete compensation was developed.[6] The process uses a flow of 10^3 scc/min of H_2S at 550°C for five minutes. This process results in a recrystallization of the CdS with a subsequent marked improvement in the electrical properties of the individual crystallites. Because the process proceeds to complete compensation, minor changes in processing conditions do not affect the final state reached. But evaluation of these films in light valves showed that the intercrystalline boundaries caused by the recrystallization gave an unacceptable grainy appearance to the imagery.

Thus, no optimum condition was reached in the processing of the thermally evaporated CdS films. The parallel effort in reactively sputtered CdS that is reported in Section III-B eventually provided a solution to these problems and allowed performance to be achieved superior to that of the thermally evaporated films. But the sputtered films were not completely developed at the time of the experimentation on the transmission mode light valve, and thus were not used in any of the experiments reported in the next sections.

3. Considerations for Selection of the Insulator Material

The main condition for selecting a transparent insulator for use in the light valve is the formation of a photosensitive junction on the CdS thin film surface. The requirement is to create a depletion region in the CdS where photoexcited electron-hole pairs are separated by the electrical field and thus contribute efficiently to the photoresponse. This is the basis of the successful operation of the dc optical-to-optical device light valves which use an electrolyte/semiconductor junction, and the ac light valves with an n-p CdS/CdTe heterojunction.

Theory[7] and experimental results on vacuum cleaned crystals[8] indicate that the surface barrier height should be a direct function of the work function difference between the semiconductor and electrode. This is because the intrinsic CdS surface states are localized near the band edges, which is in distinct contrast to the case of silicon. In silicon the surface states are localized in the band gap, and thus

effectively pin the Fermi level at the surface independent of the electrode work function. Results on CdS thin films,[9] primarily studied for use as field effect transistors, show much less predictable results. This is caused by the polycrystalline nature of the films and also by absorbed surface impurities[10] that give variable surface properties. Thus, in general, the barrier heights obtained on the thin films will be more directly related to the particular film deposition and environmental conditions, and must be determined directly.

Several insulators were chosen for evaluation that had good adhesion and mechanical properties and were compatible with the liquid crystal. Also evaluated were composite insulators comprised of a potentially good junction forming film deposited next to the CdS followed with a film known to be inert with respect to electrochemical interaction with the liquid crystal. The single layer insulators evaluated were Al_2O_3, SiO_x, and SiO_2, and a composite structure of MgF_2 and SiO_x was also tested.

Experimental Results on Transmission Mode Substrates and Light Valves

Electrical measurements of current switching ratio were made on both the light valve substrates with indium metal contacts with an equivalent impedance in series to simulate the liquid crystal, and on actual liquid crystal light valves. The light valves used the liquid crystal compositions in a layer 6 μm thick. The standard test conditions for light valves and substrates were an ac drive frequency of 200 Hz, at both 10 and 20 V rms, and an image light power of 120 $\mu W/cm^2$ at 525 nm. The light valves were also evaluated for image quality. The effect of a dc reverse junction bias superimposed on the ac voltage was also studied in several cases.

Initial work was done with Al_2O_3 as the transparent insulator. The results showed very low current switching ratios and hence low contrast ratio in light valve structures. This indicated that Al_2O_3 did not form a good junction with the CdS and thus was not suitable for light valve use. The emphasis then shifted to a more thorough evaluation of the other insulators mentioned above.

In this phase, sputtered SiO_2, thermally deposited SiO_x and MgF_2-SiO_x were evaluated with the three CdS heat treat processes described above. The initial results lead to several observations:

- Magnesium difluoride did not improve the junction properties of SiO_x films as had been expected from results in the literature.[9] Thus it was not pursued in successive tests.

- The indium metal contact on the substrate and an equivalent circuit representation of the liquid crystal was only an indicator of switching ratio performance and was not accurate quantitatively. The correlation was poorer on the recrystallized films than the standard heat treat films. This is likely the result of poor surface coverage of the insulator over the CdS, particularly in the case of the recrystallized films with a very pronounced texture.

- The flash heat treatment led to nonuniform photoelectrical properties across the substrate, indicating nonuniform compensation. Thus, it was also dropped from further evaluation.

- Reverse dc bias of the junction improved the switching ratio of the partially compensated films, but not the recrystallized films.

Results typical of those finally obtained for the two thermal processes with the sputtered SiO_2 and thermally deposited SiO_x are given in Table 7. The data indicate that the recrystallized CdS gives higher switching ratios than the standard heat treatment, and that the SiO_x apparently forms a better junction than the SiO_2. In fact, the switching ratio of greater than 6 obtained with the recrystallized CdS and SiO_x appeared to be an indication that a good junction could be formed. However, even though good measured switching ratios could be obtained in actual light valves, the laser projected imagery suffered from poor contrast and image spreading. Both of these problems are symptomatic of poor junctions. These problems will be discussed in the next section.

Table 7. Current Switching Ratios of CdS/Insulator Substrates and Light Valves for 120 μW/cm^2 Input Light Power at 525 nm

Substrate CdS Treatment	Insulator Thickness 0.5 μm	Applied Voltage at 200 Hz, rms	Current Switching Ratios	
			Equivalent Circuit	Light Valve
Recrystallization	SiO_x	10v	4.00	6.54
		20v	4.00	7.00
Recrystallization	SiO_2	10v	3.36	4.88
		20v	3.29	3.88
Standard	SiO_x	10v	3.40	3.38
		20v	3.18	2.79
Standard	SiO_2	10v	2.54	2.36
		20v	2.23	

T1650

5. Problems Associated with the Transmission-Mode AC Light Valve

While there were some positive indications from the electrical measurements, a practical transmission mode light valve was not realized. The low contrast, image spreading, and mottled and speckled imagery observed are directly related to the problems of forming a good junction with an insulator to CdS, and obtaining microscopically uniform, pinhole-free coverage on a rough polycrystalline surface. Although systematic diagnostics were not carried out, it is likely that holes or irregularities in the insulator provided a direct contact of the liquid crystal on the CdS which formed a good junction and thus increased the measured switching ratio. This also explains the lower switching ratios obtained with indium contacts, particularly on the recrystallized films. The contact of indium on CdS makes an ohmic contact and thus higher dark current would result in a lower switching ratio. The image spreading observed can be the result of a

partially conductive surface channel at the insulator/CdS interface. A surface state condition can result where an accumulation instead of depletion of electrons occurs at the surface resulting in the relatively easy transfer of charge in the plane of the substrate.

6. Further Development of the Transmission Mode Device

The work described above was the extent of the work on the transmission mode light valve. Two later developments in the program – sputtered CdS and chemomechanical polishing of the CdS surface – would have been the next steps in this development cycle. In the work continued on the reflection mode device, the sputtered CdS has shown much less dependence than the thermally evaporated films on surface parameters in its photoelectric properties, making junction formation a less critical task. And the chemomechanical techniques described in Section IV-C have allowed a smooth, structureless surface to be obtained on the CdS surface that permits microscopically uniform coverage by a thin film coating. These factors were very significant in the development of the reflection mode device and they can play the same role in further development of the transmission mode light valve if this configuration becomes useful in a particular application. However, within the context of the present contract report, the work on the liquid crystal in which the DSM mode was dropped and the hybrid field-effect mode adopted greatly reduced the demand to produce an ac device with a higher switching ratio.

B. CdS/CdTe Photosensitivity

Since the beginning of this reporting period, one of the main objectives for device improvement has been to improve the device input sensitivity. This objective became critically important with the transition from a dc to an ac device and with the consequent reduction in sensitivity for the same CdS films. This improved sensitivity objective has been supported with internal IR&D funds on three separate research fronts. First, an attempt was made to understand the physical photoelectric

nature of the ac substrate operation. Second, an attempt was made to relate process variables to photoelectric properties. Third, again on a parallel IR&D program, an attempt was made to develop and optimize sputtered CdS films with improved sensitivity by incorporating the understanding obtained in the first two research areas.

The results obtained in each of these three research areas are described below:

Model of Photoelectric Performance – AC Light Activated Charge Storage Diode

– The ac light valve substrate consists of a CdS photoconductor layer on an Indium Tin Oxide coated glass electrode. The CdS layer is overcoated with a p-type CdTe blocking layer and then a dielectric mirror. When a liquid crystal is sandwiched between this substrate and a second ITO coated glass counterelectrode, the ac light valve is formed. The equivalent circuit for this device consists of two parts – a light-sensitive element and a set of passive components. The passive components are easily represented as an ideal capacitor for the mirror and a parallel resistor-capacitor combination for the liquid crystal.

The physics describing the photoelectric properties of the CdS-CdTe light sensitive element is the topic of the present section. It has been found that this CdS-CdTe light-sensitive elment acts as a light activated charge storage diode. The key element controlling the operation of this diode structure is the ac capacitive impedance associated with the diode depletion width. It is noted that light-injected charge controls this depletion width capacity. The way this occurs is briefly reviewed below.

As the key element is the depletion width of the charge storage diode, the characteristic diode curves are the Q versus V curves of Fig. III-2. In these curves, V is the diode back bias voltage and Q is the charge on the indium tin oxide (ITO) ohmic contact to the CdS film. Light intensity is the parameter producing the family of curves shown. Our explanation begins with the dark state. In that case, the CdS layer

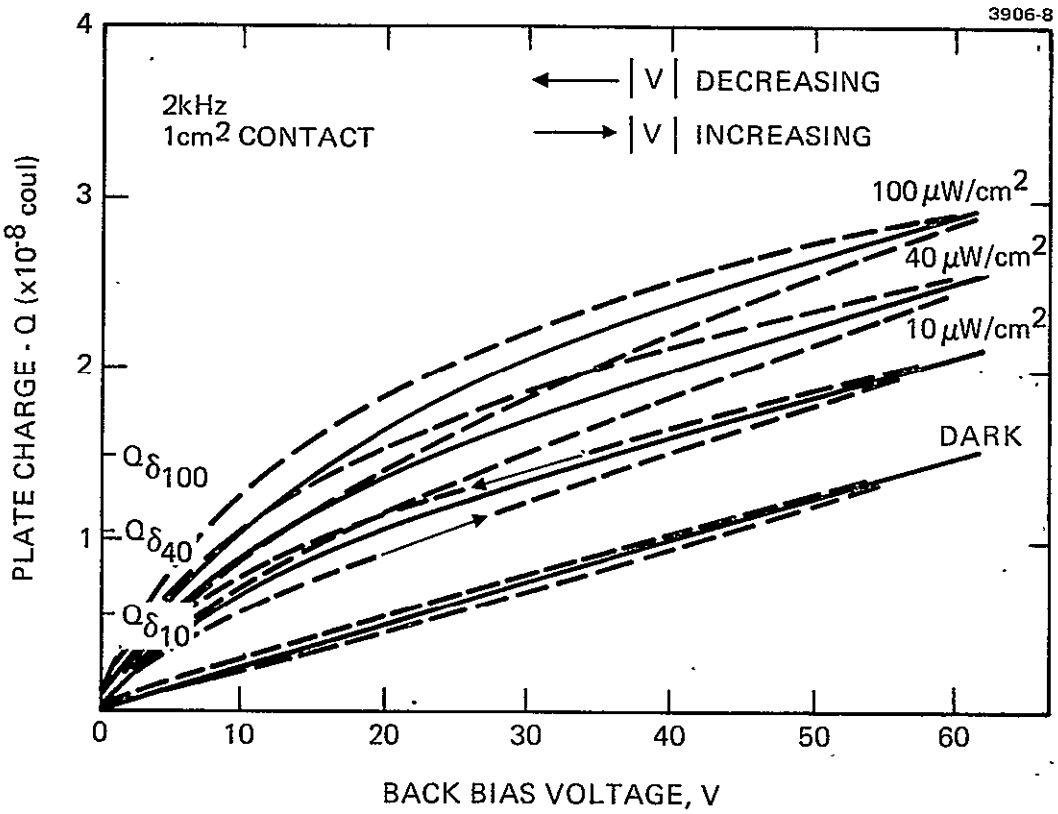

Fig. III-2. Experimental plate charge versus back bias voltage curves for the charge storage diode. Data are presented for various light levels. The dashed curves represent scope curve traces for the |v| increasing |v| decreasing cases. The solid curves represent the averaged case.

in the diode is prepared with high enough ρ that the diode depletion width sweeps easily from the CdS/CdTe interface all the way through the CdS film (~16 μm) for negligibly small voltages. Thus in the dark, the ac impedance of the photosensor is simply that of a 16 μm thick CdS dielectric capacitor. So for the dark case, the Q versus V curve in Fig. III-2 is simply a straight line.

Now, when the diode is illuminated light injects electron hole pairs in the bulk of the CdS film near the CdTe interface. The injected holes are captured in the CdS at recombination centers forming a stored charge. To explain the Q versus V curves of Fig. III-2 for the illuminated condition, note that if the diode is in the zero back bias voltage condition, the light-injected electrons are captured at trap centers in the CdS and the hole charge is compensated. Thus, the ITO plate charge is zero at zero voltage. As the voltage varies from zero, however, since some of the electrons are mobile while the holes are not, the shallow electron traps act effectively as donors and the depletion width varies with voltage in a fashion controlled by an effective donor concentration created by light-injected electrons captured at shallow trap centers. When the voltage reaches the point that the shallow trap centers are depleted, the charge Q has been removed from the film (Fig. III-2) and the film will again charge as a 16 μm dielectric capacitor and the Q versus V curve slope becomes equal to the dark state Q versus V curve slope.

It is clear from the above discussion that the electron population at the shallow trap centers is the light-dependent quantity which characterizes the photosensor response. This quantity can be related to light intensity and sensor on and off times by assuming a three-level model for the CdS film. These three levels are a recombination center, a shallow trap center, and a deep trap center. The deep trap center plays an important role in limiting performance. Referring to the earlier discussion, not all electrons trapped are free to move at the frequency of the applied ac voltage. Thus they limit sensitivity as many of the light-injected electron-hole pairs are then uneffective. This model is treated more fully, both theoretically[11] and experimentally[12]

in the literature. It is noteworthy here, however, that this model indicates that a 20-fold improvement in the switching ratio-time response product is still theoretically possible for the best presently sputtered CdS films.

The above described model fits well the three fundamental experimental observations illustrated by the data in Table 8 and Figs. III-2 and III-3. Thus, the CdS light absorption (Table 8) controls the device spectral sensitivity; sensitivity improves with lower operating voltages (Fig. III-3); and device wave shapes can be predicted fundamentally by Q versus V curves developed from a depletion width model (Fig. III-2).

Table 8. CdS Switching Ratio — 4 μm Thick Liquid Crystal

Wavelength, Å	Switching Ratio
Red, 6000	1.05 } 2 kHz
Green, 5260	1.77 } 100 $\mu W/cm^2$

T1649-R1

It is noteworthy that the above model explains the sensitizing action of the ac substrate in terms of a photocapacity effect rather than a photoconductive effect. The photoconductive effect explains the sensitizing action in a dc substrate. The photocapacitive effect suffers from an a priori loss of sensitivity but at the same time allows faster substrate response times. Therefore, it is not appropriate to think of the CdS films as slow photoconductors. This photocapacity model provides us with two salient design features for improved substrate sensitivity.

First, writing light should be absorbed near the CdTe interface where it has a maximum effect on depletion width charge. This runs counter to the usual case for uniform films where the light is absorbed exponentially from the input side near the ITO.

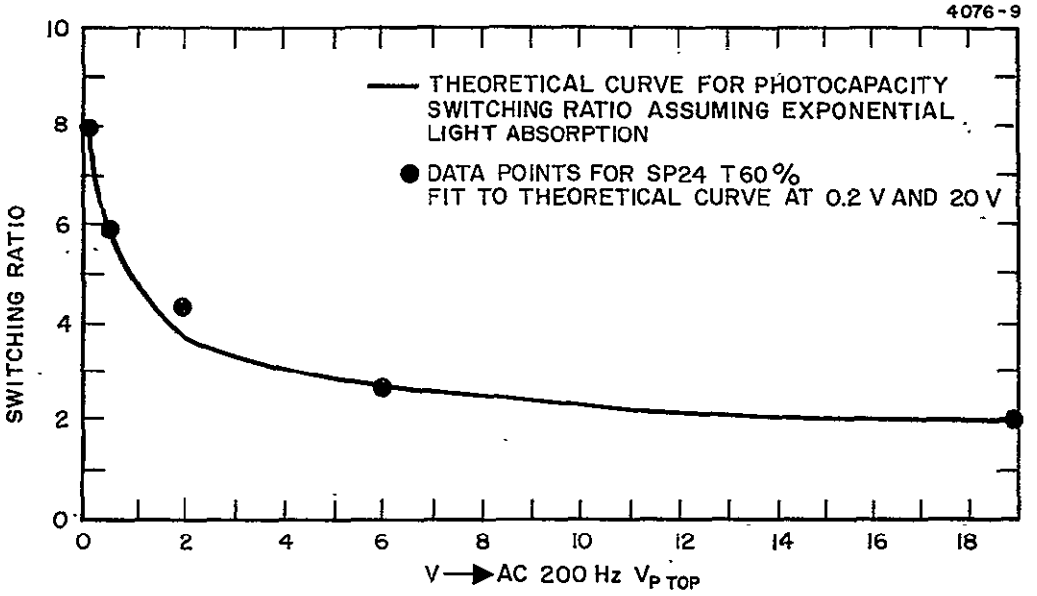

Fig. III-3. Switching ratio for a CdS film measured through a capacitive short as a function of peak to peak ac voltage amplitude.

Second, the CdS films should be of high quality with few atomic point defects. This requirement follows from the necessity that light injected electrons contribute to the shallow trap population where they are free to move and change the depletion width with each cycle of the ac voltage. Electrons falling in deep traps of the sort caused by point defects, are not sufficiently free to move. High deep trap density will degrade both light sensitivity and turn on time.

2. Cadmium Sulfide Process Variables as they Affect Device Sensitivity

During the period covered by this report, work has been done on three different methods of preparing CdS films.

- Cadmium sulfide evaporation followed by H_2S standard heat treat (refer to Technical Report No. 6).
- Cadmium sulfide evaporation followed by H_2S recrystallize heat treat (refer to Technical Report No. 6).
- Cadmium sulfide sputter reactive deposition.

Tables 9 and 10 summarize data for equivalent circuit light valve performance with each of these three types of films. As can be seen, the sputtered films are better in every respect. They are approximately an order of magnitude more sensitive and more than an order of magnitude faster.

These improvements have resulted in part from one of the two criterion set forth in the section on the photoelectric performance model. Increased light absorption is possible near the CdTe interface by simply lowering the substrate temperature during film deposition. This produces graded absorption films.

However, a dramatic improvement has resulted in response time as well in sputtered films. This is not a result of model considerations, but apparently from the fact that the sputtering process is a lower temperature process. A correlation of the thickness of ITO and/or higher temperature processing of CdS with a long decay tail resembling that of standard heat treat films has been observed. The problem of substrate response time is still being actively pursued.

Table 9. Substrate Performance Data

CdS Type	Surface Preparation	100 μW/cm² Switching Ratio	Saturated Switching Ratio	100 μW/cm²	
				On Time, msec	Off Time
Evaporated and H_2S heat treated, 12 μm thick 200 Hz	Before polish, Ag contact	1.3	2.5	20	15 sec
	Chemomechanical polish, Ag contact	1.3	2.5	20	15 sec
	Chemomechanical polish, CdTe contact	1.3	2.5	20	15 sec
Sputtered CDS — uniform 18 μm thick 200 Hz	Before polish, Ag contact	1.8	3.5	20	250 msec
Sputtered CDS — graded 18 μm thick 200 Hz	Before polish, Ag contact	2.1	3.5	30	100 to 500 msec
	Chemomechanical polish, CdTe contact	2.1	3.5	30	350 msec
2 kHz	Chemomechanical polish, CdTe contact	1.6	2.0	50	100 msec

T1653

Table 10. Switching Ratio and Time Response for Different CdS Films

8 kHz Averaged Data	Dark	100 $\mu W/cm^2$ 0.5 sec Dynamic Switching Ratio	Saturation Switching Ratio	400 $\mu W/cm^2$, 30 Hz		100 $\mu W/cm^2$ Decay, Percent 3 sec
				Modulation, Percent	Decay, Percent 0.03 sec	
Standard Heat Treat	1.63	1.20	2.0	16	40	60
Recrys. Heat Treat	1.7	1.18	1.9	19	54	88
Sputtered, Standard (graded, 400 Å ITO)	1.47	1.55	2.1	49	75	100

T1652

Improvements in response time and sensitivity in sputtered films are still expected because of the flexibility of the sputtering process. The effects of the various sputter deposition variables on CdS films are still not well understood.

3. Properties of Sputtered Graded CdS Films

Table 11 summarizes data for many sputter deposition runs. The striking feature of this table (besides the improved performance indicated in Tables 2 and 3) is the good reproducibility in preparing sputtered films with controlled characteristics. This is particularly noteworthy with respect to heat-treated films.

Table 12 gives gray scale data for one of the films of Table 10. It can be seen that appreciable 200 Hz switching ratio exists for 10 $\mu W/cm^2$ input light intensity. However, despite improvements in sensitivity, decay time, and reproducibility, three problem areas exist: visible surface defects, low frequency spatial uniformity, and low light level slow on-time.

With regard to the visible defect problem, we have observed several sources of particle inclusions in CdS sputtered films such as poor glass surface polish, dust accumulation, peeling support fixture particle inclusions, and hot pressed CdS target decomposition. Of these, we have attacked each with noted improvements at each point. The glass surface polish is now quite good. Dust accumulation and target decomposition problems have been considerably reduced by sputtering up. Support fixture peeling has been eliminated. The remaining inclusions are thought to come from the hot pressed target and plans are under way to alleviate this source by using a matrix polycrystalline CdS target.

Test of a small diameter polycrystalline target has shown that target particles can indeed be dramatically reduced or eliminated. However, this solution has not yet been adopted on a production scale.

With respect to the low frequency spatial uniformity problem, we presently avoid this problem by high frequency operation. However, low frequency operation is sometimes desirable for higher sensitivity or dynamic range.

Table 11. Switching Rates and Time Response for Sputtered CdS Films

8 kHz Sample	Dark	Switching Ratio 0.1 sec	Switching Ratio 1 sec	Dynamic Switching Ratio 0.5 sec	Saturation Switching Ratio	Modulation, Percent	Decay, Percent 30 msec
SP23e	1.4	1.50	1.56	1.56	2.1	71	83
SP26d	1.4	1.46	1.46	1.46	2.0	58	100
SP30a	1.3	1.64	1.85	1.85	2.1	50	77
SP31a	1.1	1.53	1.61	1.61	2.4	60	85
SP32a	1.3	1,92	2.0	2.0	2.57	84	84
SP34a	1.3	1.53	1.69	1.69	2.3	73	84
SP37e	1.3	1.50	1.62	1.62	2.2	64	90
SP37f	1.5	1.43	1.50	1.50	2.1	60	100
SP43a	1.6	1.37	1.37	1.37	1.75	25	55
SP44	2.0	1.42	1.52	1.52	1.80	25	53
SP45f	1.9	1.52	1.52	1.52	2.0	45	69
SP48c	1.4	1.35	1.42	1.42	2.1	50	88
SP49a	1.8	1.33	1.33	1.33	2.0	55	100
SP56	1.7	1.52	1.64	1.64	2.05	35	57
SP66c	1.3	1.46	1.60	1.60	2.3	25	44
SP67b	1.5	1.40	1.46	1.46	2.15	44	73

T1650

Table 12. Sputtered 12 μm CdS Film

Light Intensity	Switching Ratio	On 60%	Off 70%	
10 $\mu W/cm^2$	1.43	100 msec	4 sec	
40	1.7	30	1.5	
100	1.85	15	600 msec	200 Hz
400	2.1	7	200	
sat	2.35	≤5	70	
10	1.1	250 msec	30 msec	
40	1.3	50	30	
100	1.5	20	50	2 kHz
400	1.75	10	30	
sat	2.1	≤5	15	

T1654

It is presently thought that low frequency spatial variations come from breakdown of the sensitive CdS-CdTe junction. It is then reasoned that CdTe polishing would be more desirable than CdS polishing to avoid damaging that critical interface. We have successfully polished CdTe on CdS but no further work has been done to verify the junction damage hypothesis.

Finally, with respect to improved turn-on time, we predict that (based on the charge storage diode model), theoretical improvements of over an order of magnitude are possible. These improvements will result from lower deep trap densities. Lower deep trap densities are expected if the orange low temperature layer of CdS near the CdTe layer is replaced by a $CdS_{1-x}Se_x$ layer. Graded light absorption will then result from a graded band gap structure with fewer atomic defects.

C. Reflective Mode AC Light Valve Dielectric Mirror

1. Design Considerations

The dielectric mirror used in the large screen projection reflective mode ac light valve is designed to have a broad spectral reflection band of greater than 85% from 400 to 650 nm. For use at a specific wavelength, such as the helium neon laser readout at 632.8 nm of the optical data processing light valve, it is advantageous to design a mirror that has a narrower reflection band centered at the desired wavelength. This has two primary advantages:

- The mirror can be designed to give a higher reflection at the specific wavelength than will be the result of the broad spectral band mirror.
- The mirror will require fewer high-low index film pairs and thus will be thinner in total thickness. The result will be that more of the voltage switched by the light activation of the photoconductor will fall across the liquid crystal layer instead of the dielectric mirror.

The design of the dielectric mirror requires calculation of the reflectivity of a multilayer stack of transparent dielectric quarter-wave films of alternate high and low indices of refraction, n_H and n_L. The general formula relating the normal incidence reflectivity for a stack of films of abritrary thickness and index of refraction is given by[13]:

$$R = \left(\frac{n_o - \frac{C}{B}}{n_o + \frac{C}{B}}\right)\left(\frac{n_o - \frac{C}{B}}{n_o + \frac{C}{B}}\right)^*$$

$$\begin{bmatrix} B \\ C \end{bmatrix} = \left\{\prod_{r=1}^{N} \begin{bmatrix} \cos \delta_r & i \sin \delta_r / n_r \\ i n_r \sin \delta_r & \cos \delta_r \end{bmatrix}\right\} \begin{bmatrix} 1 \\ n_{N+1} \end{bmatrix}$$

where

$$\delta_r = \frac{2 n_r d_r}{\lambda_o}$$

and

N = total number of films in stack

n_o = index of incident medium

n_r = index of r^{th} film in stack

n_{N+1} = index of substrate

d_r = physical thickness of r^{th} film

λ_o = peak wavelength.

This formula was solved by computer for the following alternating pairs of high and low index dielectric materials with an optical thickness for all films of one quarter wave:

1. Zinc Sulfide (ZnS) $n_H = 2.35$
   Cryolite (Na_3AlF_6) $n_L = 1.33$

2. Titanium dioxide (TiO_2) $n_H = 2.45$
   Silicon dioxide (SiO_2) $n_L = 1.44$

The substrate was the CdTe light-blocking layer of index $n_{N+1} = 2.67$. The peak wavelength is taken as 632.8 nm. The results are given in Table 13 for up to ten alternating layers.

Table 13. Reflectivity of Dielectric Mirrors
Substrate: CdTe n = 2.67 λ_o = 632.8 nm

Number of Films on Substrate	Transmission, % ZnS/Na_3AlF_6	Transmission, % TiO_2/SiO_2
0	23	23
1	6.03	3.3
2	63.88	61.14
3	44.36	35.54
4	86.45	84.42
5	77.28	70.35
6	95.45	94.32
7	92.08	88.58
8	98.52	98.00
9	97.39	95.90
10	99.52	99.30

T1655

The results show that after large initial increases, the reflectivity changes very slowly (94 to 99%) after a total of six films are deposited. With just a four-layer mirror, a peak reflectivity of ~86% can be obtained. The broad spectral band light valve dielectric mirror typically has 14 layers so that a reduction of total mirror thickness (considering a six-layer narrow band mirror) from 1.2 to 0.5 μm will result. Such a reduction of thickness becomes a factor in light valve performance when the liquid crystal layer thickness is of similar

thickness, i.e., 2 μm. For this thickness of liquid crystal, under the normal operating conditions of the light valve, the maximum switching ratio obtainable can be increased from 2.50 to 2.75 by this thickness reduction.

Thus, the mirror design for the optical data processing light valve was finalized as a six-layer mirror centered at 632.8 nm. This design is a good tradeoff between overall reflectivity and a minimization of total mirror thickness.

The reflectivities presented are for the dielectric mirror without any additional layers. However, the liquid crystal alignment technique (as described in Section II-D) requires an amorphous layer of SiO_2 in direct contact with the liquid crystal. To minimize reflection loss from this additional low index film, the optical thickness is chosen to a multiple of a half-wave of the peak wavelength. Then this film acts as an "absentee layer" in that it does not reduce the reflectivity but maintains it at the initial value.

2. Dielectric Mirror Fabrication

The dielectric mirror fabrication techniques have been developed under parallel internal research programs and on other contracts. In summary, the prime consideration was to choose optical materials that have electrical, mechanical, and optical properties compatible with ac light valve operation. Besides the requirements of being transparent dielectrics of either high or low index, the films must have high dielectric breakdown strengths to withstand the electric fields used in the light valve. In addition, the films must be matched for stress to avoid crazing and lifting from the substrate, and they must be inert in contact with the liquid crystal.

After experimental evaluation of many systems, two pairs were found to meet these requirements: the aforementioned thermally evaporated zinc sulfide/cryolite and reactively sputtered titanium dioxide/silicon dioxide. The pair used in all the optical data processing light valves was the thermally evaporated ZnS/Na_3AlF_6 in combination with a passivating layer of either Al_2O_3 or SiO_2. (Because of

processing problems and equipment time limitations, the potentially superior system of reactively sputtered TiO_2/SiO_2 has not been used routinely in light valve production.) The zinc sulfide/cryolite mirrors are deposited with a multihearth electron beam evaporator under a vacuum of $<1 \times 10^{-5}$ Torr. The film thicknesses are monitored optically using interference filters to choose the peak wavelength, and the substrates can be heated during deposition up to 350°C by a bank of quartz infrared lamps.

The amorphous SiO_2 film used for liquid crystal alignment and as an inert interface is rf sputtered by conventional techniques.

3. Antireflection Coatings for the Light Valve Counterelectrode

Observations of the projection screen of the initial 45° twisted alignment light valves with laser readout between crossed polarizers showed a series of parallel fringes not associated with the fringes due to liquid crystal thickness nonuniformity. The fringes appeared to be associated with interference between reflections from the two counterelectrode interfaces; however, direct reflections from the interfaces cannot pass through the crossed analyzer because there is no net phase retardation in the isotropic counterelectrode. An explanation for this phenomenon is possible if back reflections from the counterelectrode surfaces through the liquid crystal to the dielectric mirror are considered. This situation is illustrated in Fig. III-4(a) where two possible reflections from the two counterelectrode surfaces are shown passing through the liquid crystal, reflecting from the dielectric mirror and leaving the light valve. (The non-normal angle is for clarity.) If any birefringence exists in the liquid crystal due to a partially activated state, a phase retardation will occur in the two back reflected rays. This retardation will allow a component of the reflected rays to pass the analyzer and thus be visible on the projection screen. And then if the counterelectrode surfaces are not parallel, a series of parallel interference bands will be seen.

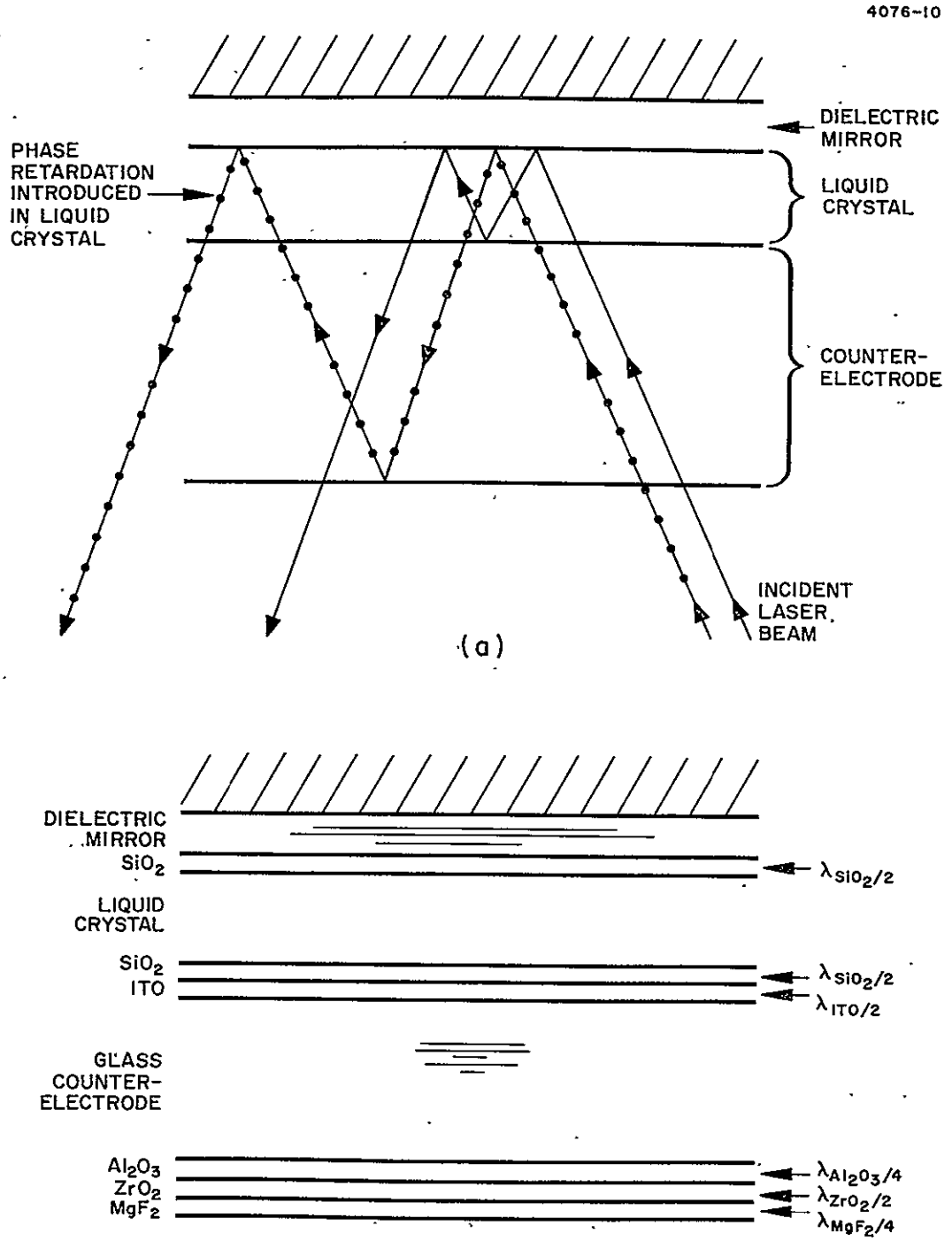

ig. III-4. (a) Schematic of possible internal coherent light reflections in light valve. (b) Schematic of antireflection properties of light valve films used to eliminate reflections.

The solution to this problem is to ensure that the counter-electrode surfaces were extremely parallel after the glass polishing procedure. This is described in Section IV-A and IV-B. The other step was to antireflection-coat the surfaces to minimize the magnitude of the backreflected rays. Without antireflection coatings the reflectivity from the counterelectrode surfaces could be as high as 11%. The antireflection-coated counterelectrode configuration is shown in Fig. III-4(b). A three-layer quarter-half-quarter wave coating[14] of Al_2O_3, ZrO_2 and MgF_2 was deposited on the outer surface of the counterelectrode which resulted in a reflection of <0.3% at this interface. (The common single layer AR coating of MgF_2 has a minimum reflectivity of 1.3%.) The interface between the glass, indium tin oxide (ITO), silicon dioxide, and liquid crystal is treated by making the ITO and silicon dioxide half-wave in optical thickness at 632.8 nm so that they act as "absentee layers" with no net reflectivity change. Then because of the close index match between the glass and liquid crystal, the reflectivity will be near zero. Because of the absorption in the ITO, this condition is not exactly met, and experimentally, total counterelectrode reflectivities of <0.8% have been observed. These procedures have eliminated the set of interference fringes and thus the AR coatings have been incorporated in all ODP light valves.

IV. OPTICAL QUALITY

A. Compatibility of Commercially Available Substrates

Prior to the more critical requirements of optical flatness and parallelism imposed by the Optical Star Field program, ac light valve research was carried out on commercially available indium-tin oxide coated glass. Measurements of these 1/8 in. substrates, from both Pittsburgh Plate Glass and Optical Coating Laboratories of Santa Rosa, California, showed completely unacceptable optical properties.

Silvering quality 1/4 in. indium-tin oxide coated substrates were purchased from Optical Coating Laboratories, Inc. and proved to be considerably better than the 1/8 in. glass. Hand selection, with a rejection of approximately 20%, yielded substrates flat to within one-half wave and parallel to within two waves across the 1-3/4 in. substrates. Surface condition of these substrates is typical of that of float processed glass. Random handling abrasions, a relatively low density $<5/cm^2$ of pits and inclusions can be seen under low power microscopic inspection. While these substrates represented an improvement over previously used material, it was evident that they would not satisfy the program goals. The best surface flatness and finish obtainable is desirable on the CdS side of the substrate, while standard commercial polish would suffice for the input side. The opposing substrate, on the other hand, requires both faces to be flat and also parallel with one another, and possess a scatter-free surface.

To this end, polishing experiments were performed at the HRL polishing shop directed toward producing one quarter wave or better surfaces on 1/4 in. and 3/8 in. glass. While excellent surfaces could be obtained on this material when mounted on the polishing backing plate, removal from the plate caused deformation to occur. These experiments led to the use of 1/2 in. thick, fine annealed BK7-A or BSC-2 glass as substrate material. Twelve optical flats of BSC-2 glass 1/2 in. thick by 1-3/4 in. x 1-1/4 in. were purchased from Esco Products of Oak Ridge, New Jersey. These flats were one-tenth wave

on both faces and parallel to 0.000024 in. Careful inspection revealed a uniform haze of extremely fine pits observable only under intense light and a dark background. This finish is standard for most optical work and results from inadequate fine grinding before polishing. Larger pits which may be filled with minute quantities of glass and polishing oxides can be the source of anomalous film growth patterns and contamination.

Subsequent orders specified a reticle quality finish. These substrates, carefully ground with successively finer grits to a 5 μm finish before polishing with ceric oxide have been found to yield a completely defect-free surface and have become the standard used for all critical evaluation and delivery cells.

B. Reprocessing Studies

Investigations were carried out to determine whether the substrates could be reused. Optical flats were carefully inspected interferometrically and microscopically before coating with ITO and again after removal of the coating. No significant change in the number of surface defects or flatness of the substrates were observed. Removal of the conductive coating was accomplished by using the RCA Cleaning Procedure.[15] Hydrogen peroxide and ammonium hydroxide to remove organic contaminants by oxidation followed by hydrogen peroxide with hydrochloric acid for desorbing metals and metal oxides.

Confirmation of the above visual observations was obtained by an SEM study made on two 1/2 in. substrates, one with an etched surface and one unetched. Again no significant change was observed because of etching.

Similar results were obtained with indium-tin oxide coated substrates on which CdS had been vapor deposited. Concentrated nitric acid was used to strip the CdS film before using the RCA cleaning procedure. No changes in surface finish or flatness were observed.

Sputtered CdS films, having exhibited significantly better electrical properties, have replaced the vapor deposited films in our ac light valve programs. These films possess an intrinsic compressive stress which bows the flat glass substrate to four fringes or two waves convex. To compensate for this effect, substrates were ground and polished four fringes concave. The stress of the films then brings the optical figure to flat within one half wave or better. Optical flatness better than one half wave might be obtained by the use of specialized polishing techniques that will be the subject of future investigations.

Twelve substrates that had CdS sputtered onto them were stripped off and inspected. All showed some strain when viewed under crossed polarizers. Half showed some deformation of the four-fringe concave figure. Those that showed no deformation of the original figure were reprocessed, but all of these showed some deformation of figure after CdS coating. This group was again stripped of CdS and all 12 samples were annealed according to the following schedule:

1. Room temperature to 560°C and hold for two hours
2. 560°C to 520°C at 5°C/hour
3. 520°C to room temperature at 20°/hour.

This annealing schedule did not completely remove all traces of strain. One local supplier of optical glass, Industrial Glass Co. of Los Angeles, uses a ten-day cycle for fine annealing of optical parts. Considering the fact that the parts are reground and polished after annealing, only the cost of the rough blank would be saved in the stripping and annealing operations. This makes salvaging uneconomical except when dealing with larger quantities. Substrates are now used on a one-time basis. The more costly opposing electrodes, of course, do not suffer from deformation due to stress in the films and, if not damaged in handling, may be recycled several times.

C. Substrate Handling

1. Substrate Polishing

The transmission mode ac light valve applicable to the Star Tracker Coherent Optical Correlator System requires optically flat, ripple-free, scratch-free, contamination-free specular surfaces on the CdS films. Both the vapor deposition method and sputtering method produce films that have a scattering, nonspecular surface finish.

Three practical methods available for the polishing of semiconductors are mechanical, chemical, and chemomechanical.

Mechanical polishing with fine abrasives produces flat substrates, but there is always attendant subsurface damage and fine sleeks are difficult to avoid.

Chemical etching of imperfect crystal lattcies results in surfaces free of subsurface damage, but not optically flat.

Chemomechanical polishing is a compromise between the two. The abrasive, softer than the material being polished, is dispersed in a chemically reactive solute or incorporated into the matrix of the polishing pad. The reactive solute acts as a mild chemical etchant, while the polishing gently planes the surface, removing the reaction product, thus producing a flat surface free of damage.

Little work has been done on polishing of II-VI compound such as CdS. The chemical polishes listed, such as fuming nitric acid plus glacial acetic acid or $K_2 Cr_2 O_2$ in 16N sulfuric acid, developed hexagonal pits and a discontinuous, irregular sulfide film.

Several chemical etchants have been reported for the III-V semiconductors and we have studied their effects on our CdS films. The etchant consists basically of an organic liquid in which a halogen, generally Cl_2 or B_2, is dissolved. During the program the following chemical etch solutions have been investigated:

1. Bromine in Methyl Alcohol

For slow etching rate, 0.01 to 1.0% Br_2 in methanol was tested. Although the low

concentration solution did not alter the surface after 15 min of polishing, it reacted with the CdS immediately upon contact, forming a dull surface with pits (orange peel-like). As a result, it was judged to be unacceptable for this role.

2. Iodine in Methyl Alcohol

Iodine dissolved in alcohol solvent is less reactive with the CdS surface; it resulted in no surface effects such as pits or haze. One to two percent iodine in methyl alcohol solution is a useful etchant, but did not provide the polish desired. Furthermore, we found that the very slow polishing rate of this chemical could not be increased by higher iodine concentration.

As a result of these investigations, a chemomechanical experiment was performed. Good chemomechanical polishing was achieved on evaporated CdS with an etching solution of iodine and cab-o-sil in alcohol, using a bulbous paper lap. Cab-o-sil is a submicroscopic fumed silica with very high chemical purity, extreme fineness (particle size from 70 to 500 Å), and large external surface area. This silica powder was added to the etching solution for multiple purposes:

1. Gentle mechanical polishing of the surface
2. Increasing the viscosity of the solution, resulting in a more even polishing across the surface
3. Reducing solvent evaporation and create a thin lubricating layer between the polishing pad and CdS to eliminate mechanical scratching of the substrate.

Comparing the chemomechanical polished films in completed devices with films that were mechanically polished, it was found that although much less macrosurface damage was observable in the chemomechanically polished films, they showed only slight improvement in image quality. We attributed this observation to the display system used for evaluation, which is very sensitive to the orange-peel-like surface characteristics of the chemomechanical polish techniques.

These early experiments were performed by hand polishing methods and necessarily suffered from lack of control. The next step was to control more accurately the polishing speed, etchant flow and interaction time. Figure IV-1 shows the automatic polishing mechanism developed for this purpose.

The machine is a Lapmaster 12, from Crane Packing Co., modified specifically for our purpose. A 12 in. polishing wheel rotates at 60 rpm. Buehler AB Kitten-Ear polishing pads are used. Three idler wheels are attached to the frame of the machine 120° apart so that the drive plates, driven from a central friction drive wheel, rotate freely against them. Three substrate holders are symmetrically attached to the drive plates by means of adjust screws. The speed of the friction drive wheel may be adjusted to rotate the drive plates at a rate of 0 to 10 rpm. The polishing pad is precharged with a solution of transene and cab-o-sil. The solution of 2% iodine in transene is introduced by pipette feed. Polishing pressure may be adjusted with weights secured to the drive plates.

Experiments were performed at optimizing the polishing process. Polishing pressure, drive plate speed of rotation, iodine solution rate of introduction, and time of polish are all independently adjustable parameters. It was found that by limiting the iodine solution rate to 1 drop/sec, so that a relatively dry pad is maintained and increasing the polishing time to 24 min with a minimum of polishing pressure 18 g/cm^2, the orange-peel effect could be greatly reduced. This procedure yields consistent results of a highly specular finish with little or no streaks. Streaks and scratches that do occur are found to be caused from edge chipping or inclusions in the CdS coming loose during the polishing run. The polishing cycle is terminated with a 2 min polishing with transene only, as a first step in the cleaning process.

2. Contamination Studies

Cleaning of substrates after polishing proved to be more of a problem than first suspected. The polished CdS layer, while

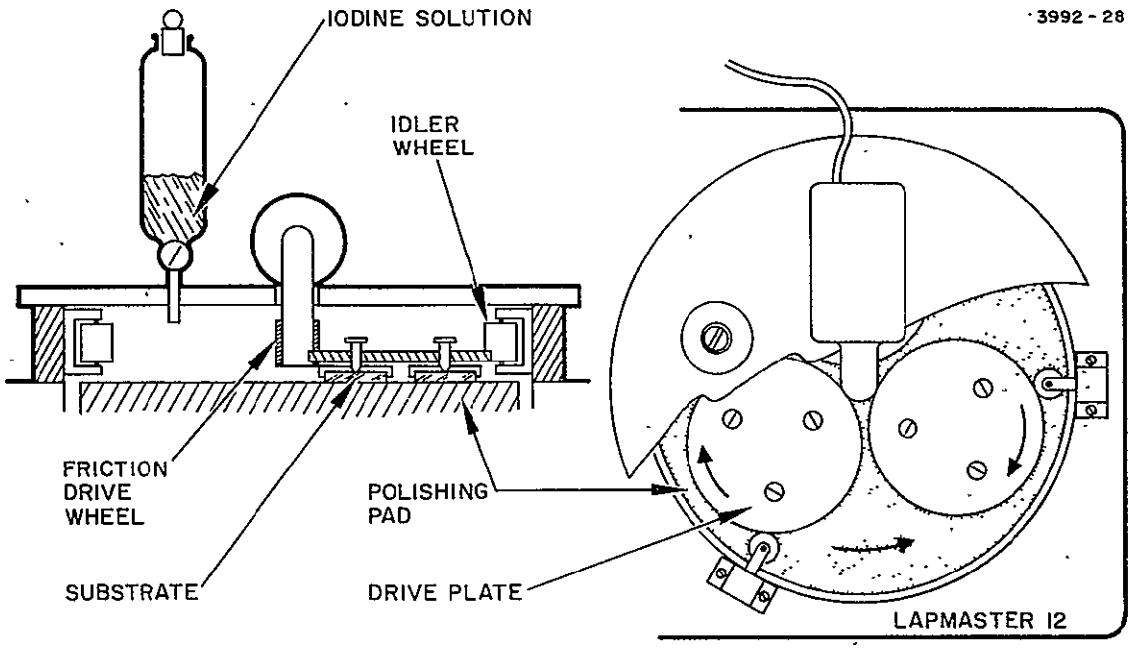

Fig. IV-1. Chemomechanical polishing machine.

specular in finish, scatters light somewhat as a result of the very fine crystalline nature of the films. This makes critical examination of the surface difficult. Many samples showed random patches of haze only after the subsequent deposition of CdTe. As an attempt to identify the cause of the haze, which severely affects the optical properties of the film, and which may also strongly influence the photosensor response of the light valve, an Auger analysis of the CdS film surface was made. Photosensor measurements were made on the same films to provide additional correlation. It was hypothesized that this haze was particles of Cab-o-Sil polishing powder imbedded in the soft CdS surface that had not been removed by subsequent cleaning. Four types of evaporated CdS film surfaces (all having been H_2S thermal processed) were analyzed:

1. No polish
2. Chemomechanical polish with Transene-Iodine-Cabosil slurry
3. Mechanical polish with Linde B on Kitten-Ear mat
4. Mechanical polish on bibulous paper.

Photosensor measurements on the substrates indicated that the non-polished and chemomechanical polished samples showed similar photoelectrical behavior; the mechanically polished samples showed a severe increase in dark current and a longer response time. The effect of ion beam sputtering of the CdS surface in argon was similar to mechanical polishing; mild anneal in air or in argon of mechanically polished films tended to improve their photoelectrical characteristics.

The Auger analysis of these same films showed the same impurities on all samples. Carbon, oxygen, and chlorine in relatively similar quantities were found on the surfaces; sputter etching of less than 50 Å greatly reduced the quantity of these materials indicating that the impurities were absorbed on the surface rather than being distributed in the bulk of the film. There was no evidence of polishing compound residue on the polished samples which indicates that the

chemomechanical polish haze is a surface texture of cadmium and/or sulfur. In addition, a correlation was found between the cadmium to sulfur ratio left following polishing and the surface treatment. In general, high cadmium to sulfur ratios were indicative of the no polish and chemomechanically polished substrates; ion beam sputtering and mechanical polishing tended to produce lower ratios. The physics underlying these observations is not yet clear. However, it appears that excess cadmium, which creates shallow donors, gives an accumulated surface condition that is beneficial to good photoelectrical performance of the CdS in the light valve.

3. Cleaning

Continued experience in polishing and cleaning of the substrates led to a cleaning process which has reduced the haze problem substantially. The following cleaning process is based on the general assumption that the surface haze is produced by continued chemical etching taking place after removal from the machine but before removal of the etchant in the cleaning.

1. Two-minute transene flush of the polishing pad as a termination of the polishing cycle
2. Removal from polishing machine and immediate rinse in transene (do not allow to dry).
3. Immediately ultrasonic in fresh transene (10 min)
4. Thoroughly rinse with transene from squirt bottle
5. Spin dry in warm air flow
6. Inspect, using a high intensity light at grazing incidence under 7 to 30 power B&L Stereo Microscope.

It was found that it is important to keep the cleaning solutions in active contact with the substrate. The process must be continuous to be effective.

D. Manufacturing Technique

Several methods for cell assembly were attempted to obtain reproducible, uniform twisted nematic alignment in the light valve devices. Of the three methods most commonly used, one remained as the most consistent for all light valves fabricated.

The first and most consistent method is to apply the liquid crystal in a narrow (~1/8 in.) strip across the width of the mirror substrate approximately one fourth of the length from one end with a clean glass rod. A Mylar spacer is placed on this substrate so that the aperture edge is almost on this strip of liquid crystal (trying to keep the aperture completely clear, and free of any liquid crystal). Another strip of liquid crystal is then put on top of the spacer in the same place as the original strip. The opposite electrode is then placed (parallel with the first) with one edge almost completely in the second strip of liquid crystal and the substrate then slowly lowered down onto the first substrate so that the liquid crystal is spread over the entire cell aperture evenly. The two substrates are then squeezed together so that any bubbles may escape, and the assembly is tightened into a cell holder.

The second method is essentially the same as the first, except that each substrate is precoated with a thin layer of liquid crystal to promote parallel alignment that is homogeneous on each surface. This is accomplished by initially applying a thin (~1/8 in.) strip of liquid crystal across the width of each substrate with a clean glass rod. By drawing a bead of liquid crystal, held between a clean glass rod and the substrate, across the surface of the substrate (without touching it with the glass rod), an even coat of liquid crystal is applied across the surface. It was hoped that this method would allow each substrate surface to align parallel without any interference from the opposing electrode wall forces, and then when more liquid crystal was added, and the cell assembled, the bulk liquid crystal could orient itself with respect to the prealigned walls. The problem with this method was that it wasted a lot of liquid crystal.

The third method is very simple and related to the second method. The second method is used in every way until the two substrates are ready to be put together. The substrates are assembled as if for a parallel cell, and after a few minutes, the electrodes are rotated with respect to each other to the desired angle. The problem with this method is that a circular aperture is desirable to avoid cutting the corner of a square aperture when the substrates are twisted.

1. Spacers

Depending on the desired thickness, the spacers used were either Mylar film of the desired thickness, or for thinner cells, SiO_2 evaporated in a spacer pattern directly on the electrode opposing the mirror.

Mylar spacers, 6.3 and 12.7 μm, were used for thicker cells and were obtained, precut, from an outside source. The spacer was in the same configuration as a picture frame, with the border extending over the edges of the substrates to avoid shorting between the electrodes.

For the thinner cells, 2 or 4 μm films of SiO_2 were deposited directly on the transparent electrode in a pattern similar to that of the Mylar. These cells were made from thicker glass substrates to avoid warpage when the screws in the cell holder were tightened.

2. Thickness Uniformity

To ensure uniform thickness, especially in the 2 and 4 μm cells, 1/2 in. or 3/8 in. glass was used after being polished to $\lambda/10$ or $\lambda/4$ specifications or optical flats were used directly (see Section IV-A). These glass substrates, together with the evaporated SiO_2 spacer, ensured uniform thickness across the cell aperture. In addition, 1/16 in. thick rubber pads were placed in the cell holder between the cell and the holder itself to control thickness when tightening the cell holder screws. This allowed fine thickness tuning when the cell was in the projection system.

V. DEVICE PERFORMANCE EVALUATION AND RESULTS

This section describes the equipment and the procedures used in testing the ODP light valve for the following properties:

1. Sensitometry (percent transmission versus exposure light level)

2. Modulation transfer function (MTF) showing percent of intensity modulation as a function of resolution

3. Response time, rise times to 90% transmission, decay times to 10% transmission, and cycle times as a function of exposure time and intensity level

4. Optical quality, including flatness of facing electrode and liquid crystal layer, and blemishes and liquid crystal alignment interruptions on the surfaces.

A. Test Setup Description

The test facility used consists of two main projection systems: (1) a 500 W xenon arc reflection mode projection system (Fig. V-1) for use where high intensity projection light levels are needed to improve signal-to-noise in the measuring instruments, and (2) an 18 mW, helium-neon laser optical data processing projector and test bench (Fig. V-2). The associated instruments used for specific tests are described under the appropriate test heading below. Both projectors, however, are used for observing optical quality and general performance in an ODP light valve.

1. The Sensitometry Measuring System

The sensitometery measuring system consists of the xenon projector assembly (Fig. V-1) for operating the light valve and a calibrated radiometric intensity level detector (United Detector Technology Model 11A) placed in the transmission image plane of the light valve. A red filter (615 nm wavelength peak transmission) is placed in the projection beam to simulate helium-neon laser emission

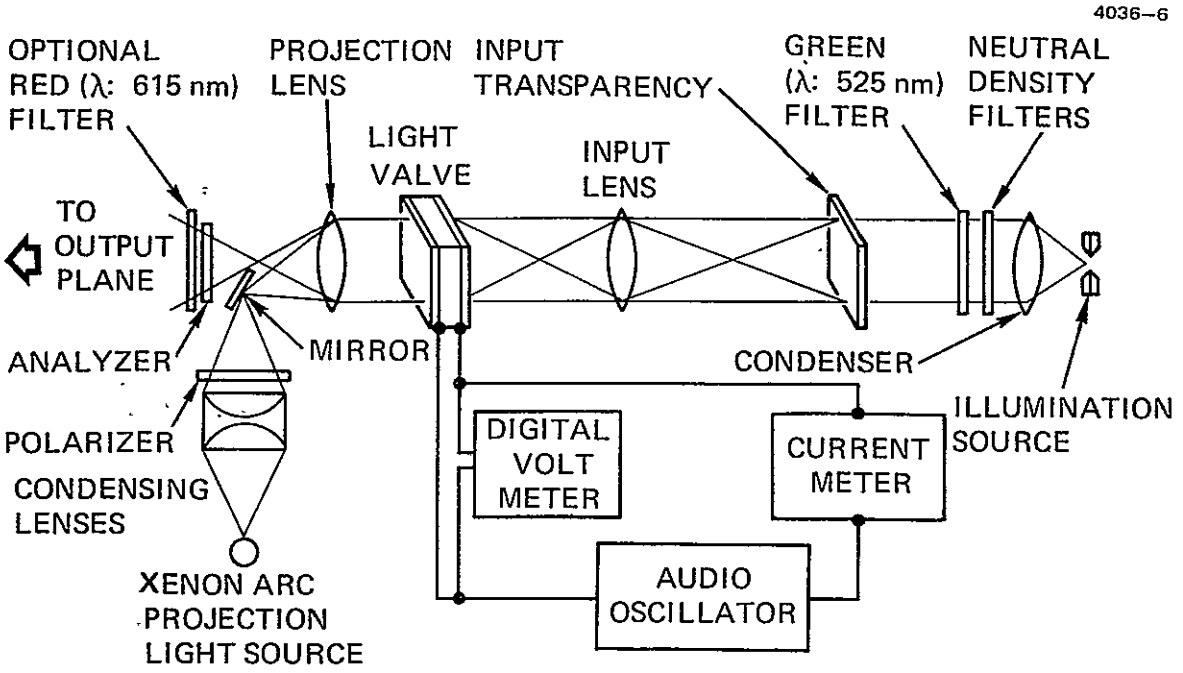

Fig. V-1. Schematic of reflection mode projection system for the field-effect ac light valve.

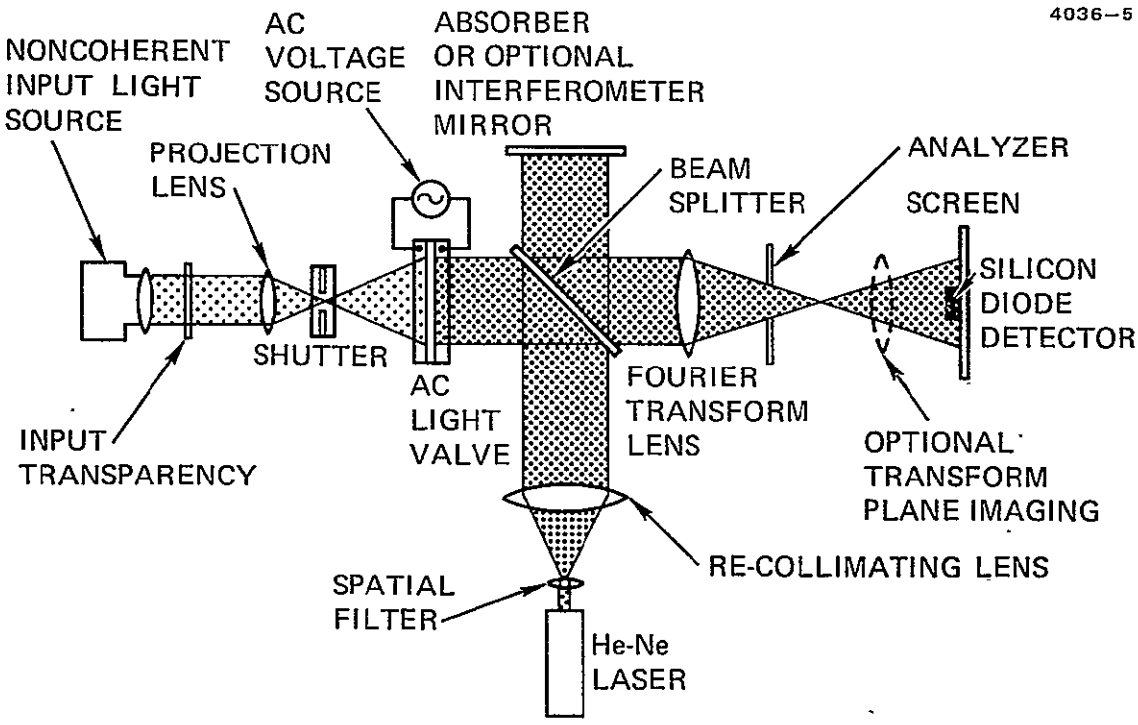

Fig. V-2. Schematic of optical processor using reflection mode ac light valve.

incident on the radiometric detector. A green filter (525 nm lambda) to simulate the P-1 phosphor is placed in the illumination beam. An ac bias voltage is applied across the light valve at or slightly below the dark threshold of optical response (Vth). The illumination light level at the input to the light valve (CdS layer) is then varied by inserting the calibrated neutral density filters in the beam. The transmission intensity in the image plane of the projection beam is then recorded as a function of input light intensity to yield a typical sensitometry curve as shown in Fig. V-3.

Modulated Transfer Function Measuring System

The modulated transfer function (MTF) measuring scheme utilizes the same xenon projector assembly as the sensitometry system above. A Sayce Resolution Chart is used to image a continuously varying spatial frequency line pattern at the input to the light valve (10 lines/mm to 200 lines/mm). When an operating bias is applied to the light valve the line pattern is projected to the image plane with magnification of 50 to 70x. The projected line pattern is then mechanically scanned with a photodiode detector which is 500 μm in diameter. The intensity distribution of the image (lines and spaces) is then recorded on an x-y recorder as a function of detector position on the line pattern. The limiting spatial frequency of this system when used with 70x magnification in the projection plane and a 500 μm diameter detector is 140 lines/mm at the light valve. The data obtained in this manner show contrast as a function of resolution for the light valve and the projection optics. Using the equation

$$\frac{I_L - I_S}{I_L + I_S} \times 100 = \% \text{ modulation},$$

where I_L is the intensity at a line and I_S is the intensity at a space, the percent modulation for the light valve and projection optics at each spatial frequency may be calculated. This percent modulation product of light valve and optics must then be divided by the percent modulation

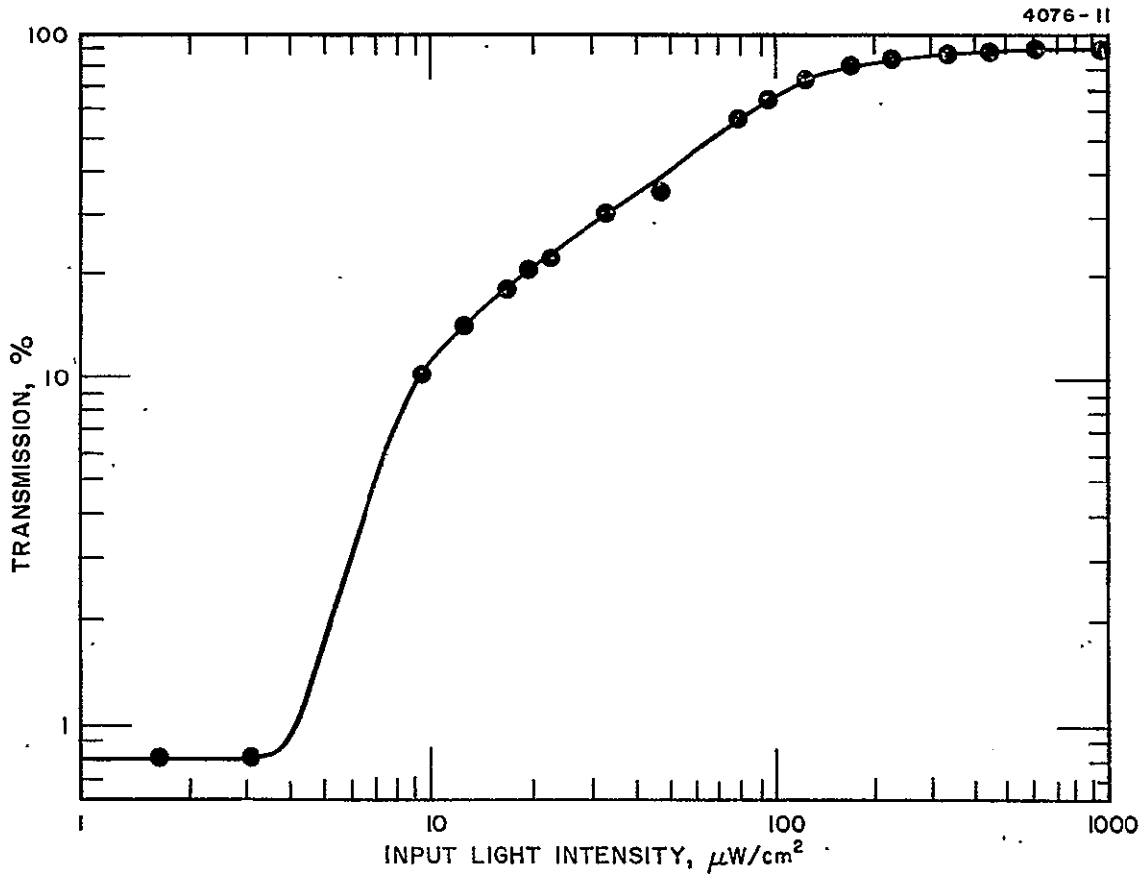

Fig. V-3. Sensitometry of the optical data processing light valve.

caused by the optics (also a measured value) at each spatial frequency to obtain the data for plotting the light valve MTF curve. A characteristic MTF curve of the light valve is shown in Fig. V-4. When contrast ratio is defined as I_L/I_S, then 50% modulation corresponds to a contrast ratio of 3:1.

3. Response Time Measurements

The laser optical data processing bench was used for all response time measurements. The exposure time of the illumination beam was controlled by an Ilex Universal No. 4 shutter. The exposure intensity was controlled by the voltage applied to the tungsten lamp illumination source. The input image transparency used was a Standard Air Force Resolution Chart. The projection optics were chosen to place the coherent readout image on the projection screen with approximately 20x magnification. A silicon photodiode with a response of better than 10 kHz was placed in the large rectangle of the projected image to generate a signal proportional to the projection intensity as the light valve is switched on and off. A Tektronix model 454 oscilloscope and a Tektronix model C-40 camera were used to record the photodiode signal as a function of time to give the rise, decay, and cycle time data. The oscilloscope calibrated sweep was used as the time reference and the shutter exposures were calibrated to this reference. The exposure intensity was calibrated to a United Detector Technology Model 11a Radiometer. The ac 10 kHz bias voltages applied to the light valve for time response measurements were set at the threshold voltage (Vth) unless otherwise indicated. The image was observed on the output screen during the measurements to verify that high resolution images were being projected. Some typical response measurements will be shown and discussed in Section V-C.

4. Device Optical Quality Evaluation

Both the large xenon projector and the laser projector were used to evaluate various characteristics of optical quality. The

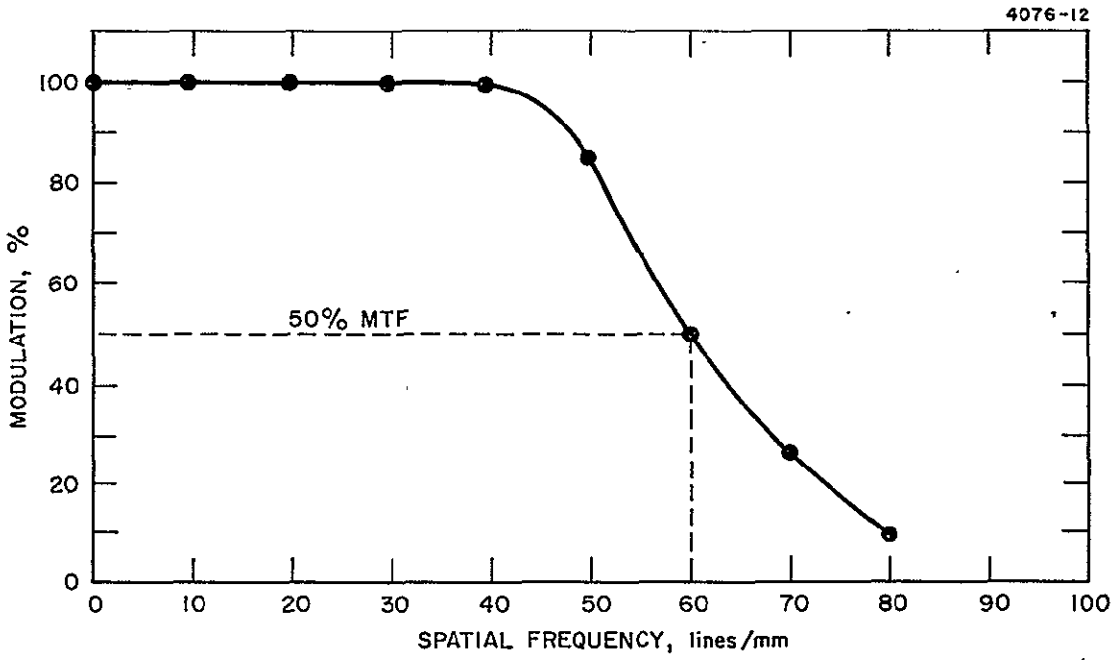

Fig. V-4. Modulation transfer function of the optical data processing light valve.

xenon projector with high magnification was used to observe blemishes in the films to assist in ascertaining their origin, to observe and adjust thickness and uniformity of the liquid crystal layer, to check for birefringence caused by strains in the facing electrodes; and to evaluate the optical characteristics of films such as antireflection coatings.

The laser projector bench was used to further evaluate antireflection coatings by observing fringe contrast in the output plane, to evaluate the flatness of substrates and mirrors by observing the modulation or bending of the coherent wave front when used in the Michelson interferometer configuration, to measure light valve mirror reflectivity or projection beam insertion loss, and to project the transform plane image onto the screen for observation of scattering and cleanliness.

B. Operating Conditions

The light valve operating conditions for all of the testing described here fall into a relatively narrow range. This is primarily because of the similarity in the characteristics of the components which make up the device. Ranges for typical operating conditions are given below.

1.	Operating frequencies of excitation voltage	1 to 20 kHz
	Nominal	10 kHz
2.	Operating excitation voltage amplitude	5 to 7.5 V rms
	Nominal	6.0 V rms
3.	Input illumination level at 5250 Å λ	10 to 600 $\mu W/cm^2$
	Nominal	120 $\mu W/cm^2$
4.	Readout beam at 6328 λ E Vector Horizontal	>3 mW/cm^2

C. Test Results

The following paragraphs contain a description of the test results and some explanation to assist in understanding the data given in graphs and photographs.

1. Sensitometry

The sensitometry curve shown in Fig. V-3 is that of a typical ODP light valve, Cell SP48E. The large xenon projector was used to record these data because of the large dynamic range of illumination light available in that system. The illumination light was filtered to simulate a P-1 phosphor with a central wavelength of 5275 Å and a 50% bandwidth of 233 Å. The projection light was filtered to 615 nm wavelength to enable the use of a radiometric detector. The excitation voltage was 6.09 V rms at 20 kHz with rms current of 5.05 mA. The transmission value obtained with the light valve turned off and the polarizers parallel is represented as 100% transmission on the graph. The analyzer was then crossed to run the data. It can be seen from the graph that with input intensity of 170 $\mu W/cm^2$ the steady state contrast is greater than 100:1. The gray scale content or "shades of gray" of the output can be derived from this curve. If we use the standard sensitometric gray scale step of 0.15 N.D. per step plotted along the input axis of this curve, then cross plot the points of intersection to the output axis, we find that the output contains approximately nine shades of gray.

2. Modulation Transfer Function

The modulation transfer function (MTF) shown in Fig. V-4 is that of Cell SP48E. These data were taken with the large xenon projector, using white projection light to improve the signal to noise of the detector in the high resolution areas of the scan (see test setup description Section A-1). It is expected that the MTF would be higher with monochromatic light, though much more difficult to measure. The MTF of the addressing image has been measured to be 100% at 60 lines/mm when used in the projection mode. The lens used is a

1.0:0.5 finite conjugate lens. Therefore, we may assume that the MTF of the input image for this curve is 100% at greater than 60 lines/mm.

Response Time

The response time data given here have been taken from several ODP light valves, since this is their most widely varying characteristic at the present time. Response times shown here are believed to be mainly controlled by the CdS substrate. This belief is supported by data taken in CdS film studies. The somewhat unusual exposure times are the result of the characteristics and position of the shutter used and the times given are the actual calibrated values. The off-state transmission is within the width of the oscilloscope trace and contract in all cases is better than 30:1. The noise on the top flat portion of the trace is caused by vibrations in the optical bench which in turn cause amplitude noise on the photodetector. Two traces were recorded on one photograph in order to ensure acquisition. Figures V-5 through V-10 are oscilloscope traces of response characteristics with a brief explanation of each.

4. Optical Quality Evaluation

Optical quality tests were made, using the optical data processing bench setup, with and without the optional Michelson Interferometer Mirror, Fig. V-2, and with the large xenon projector assembly, Fig. V-1. Data were recorded both visually and on photographic film. The optical quality characteristics evaluated were uniformity caused by spots and blemishes on the films, liquid crystal alignment, thickness of liquid crystal layer, and substrate impedance variations; and coherent wavefront distortion of the reflected wave.

a. Optical Uniformity — Optical uniformity is controlled by a complex interrelationship of several factors which are difficult to isolate and required the use of both projectors (Fig. V-1 and V-2), to assist in analysis. These factors are the spatial uniformity of the dark (off state) and the illuminated (on state) impedances of the substrate (includes CdS, CdTe and mirror layers); thickness gradients

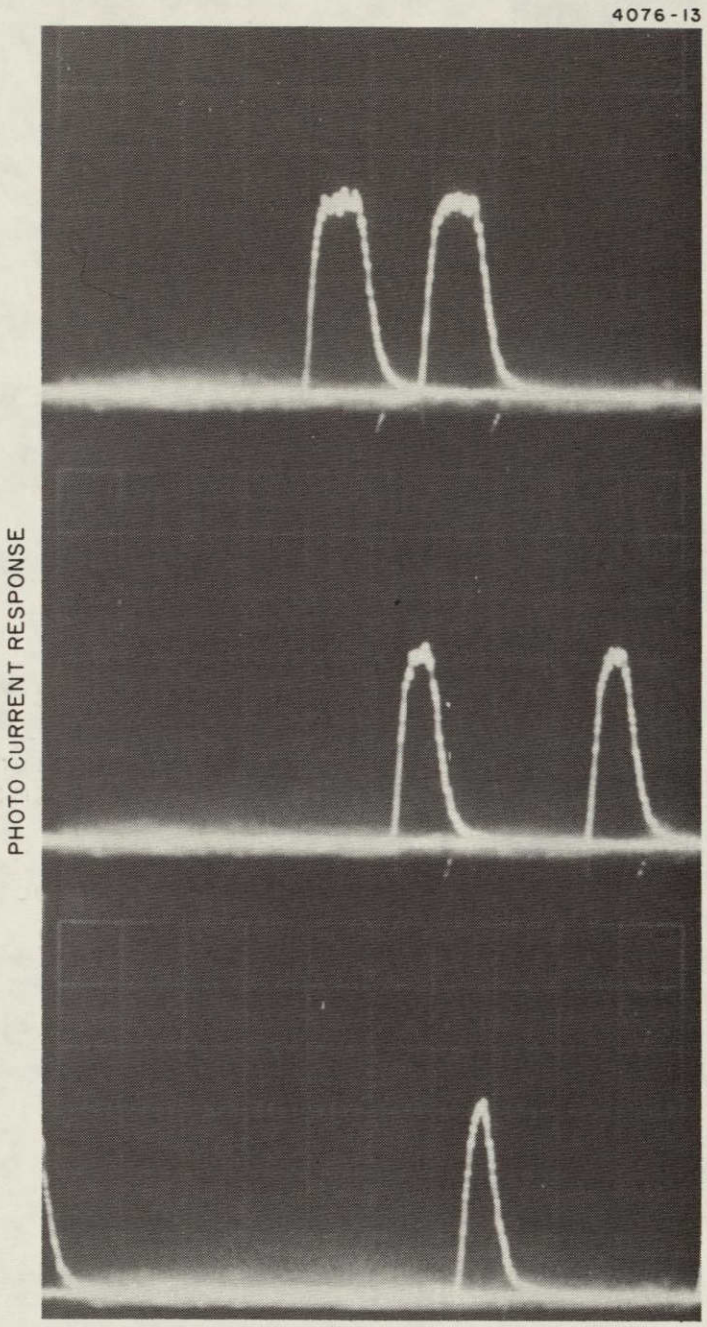

Fig. V-5.
Cell SP49E (A relatively fast film). Cycle time to saturation as a function of exposure time.
Conditions:
Sweep time, 50 msec/cm;
Bias Voltage (V_{th}, 5.4 V rms at 10 kHz; Illumination Level, 350 $\mu W/cm^2$;
Top Photo Exposure Time, 40 msec; Center Photo Exposure Time, 23 msec;
Bottom Photo Exposure Time, 18 msec.

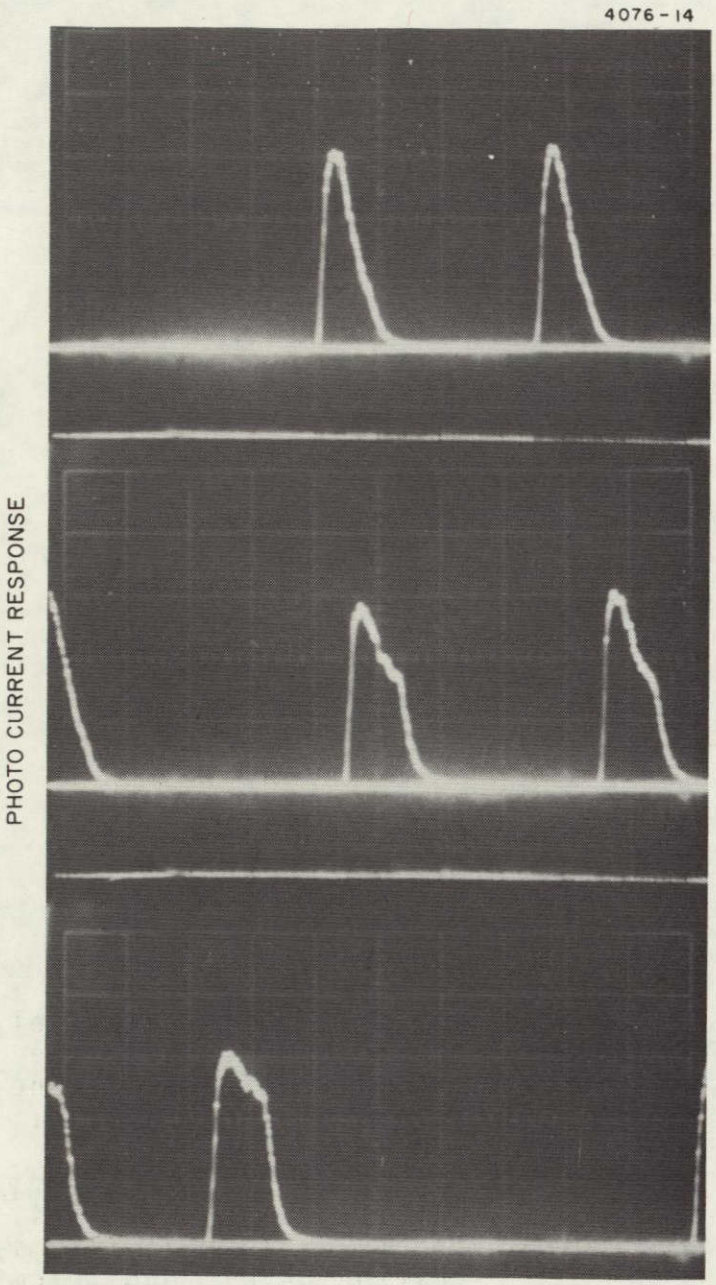

Fig. V-6.
Cell SP49E. Cycle time to saturation as a function of input light level. Conditions: Sweep Time, 50 msec/cm; Bias Voltage (V_{th}), 5.4 V rms at 10 kHz; Exposure Time, 40 msec; Top Photo, 60 $\mu W/cm^2$; Center Photo, 160 $\mu W/cm^2$; Bottom Photo, 350 $\mu W/cm^2$.

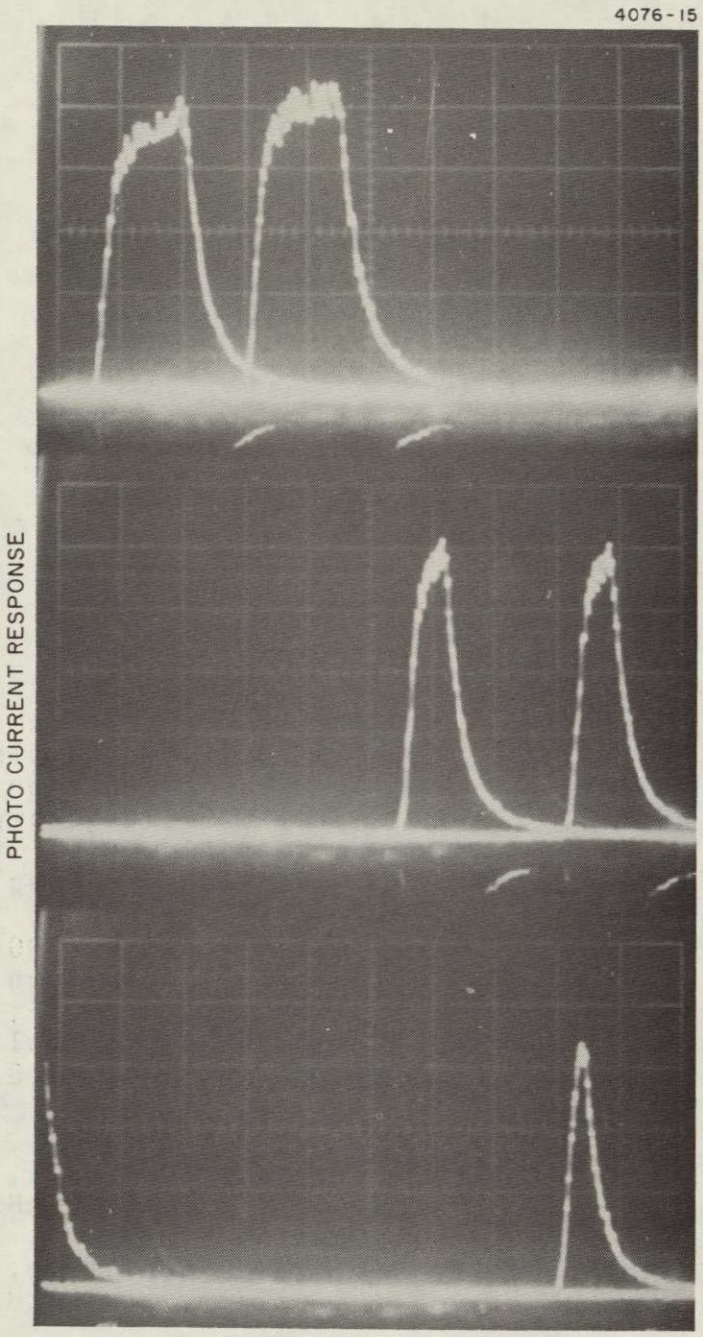

Fig. V-7. Cell SP48B (Medium Speed Film). Cycle time to saturation as a function of exposure time. Conditions: Sweep Time, 50 msec/cm; Bias Voltage (V_{th}), 5.2 V rms at 10 kHz; Illumination Level, 350 $\mu W/cm^2$; Top Photo Exposure Time, 100 msec; Center Photo Exposure Time, 40 msec; Bottom Photo Exposure Time, 23 msec.

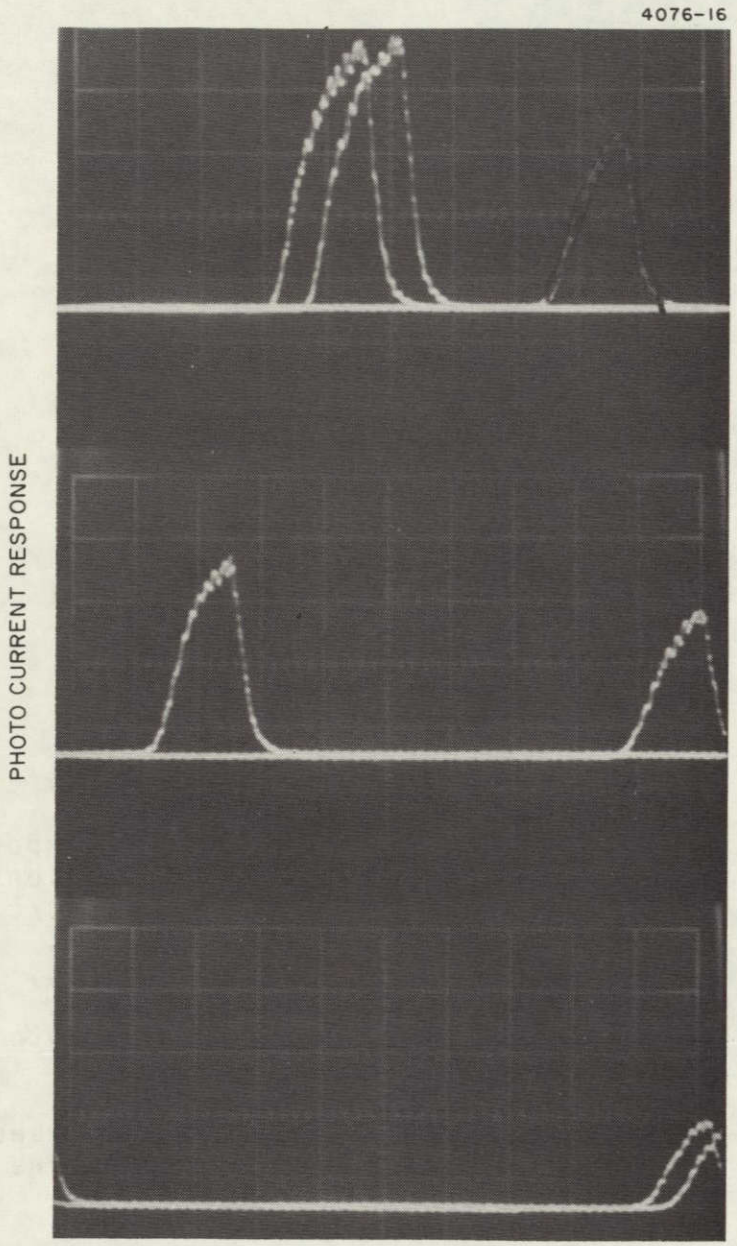

Fig. V-8.
Cell SP48E (Medium Speed Film). Cycle time as a function of bias voltage amplitude (below V_{th}). Conditions: Sweep Time, 50 msec/cm; Exposure Time, 100 msec; Illumination Level, 350 $\mu W/cm^2$; Top Photo Bias Voltage Amplitude, 4.8 V rms at 10 kHz; Center Photo Bias Voltage Amplitude, 4.3 V rms at 10 kHz; Bottom Photo Bias Voltage Amplitude, 3.8 V rms at 10 kHz.

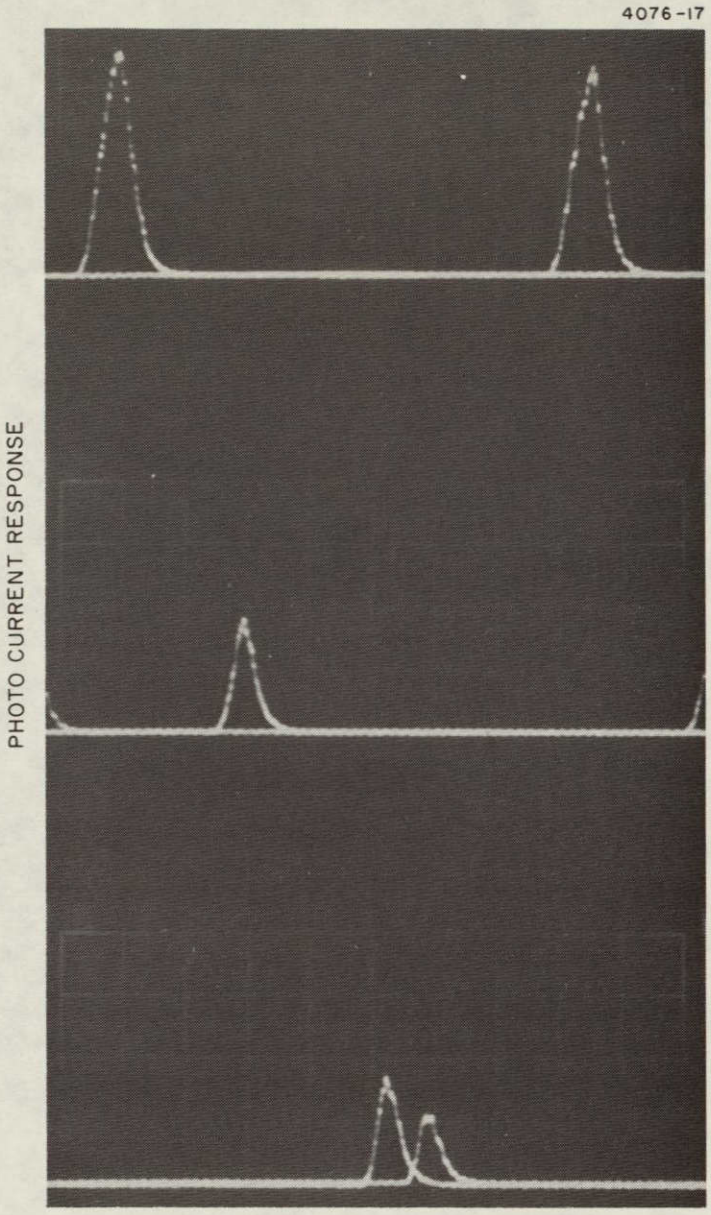

Fig. V-9.
Cell SP48E (Medium Speed Film). Cycle time as a function of exposure time showing limitation of transmission amplitude. Conditions: Sweep Time. 50 msec/cm; Bias Voltage, 4.8 V rms at 10 kHz; Illumination Level, 350 $\mu W/cm^2$; Top Photo Exposure Time, 40 msec; Center Photo Exposure Time, 23 msec.

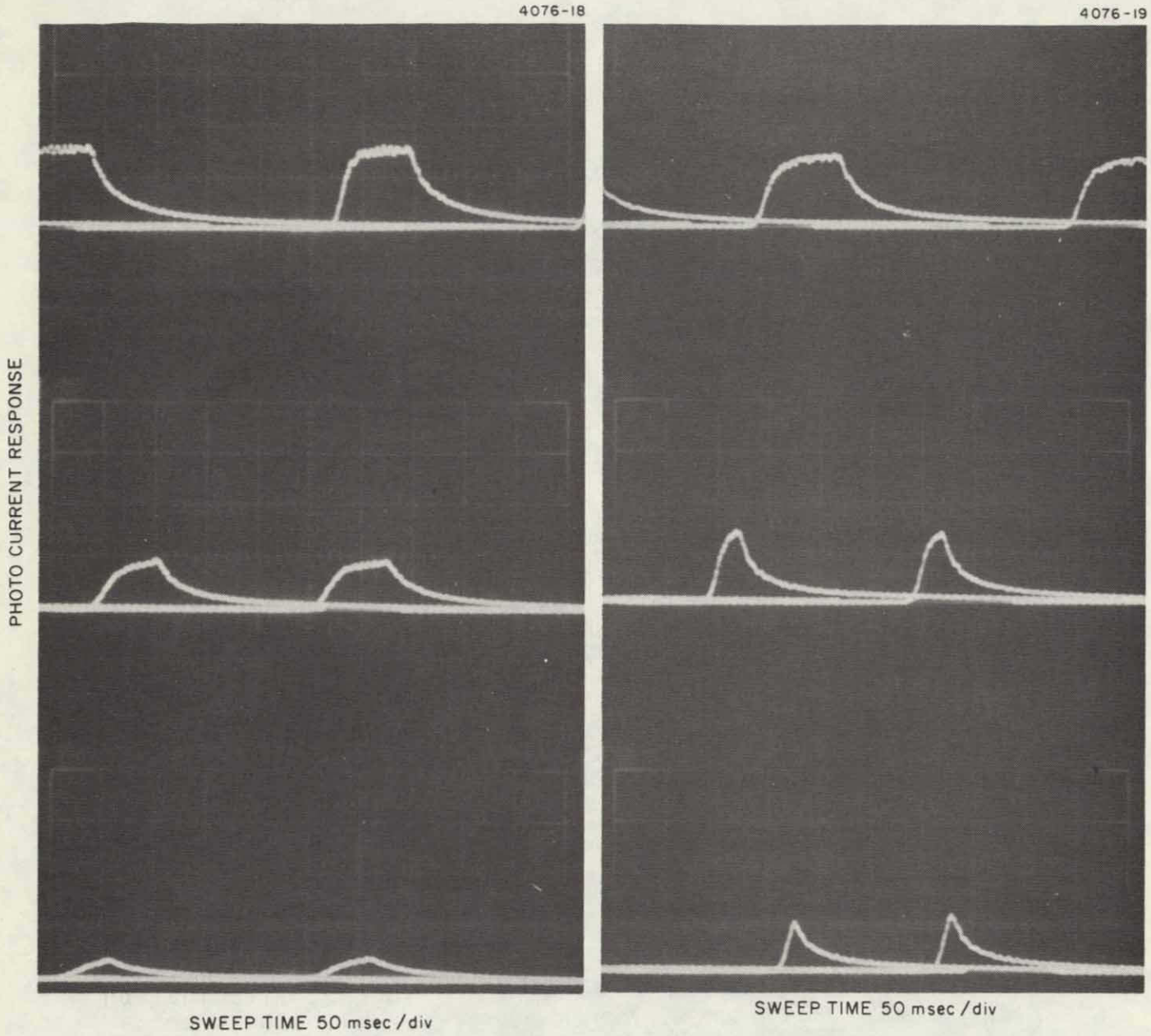

Fig. V-10. Cell a2d (Slow speed film). Demonstration of the relative effects of Exposure Time and Illumination Level on the same light valve. Common Conditions: Sweep Time, 50 msec/cm; Bias Voltage (V_{th}), 5 V rms at 10 kHz.

Photo	Exposure Time, msec	Illumination Level, $\mu W/cm^2$
Top Left	100	350
Center Left	100	160
Bottom Left	100	60
Top Right	100	350
Center Right	40	350
Bottom Right	23	350

of the liquid crystal layer; and surface alignment of the liquid crystal layer. Measurements of these characteristics were made visually as described below.

b. Substrate Impedance Uniformity – The substrate impedance is determined by the resistance and capacitance of the films (mirror, light-blocking layer, and CdS). In the final device these series impedances are in turn in series with the liquid crystal to further complicate their analysis. The large xenon projector was used to test for substrate uniformity because the illumination light is uniform and intense enough for light saturation. Visual observation of transmission uniformity on the output screen was made at 50x magnification. Characteristics isolation tests were made as follows.

The thickness of the liquid crystal layer was first evaluated to determine its role in subsequent tests. Thickness is then adjusted where possible. With bias voltage at low frequency (200 Hz), where the resistive component of the overall impedance is significant, the substrate is then switched at operating illumination intensity (100 $\mu W/cm^2$), and saturated illumination intensities (1.7 mW/cm^2). The optical response threshold and maximum transmission may then be observed on the output screen as a function of localized resistance variations. Film interface nonuniformities can usually be seen in this test. The bias voltage is then changed to high frequency (100 kHz) and the same tests repeated as above. Here the impedance is predominantly capacitive and the response observed is mostly a function of film thickness. The overall result of these tests, when correlated, is to give a good approximation of the quantity each film contributes to nonuniformity.

c. Liquid Crystal Thickness – Thickness gradients in the liquid crystal layer were identified by finding the product of several test techniques applied to a given area of a device. The large xenon projector with its broad spectral band of linearly polarized light was used to detect thickness gradients across the aperture by observing

color variation on the output screen when the device is in the off state. This is possible since transmission (T) is proportional to $\Delta d\, \Delta n/\lambda$ where Δn is the optical birefringence, Δd is the thickness differential, and λ the transmitted wavelength. Thickness gradients thus observed can be correlated with interference fringes observed on the device when its aperture is viewed on the optical data processing bench in the following manner. The high intensity laser light which is incident upon the device in the ODP bench is scattered slightly at the mirror surface and at the ITO surface. This small quantity of scattered light can be seen when viewed off axis. Interference occurs when $\Delta d \cdot n = k\lambda/2$ where n is the average effective index in the medium Δd, and k is the number of fringes observed. The number and shape of the fringe or fringes indicates the nature of Δd.

d. Surface Alignment – Surface alignment of the LC was viewed in the polarized light of the large projector at high magnification. Alignment interruptions or changes in direction were observed on the output screen as disclination lines and areas of contrasting spectral transmission characteristics. The shape, size and location of these aided in indicating their cause. Some examples are holes and scratches from substrate polishing, unsuccessful surface treatment, damage occurring during assembly, or contamination on the surface.

(1) Coherent wavefront distortion tests – Tests for phase distortion of the laser beam wavefront were made on the optical data processing test bench. The optional mirror (Fig. V-2) was used in the Michelson Interferometer Mode to interfere the reference beam with that of the light valve mirror. The output plane of the system was then observed and photographed for fringe curvature to determine the quantity of bowing in the substrate mirror ($\Delta \ell$). By counting the number of interference fringes (k) displaced across the aperture and using the equation $\phi = (2k-1)\,\pi$ radians we can calculate the total phase shift of the light valve reflection with respect to the reference beam (ϕ).

Then $\phi/2\pi = N_\lambda$ the number of wavelengths in the path difference, $2\Delta\ell$. The actual bow of the mirror is found using the equation $\Delta\ell = N_\lambda \lambda/2$. A photograph of a typical light valve with curvature of 1 to 2 wavelengths is shown in Fig. V-11.

D. Physical Description of Delivered Devices

The delivered light valves are essentially the same physical configuration as the optical-to-optical device with the exception that the substrate glasses are 12 mm thick. The overall thickness of the delivered ODP light valves is therefore ~37 mm.

The cell holders, Fig. V-12 (a) and (b) are machined from 6061 aluminum stock and are black anodized prior to use. The base, or terminal block, Fig. V-13, is machined from lucite to accept standard G-32 banana pins with wire lugs. Two-inch leads of stranded No. 26 Teflon-coated wire are soldered to the wire lugs and attached to the electrodes at their opposite ends by means of small alligator clips or small beryllium copper clips made from 1/4 x 5/8 x 0.020 in. thick sheet beryllium and bent into a U-shaped clip that slips over the end of the electrode (see Fig. V-14). The terminal block is then attached to the holder by two 6/32 x 5/8 in. roundhead screws.

A photograph of the component parts of the light valve is shown in Fig. V-15, and the assembled device is shown in Fig. V-14.

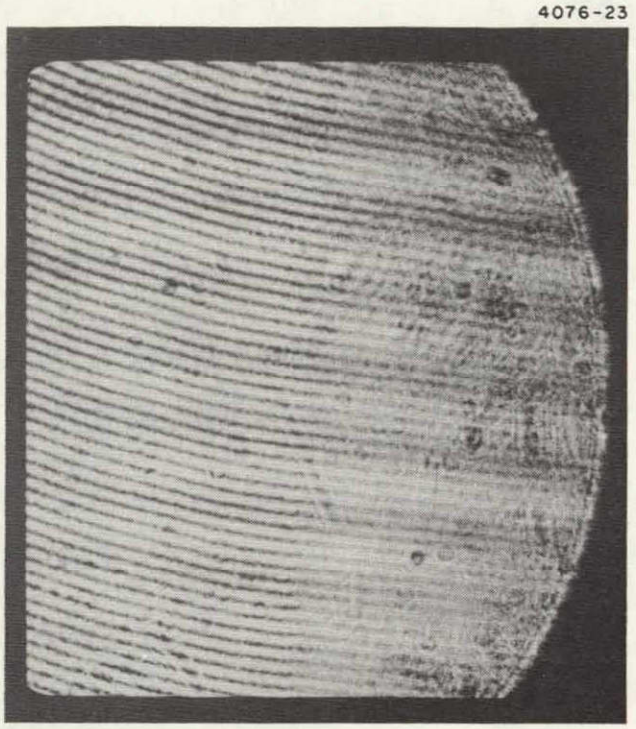

Fig. V-11. Interference fringes showing bow in substrate mirror.

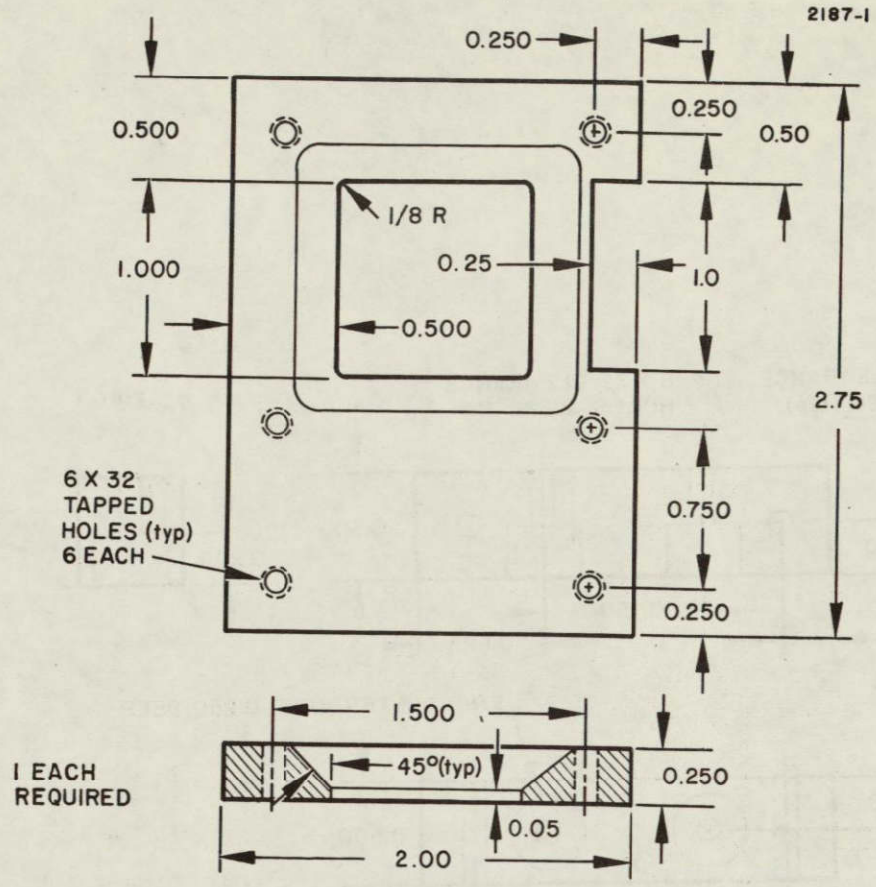

NOTE: ORIENTATION OF 45° BEVEL IMPORTANT

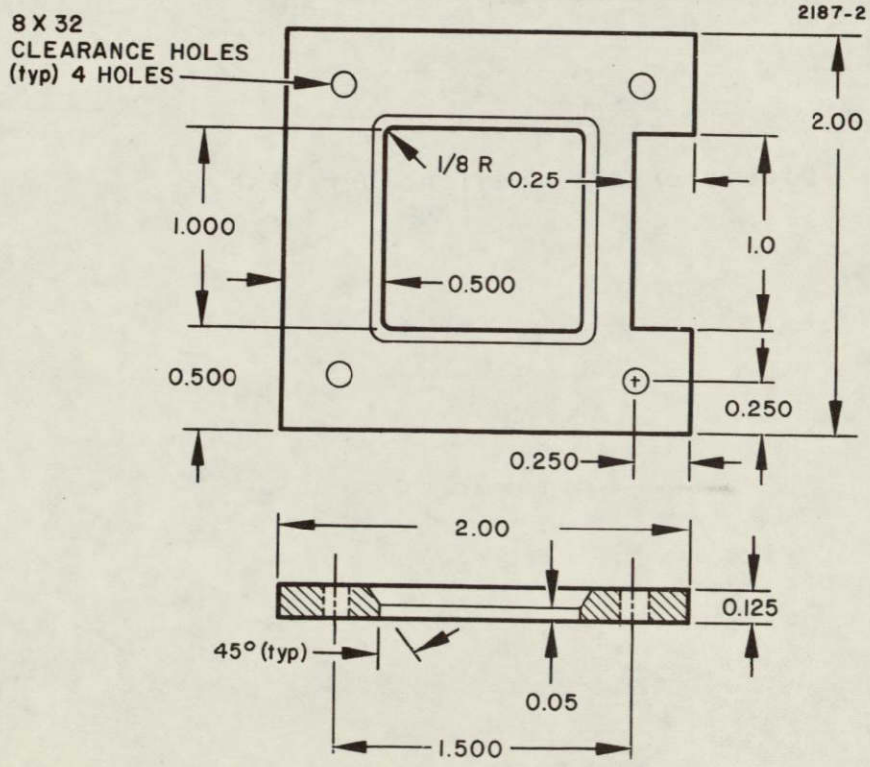

Fig. V-12.
Liquid crystal
cell holder.

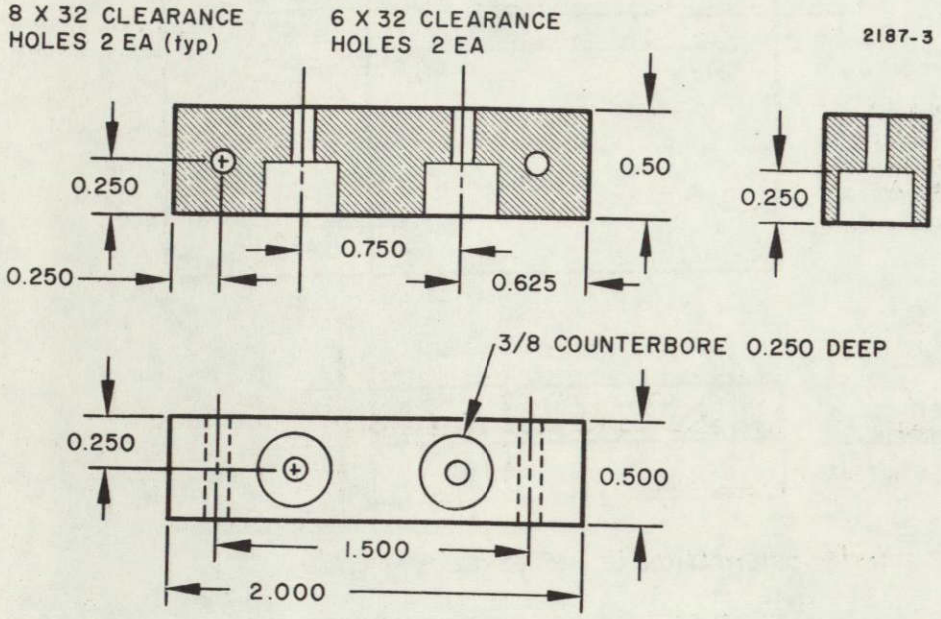

Fig. V-13. Liquid crystal cell holder base.

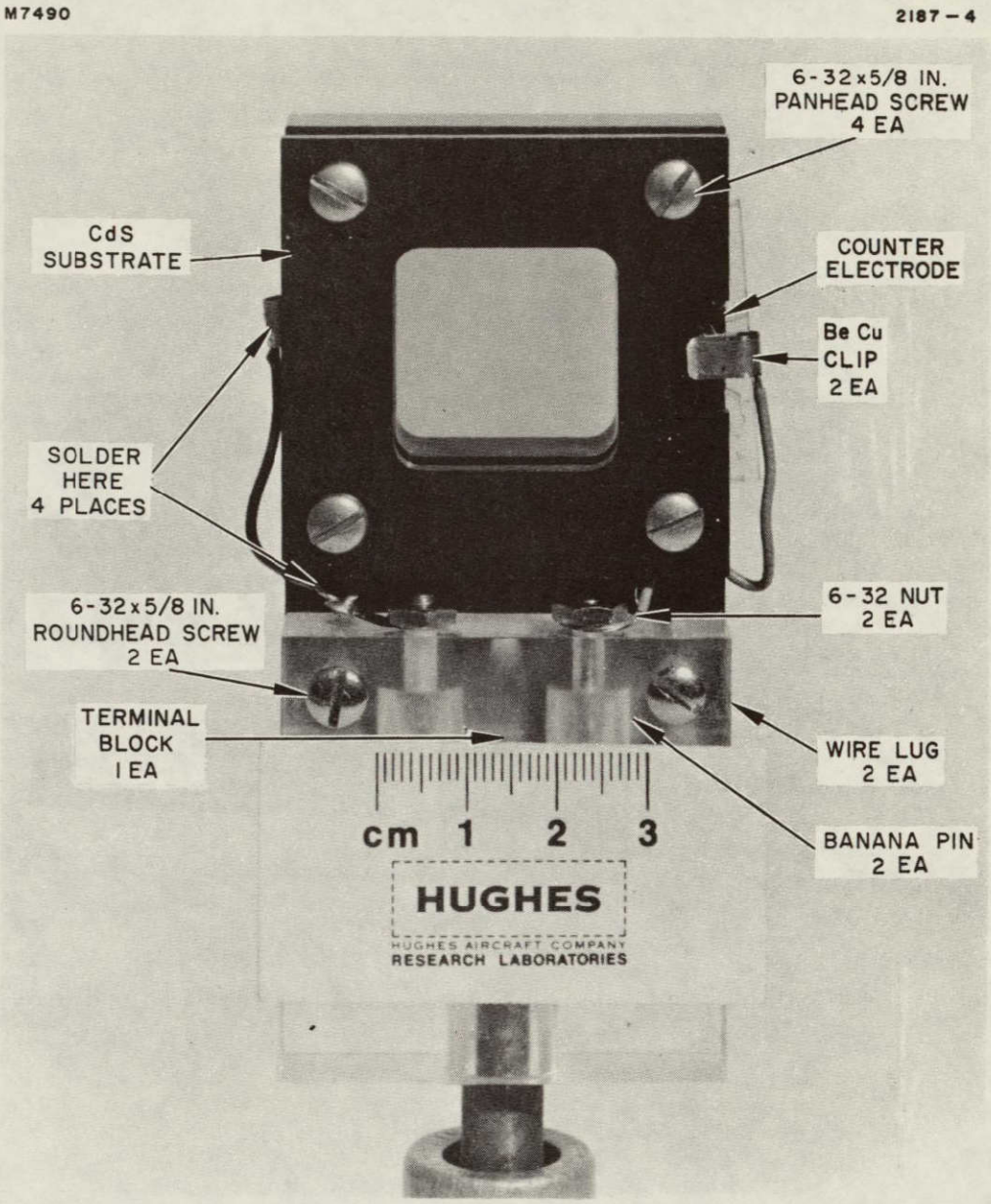

Fig. V-14. View of assembled cell.

M9755

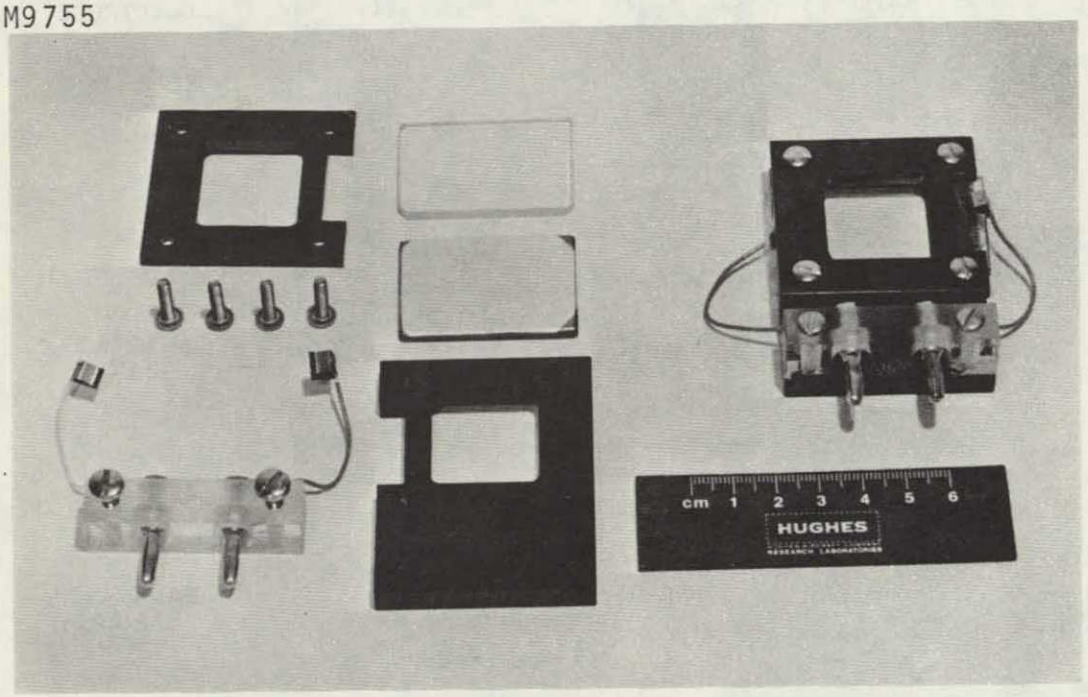

Fig. V-15. Exploded view of photoactivated liquid crystal light valve device.

REFERENCES

1. G.H. Heilmeier, et al., Proc. IEEE 56, 1162 (1968).

2. L. T. Creagh, et al., IEEE Trans. on Electron Devices ED-18, 672 (1971).

3. Dwight W. Berreman, J. Opt. Soc. Am. 43, 1374 (1973).

4. J. E. Bigelow and R. A. Kashnow, G. E. Technical Information Series Report No. 74, CRD 090, June 1974.

5. F. J. Kahn, Appl. Phys. Lett. 22, 386 (1973); F. J. Kahn, G. N. Taylor, and H. Schonborn, Proc. IEEE 61, 832 (1973).

6. L. M. Fraas, W. P. Bleha, and P. O. Braatz, J. Appl. Phys. 46, 2 491 (1975).

7. C. A. Mead, Solid-State Electronics 9, 1023 (1966).

8. R. K. Swank, Phys. Rev. 153, 844 (1967).

9. A. Waxman, Solid-State Electronics 9, 303 (1966); C. A. Nevgebauer, D. C. Miller, and J. W. Hall, Thin Solid Films 2, 57 (1968).

10. W. Palz and S. Ravelet, Solid-State Electronics 13, 1241 (1970).

11. L. Fraas, W. B. Bleha, and J. Grinberg (to be published).

12. L. Fraas, W. P. Bleha, and J. Grinberg (to be published).

13. H. A. Macleod, Thin Film Optical Filters (American Elsevier, New York, N. Y., 1969), p. 20.

14. J. T. Cox, G. Hass, and A. Thelen, J. Opt. Soc. Am. 52, 965 (1962).

15. W. Keon and D. Pustinen, RCA Review, June 1970, p. 167.

APPENDIX

OPERATING INSTRUCTIONS FOR DELIVERED DEVICES

The delivered ODP light valves are laboratory models and must be handled with care to avoid degradation of their optical and electrical properties. The following paragraphs contain information intended to assist the user in their handling, operation, and storage.

1. Handling of ODP Light Valve

The cell assembly consists of a stack of plates of different materials held together by four 6-32 screws only. Two neoprene pads are contained in the stack to provide a relatively constant pressure to the glass substrates. The following is a list of recommendations to assist in preventing handling damage.

a. Always handle and mount the device by the base plate or lucite block, never by the glass substrate or front faceplate.

b. Do not apply an external force to the stack in any direction.

c. Do not turn the four 6-32 assembly screws. They have been set for optimum performance during fabrication. Any change will only degrade device performance.

d. The lucite block may be removed if a different mount is desired, but alternate mounting fixtures should be attached only to the base plate, taking care not to distort the base plate in the process of making the modification.

e. The input and output surfaces may be cleaned if necessary with lens tissue and a very small quantity of lens cleaning solvent. Extreme care should be taken to assure that solvent is applied to the light input and output aperture surfaces only. Solvents that attack the neoprene pads should not be used, of course.

Severe temperature environments should be avoided in these laboratory models. Operation at room temperature in dry air is recommended.

g. In general, the devices should be treated as one would treat any other fragile optical component. Dropping or bumping can cause damage.

2. Storage

The delivered ODP light valves are not hermetically sealed; hence they will not be impervious to air and moisture. They should be stored in an environment that meets the following conditions:

a. Temperature should be 20 to 30°C.

b. The atmosphere should be air with humidity as low as practical or dry nitrogen, if possible.

c. Devices should be placed with the back of the base plate (input side) down on a flat surface.

3. . . Operation of Delivered Devices

Electrical operation of the delivered light valves requires the use of an audio oscillator with a frequency range of from 0.4 to 10 kHz and variable output amplitude of 10 V_{rms} maximum, and ac voltage monitor, and an ac current monitor.

a. Procedure

With the output analyzer crossed to the polarization of the incident readout beam, insert the device in the optical path of the system with the base plate side (input side) toward the addressing (input) illumination, and the front face (output side) toward the coherent laser readout beam. (The light valve mirror reflection of the incident laser beam may be used to assist in adjusting the light valve normal to the optical axis of the system.) Rotate the light valve about the optical axis of the system until minimum transmission exists on the output screen. A minimum will occur at approximately each 90° of rotation. Focus the addressing (input) illumination, through the 1.2 cm thick input glass substrate and onto the CdS layer. Slowly apply the ac biasing voltage to the light valve electrodes until the image appears on the readout beam screen. Do not exceed 10 V_{rms} at the light valve electrodes. The ac current monitor in the biasing circuit will assist in determining circuit continuity (including good contact at the BeCu clips on the light valve electrodes). These clips

may be bent slightly to tighten them if poor contact is observed. The position of the clip on the electrode is also an important factor for obtaining good contact. The final adjustments of the imaging focus and the projection lens focus may now be made. The amplitude of the bias voltage and the intensity of the input illumination may be trimmed in an inverse relationship to obtain maximum contrast and resolution of the image on the output screen. Bias voltage that is too high will result in background write-up (device transmission) in the nonilluminated areas of the image. Bias voltage that is too low will result in no or low transmission in the illuminated areas. Image illumination that is too intense, poorly focused, or of low resolution will result in image spreading at the output. Image illumination that is not intense enough will result in low (or no) transmission at the output. In cases where the input image is pulsed in short duration pulses, i.e., 10 to 20 msec, the bias voltage amplitude should be adjusted to V_{th} maximum. The image intensity may then be adjusted up or down to give the required image energy density for the best contrast and resolution in the output image.

Characteristics of Delivered Devices

The following data summarize the measured performance of the delivered devices. These data characterize the devices individually for assistance to the user.

Cell SP69E (Red)

Bias Voltage at 1 kHz	5.4 V_{rms}
Illumination Level	60 $\mu W/cm^2$
Contrast Ratio (Measured at above conditions)	385:1
Resolution (Measured at above conditions)	>40 lines/mm
Time Response	See Fig. 1

Cell SP49D (Red)

Bias Voltage at 1 kHz	5.6 V_{rms}
Illumination Level	60 $\mu W/cm^2$
Contrast Ratio (Measured at above conditions)	210:1
Resolution (Measured at above conditions)	>40 lines/mm
Time Response	See Fig. 2

Cell SP69A (Green)

Bias Voltage at 1 kHz	7.3 V_{rms}
Illumination Level	60 $\mu W/cm^2$
Contrast Ratio (Measured at above conditions)	240:1
Resolution (Measured at above conditions)	>40 lines/mm
Time Response	See Fig. 3

Cell SP70B (Green)

Bias Voltage at 1 kHz	6.4 V_{rms}
Illumination Level	60 $\mu W/cm^2$
Contrast Ratio (Measured at above conditions)	110:1
Resolution (Measured at above conditions)	>40 lines/mm
Time Response	See Fig. 4